4-1988

Proceedings of the Eighteenth Annual Biochemical Engineering Symposium

Robert H. Davis
University of Colorado at Boulder

Proceedings of the

18th

Annual Biochemical Engineering Symposium

April 22-23, 1988

Robert H. Davis
Editor

Department of Chemical Engineering
University of Colorado
Boulder, CO 80309

University of Colorado at Boulder

PROCEEDINGS OF THE EIGHTEENTH ANNUAL BIOCHEMICAL ENGINEERING SYMPOSIUM

April 22–23, 1988

Robert H. Davis
Editor

Department of Chemical Engineering
University of Colorado
Boulder, Colorado 80309

PROCEEDINGS OF THE EIGHTEENTH ANNUAL BIOCHEMICAL ENGINEERING SYMPOSIUM

The eighteenth annual biochemical engineering symposium was held during April 22–23, 1988 at the YMCA of the Rockies conference center in Estes Park, Colorado, under the sponsorship of the University of Colorado. Previous symposia in this series have been hosted by Kansas State University (1st, 3rd, 5th, 9th, 12th, 16th), University of Nebraska–Lincoln (2nd, 4th), Iowa State University (6th, 7th, 10th, 13th, 17th), University of Missouri–Columbia (8th, 14th), and Colorado State University (11th, 15th). Next year's symposium is scheduled to be held at the University of Missouri–Columbia.

The symposia are devoted to talks by students about their ongoing research. Because final publication usually takes place elsewhere, the papers included in the proceedings are brief, and often cover work in progress.

Attending the eighteenth annual biochemical engineering symposium were the following:

Colorado State University—Dr. Jim Linden, Zsolt Buday, Ming Shiang, DooHyun Ryoo, Won–Ho Rho, Xiangdong Zhou, Guorong Zhang, Ahmad Hilaly, N. Raghunand, Sarah Waterman, David Mitchell, Linda Henk, Shari Hanson, Carol Harper, John Haigh, Richard Moolick, Dr. U. S. Agrawal (visiting from India)

Iowa State University—Dr. Charles Glatz, Dr. Peter Reilly, Curtis Krause, Susan Rogers, Meng Heng, Jang–You Shieh, Bipin Dalmia, Andrea Bozzano, Ramanathan Murali, Leah Patterson, Jing Zeng, Hsiu–Mei Chen, Diane Parker, Julie Hardwick, Dr. Kulbhushan Bastawde (visiting from India), Milica Radosavljevic (visiting from Yugoslavia), Dr. N. Ganesh Karanth (visiting from India)

Kansas State University—Dr. Larry Erickson, Juan Guerra, Brad Wright, Laura Berry, Travis Jones, Lourdes Taladriz, Ayush Gupta, John McDonald

University of Colorado—Dr. Robert Davis, Dr. Dhinakar Kompala, Dr. Fred Ramirez, Huaqing Zhou, Ching–Yuan Lee, Laura McBurney, Dana Andersen, Greg Ogden, Kim Henry, Kalyan Tadikonda, Brian Batt, Bill Bentley, Harold van Deinse, Seujeung Park, Doug Gee

University of Missouri–Columbia—Dr. Rakesh Bajpai, Paul Li–Hong Yeh, Horngtwu Su, Peter Ung–Nak Sohn

Washington University—Dr. Ales Prokop

18th ANNUAL BIOCHEMICAL ENGINEERING SYMPOSIUM

April 22–23, 1988 Estes Park, Colorado

Program

Friday, April 22

6:30-9:30 p.m. **Informal Reception and Buffet**

Saturday, April 23

7:30-8:30 a.m. **Breakfast**

9:00-10:15 a.m. **First Paper Session**

1. Applications of mass spectrometers in biochemical engineering. John P. McDonald, Ayush Gupta, and Lourdes Taladriz, Kansas State University.
2. Enzymatic hydrolysis of corn gluten proteins. Julie Hardwick, Iowa State University.
3. Monitoring the acetone–butanol fermentation by HPLC. Z. Buday and J. C. Linden, Colorado State University.

10:15-10:45 a.m. **Coffee Break**

10:45-12:00 noon **Second Paper Session**

4. On–line state identification for batch fermentation. Douglas A. Gee and W. Fred Ramirez, University of Colorado.
5. Role of spargers in air–lift reactors. Peter U. Sohn, University of Missouri–Columbia.
6. The interaction of microcarriers and turbulence within an airlift fermentor. G. Travis Jones, Kansas State University.

12:00-1:00 p.m. **Lunch**

1:00-2:30 p.m. **Third Paper Session**

7. Oxygen diffusion in the inter-fiber gel/cell matrix of NMR–compatible hollow fiber bioreactors. Shari L. Hanson, Bruce E. Dale, and Robert J. Gillies, Colorado State University.
8. Characterization of Ca–alginate gel beads formation. Horngtwu Su, University of Missouri–Columbia.
9. Effects of plasmid–mediated activity on bacterial metabolism and culture stability. William Bentley, Dana Andersen, Robert Davis, and Dhinakar Kompala, University of Colorado.
10. Genetic engineering of beta-galactosidase to aid in fermentation product recovery by polyelectrolyte precipitation. Diane E. Parker, Iowa State University.

2:30-4:30 p.m. **Free Time (hiking, volleyball, etc.)**

4:30-5:45 p.m. **Poster Session**

1. Biodegradation of organic compounds in soil. Lourdes Taladriz, L. E. Erickson, and L. T. Fan, Kansas State University.

2. Effect of dilution, pH and nutrient composition on the biodegradation of metalworking fluids. Ayush Gupta, L. E. Erickson, and L. T. Fan, Kansas State University.

3. A design study of tissue plasminogen activator production using mammalian cell culture. Laura Berry, Juan Guerra, and Pongstron Uralwong, Kansas State University.

4. Modeling air injection for *in situ* biodegradation of soil contaminants. Brad Wright, Kansas State University.

5. Redox potential correlation with dissolved hydrogen concentration. Xiangdong Zhou and J. C. Linden, Colorado State University.

6. Characterization of shear effects in plant and animal cell cultivations. Paul Li–Hong Yeh, University of Missouri–Columbia.

7. Modeling of ensiling fermentation. A. K. Hilaly, L. H. Henk, and J. C. Linden, Colorado State University.

8. Refolding kinetics of SLPI-A recombinant protein. S. Jachim, Colorado State University.

9. Role of ester groups in resistance of cell wall polysacharides. D. Mitchell, B. E. Dale, and H. Schroeder, Colorado State University.

10. Biosolubilization of coal. R. Moolick and J. C. Linden, Colorado State University.

11. Fungal cellulase production in fluidized bed reactors. W. H. Rho, Colorado State University.

12. Thermophilic cellulase from *Acidothermus cellulolyticus*, M. Shiang, Colorado State University.

5:45-7:00 p.m. **Dinner**

Table of Contents

Applications of Mass Spectrometers in Biochemical Engineering

John P. McDonald, Ayush Gupta, Lourdes Taladriz

Dept. of Chemical Engineering
Kansas State University
Manhattan, Kansas

Quadrupole Mass Spectrometers have become important instruments in the analysis of volatile compounds. Quadrupole analyzers have a number of advantages over other methods. Unlike chromatography, mass spectrometers are capable of on-line analysis. Other on-line instruments are limited to certain volatile compounds. Mass spectrometers are capable of monitoring any compound provided that a unique mass to charge ratio is generated by the ionizer.

Mass Separation

By means of a rotary and a turbomolecular pump, the pressure in the ionization chamber is reduced to 10^{-5} torr. Low pressure is required to insure a long mean free path and a low number of collisions between ionized molecules.

The gas inlet consists of a 50 micron i.d. fused silica capillary one meter in length. These dimensions maintain continuous laminar flow throughout the inlet system. The pressure differential across the capillary is about one atmosphere. Gas flows through the capillary at about 1.8 ml (STP) per hour.

Electron Impact (EI) ionization is the method of choice for most applications of mass spectrometry. Gas molecules entering the ionization chamber through the capillary inlet collide with electrons radiating from a hot thoriated iridium filament. These collisions result in ions and ion fragments of the parent molecule. Fragmentation is a considerable problem for high molecular weight compounds. Alternative soft ionization techniques can be used to maintain molecular integrety.

The charged particles in the ionization chamber are separated by the mass filter. The quadrupole field generated by a DC voltage and a radio frequency applied to four parabolic rods works as a mass filter. Only ions with specific mass to charge ratios will travel on stable oscillatory paths. By adjusting the DC voltage, various mass to charge ratios are focused through the exit slit and collected by a faraday cup where they register as current.

Data Acquisition

A Dycor model M200 Quadrupole Gas Analyzer (Ametek Co. Pittsburgh, Pennsylvania 15238) was interfaced with a Zenith Electronics Co. Model 120/240 Computer through their respective RS232 ports. Lotus 123 and Lotus Measure were used in establishing the data acquisition and control of all parameters. This software package was chosen for its versatility and simplicity.

The system of macro driven spreadsheets designed at Kansas State University can control any parameter or read data from the instrument directly into the spreadsheet, where it can be stored for later recall, and calculation.

Applications

The versatility of the mass spectrometer lends the instrument to a number of applications. Used in series with a gas chromatograph (GCMS) and a computerized data base, a system can be developed for separation and quantification of any number of compounds. The use of GCMS precludes on-line analysis, but gives more reliable results for gas streams with a large number of similar components.

Biodegradation Studies

Fermentation off-gas analysis has been studied by numerous researchers (Hienzle, 1987; Lloyd *et al.*, 1985; and Pungor *et al.*, 1983). Most such studies have been limited to semi-batch processes (where air is sparged through the system). Off-gas analysis can also provide useful kinetic information in batch biodegradation studies.

Experimental Methods: The mass spectrometer capillary inlet was inserted into the headspace of shake flasks through a syringe needle peircing the stopper. The capillary and syringe needle were then wrapped with parafilm "M" to ensure air-tight conditions. A mixed bacterial culture biodegradation of an oil (IRMCO 141) was being studied.

The COD concentration was approaching steady state in the shake flask experiments when the MS measurements began (at 500 and 550 hours for 2% and 5% initial oil concentrations). The objective of the gas phase analysis was to determine the oxygen uptake and carbon dioxide production rates. Specific growth rate was calculated from this data and compared with the known maximum specific growth rate.

The equations employed to evaluate the rate of oxygen uptake (OUR) and the carbon dioxide production rate (CPR) for a batch fermentation from the mass spectrometer data include a liquid phase balance on the gas species 'i'

$$V_l \frac{dC_{li}}{dt} = k_{la} (C^*_{li} - C_{li}) V_l + r_i \text{ X } V_l \qquad (1)$$

and a gas phase balance

$$V_g \frac{dC_{gi}}{dt} = F(x_{oi} - x_i) - k_{la} (C^*_{li} - C_{li}) V_l \qquad (2)$$

Adding equations (1) and (2) gives

$$V_l \frac{dC_{li}}{dt} + V_g \frac{dC_{gi}}{dt} = F(x_{oi} - x_i) + r_i \text{ X } V_l \qquad (3)$$

The gas and liquid phase equilibrium concentrations are related using Henry's law

$$C_{li}^{*} = H_i \, x_i \, P_{tot} \qquad (4)$$

Also from the ideal gas law

$$C_{gi} = \frac{P_{tot} \, x_i}{RT} \qquad (5)$$

Because the rate of biodegradation is extremely slow, the mass transfer driving force is small and

$$C_{li}^{*} = C_{li} \qquad (6)$$

is assumed.

Differentiating equations (5) and (6) yields

$$\frac{dC_{gi}}{dt} = \frac{P_{tot}}{RT} \frac{dx_i}{dt} \qquad (7)$$

$$\frac{dC_{li}}{dt} = H_i \, P_{tot} \frac{dx_i}{dt} \qquad (8)$$

Equations (3), (7) and (8) when combined result in the overall mass balance in terms of the gas phase mole fraction of species i.

$$\left(V_g \frac{P_{tot}}{RT} + V_l H_i \, P_{tot}\right) \frac{dx_i}{dt} = F(x_{oi} - x_i) + r_i \, X \, V_l \qquad (9)$$

The term '$r_i \, X \, V_l$' is either the oxygen uptake rate (OUR) or the carbon dioxide production rate (CPR) depending on whether the subscript 'i' is oxygen or carbon dioxide.

Defining:

$$n_{oi} = \left(V_g \frac{P_{tot}}{RT} + V_l H_i \, P_{tot}\right)$$

and $R_i = r_i \, X \, V_l$

results in a more compact notation.

$$n_{oi} \frac{dx_i}{dt} + F \, (x_{oi} - x_i) = R_i \qquad (10)$$

$$n_{oO2} \frac{dx_{O2}}{dt} + F \, (x_{O2} - x_{oO2}) = - \, OUR \qquad (10 \, A)$$

$$n_{oCO2} \frac{dx_{CO2}}{dt} + F \, (x_{CO2} - x_{oCO2}) = CPR \qquad (10 \, B)$$

Solving these differential equations with the initial condition at $t = 0$; $x_i = x_{oi}$, and assuming R_i is constant we obtain

$$x_i - x_{oi} = \frac{R_i}{F} \left(1 - \exp\left(- \frac{F\ t}{n_{oi}}\right)\right) \qquad (11)$$

$$\text{Let } \theta_1 = \frac{R_i}{F} \qquad (12)$$

$$\text{and } \theta_2 = \frac{F}{n_{oi}} \qquad (13)$$

The following equations were used to estimate the values of biomass energetic yield and the specific growth rate constant (Ferrer, et. al., 1979)

$$\text{RQ (Respiratory Quotient)} = \frac{Q_{CO2}}{Q_{O2}} \qquad (14)$$

Q_i = Rate of uptake or production of 'i' $\left(\frac{\text{gmoles}}{\text{hr gm DW}}\right)$

$$\eta \text{ (Biomass Energetic Yield)} = \frac{1 - 1/4\ \gamma_s\ RQ}{\gamma_s/\ \gamma_b - 1/4\ \gamma_s\ RQ} \qquad (15)$$

$$\mu \text{ (Specific Growth Rate Const.)} = \frac{48\ Q_{O2}}{\gamma_b\ \sigma_b\ (1/\eta - 1)} \qquad (16)$$

γ_b (Biomass Reductance Degree) = 4.29

γ_s (Substrate Reductance Degree) = 5.00 (For IRMCO 141)

σ_b (Weight Fraction Carbon in Biomass) = 0.462

Estimates of θ_1 and θ_2 were obtained by non-linear regression of equation 11. The iterative technique used was linearization by Taylor series expansion. (Draper and Smith, 1981)

For IRMCO 141 at 2.0 % initial oil concentration, the oxygen data resulted in an OUR of 0.00033 g mol/hr ($F = 1.8$ ml/hr; $\theta_1 = -0.181$; and $\theta_2 = 0.058$). The Carbon dioxide data gave a CPR of 0.00030 g mol/hr ($F = 1.8$ ml/hr; $\theta_1 = 0.164$; and $\theta_2 = 0.059$).

This data is presented along with the non-linear regression fits in Figure 1.

For IRMCO 141 at 5.0 % initial oil concentration, the oxygen data resulted in an OUR of 0.00058 g mol/hr (F = 1.8 ml/hr; θ_1 = -0.322; and θ_2 = 0.033). The Carbon dioxide data gave a CPR of 0.00055 g mol/hr (F = 1.8 ml/hr; θ_1 = 0.304; and θ_2 = 0.018). Figure 2 shows the data for 5.0% initial oil concentration.

From equations (14), (15) and (16) for IRMCO 141 at 2.0 % initial oil concentration, the biomass energetic yield, η, and specific growth rate, μ, are estimated to be η = 0.368 and μ = 0.00044 (1/hr). From the biomass measurements, the value of μm = 0.01 (1/hr) has been estimated. (Gupta 1988) For IRMCO 141 at 5.0 % initial oil concentration η = 0.253 and μ = 0.00034 (1/hr). From the biomass measurements, the value of μm was 0.02 (1/hr). From the OUR and the CPR values along with the information on the specific growth rate constants (μ) it appears that the biodegradation rate had indeed decreased to extremely low values for both the shake flasks at the point in time where the mass spectrometer readings were taken.

Semi-Batch Fermentations

When a gas stream is sparged through the fermentation vessel, the OUR and CPR values are easily obtained. A quasi steady state assumption is made, and the time derivative terms are dropped from equation 10. Experimental data for this case is shown in figure 3.

REFERENCES

Dawson, P. H., *Quadrupole Mass Spectrometry and its Applications*, pp. 319-329, Elsevier Scientific Publishing Company, Amsterdam (1976).

Draper, N. R., Smith, H., *Applied Regression Analysis*, John Wiley & Sons, New York, (1981).

Ferrer, A., and L. E. Erickson, Evaluation of data consistency and estimation of yield parameters in hydrocarbon fermentations, *Biotechnology & Bioengineering*, 21, 2203-2233 (1979).

Ferrer, A., and L. E. Erickson, Data consistency, yield, maintenance, and hysteresis in batch cultures of candida lipolytica cultured on n-hexadecane, *Biotechnology & Bioengineering*, 22, 421-450 (1980).

Gupta, Ayush, Biodegradation of Synthetic Components in Metalworking Fluids, Masters Thesis, Kansas State University, (1988)

Heinzel, E., Mass spectrometry for on-line monitoring of biotechnological processes, *Advances in Biochemical Engineering & Biotechnology*, 35 (1987).

Lloyd, D., S. Bohatka, J. Szilagyi, Quadrupole mass spectrometry in the monitoring and control of fermentations, *Biosensors*, 1, 279-212 (1985).

Odham, G., L. Larsson, P. Mardh, *Gas Chromatography Mass Spectrometry Applications in Microbiology*, pp. 27-52, Plenum Press, New York (1984).

Punger, E., et. al., Direct Monitoring of the Liquid and Gas Phase During a Fermentation in a Computer-Mass-Spectrometer-Fermentor System, *European Journal of Applied Microbiology and Biotechnology*, 18, 135-140 (1983).

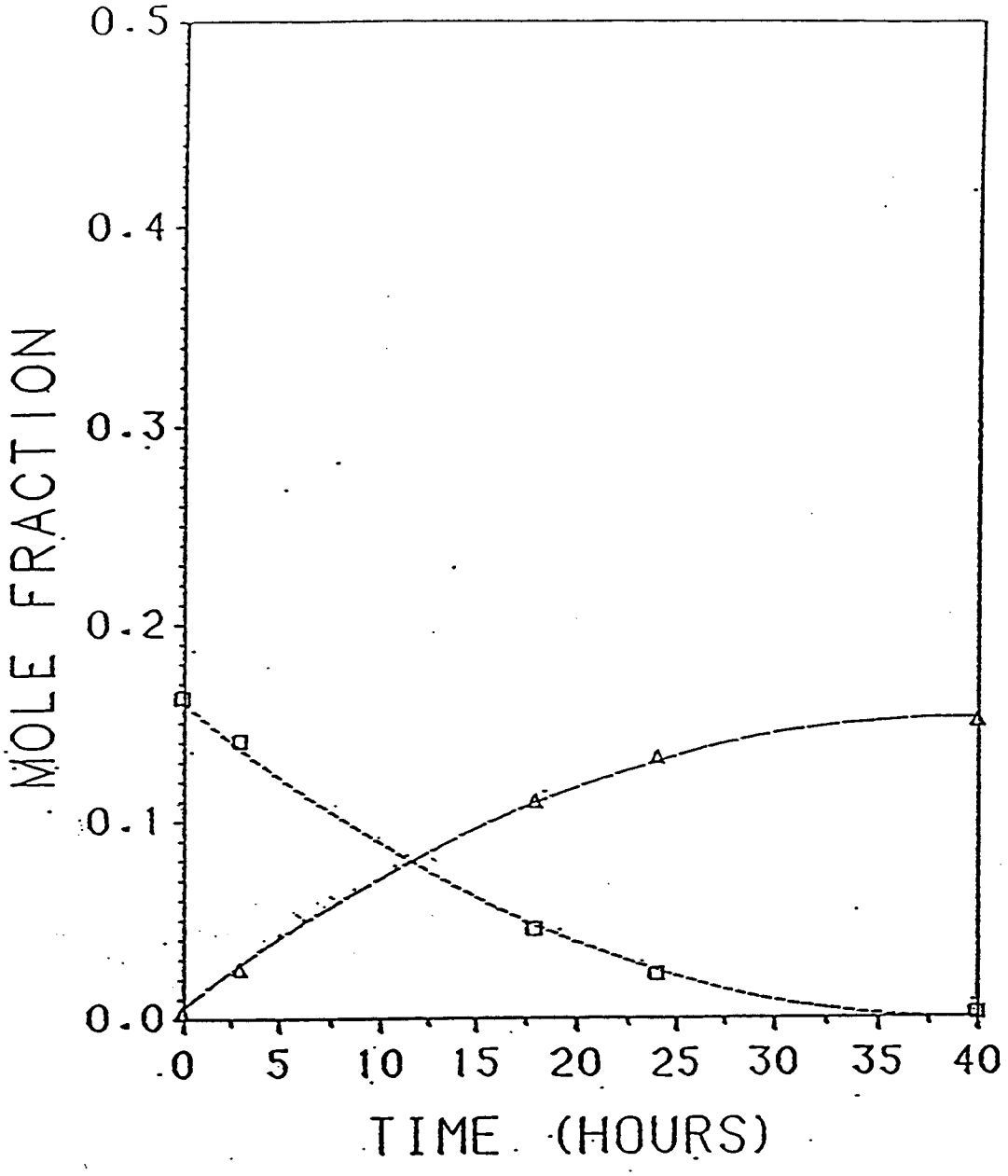

Figure 1. Carbon dioxide (Δ) and Oxygen (□) variation with time in the gas phase for mixed population of microorganisms growing on oil sample IRMCO 141 at an initial oil concentration of 2.0%. Dotted lines are the non-linear regression best fit.

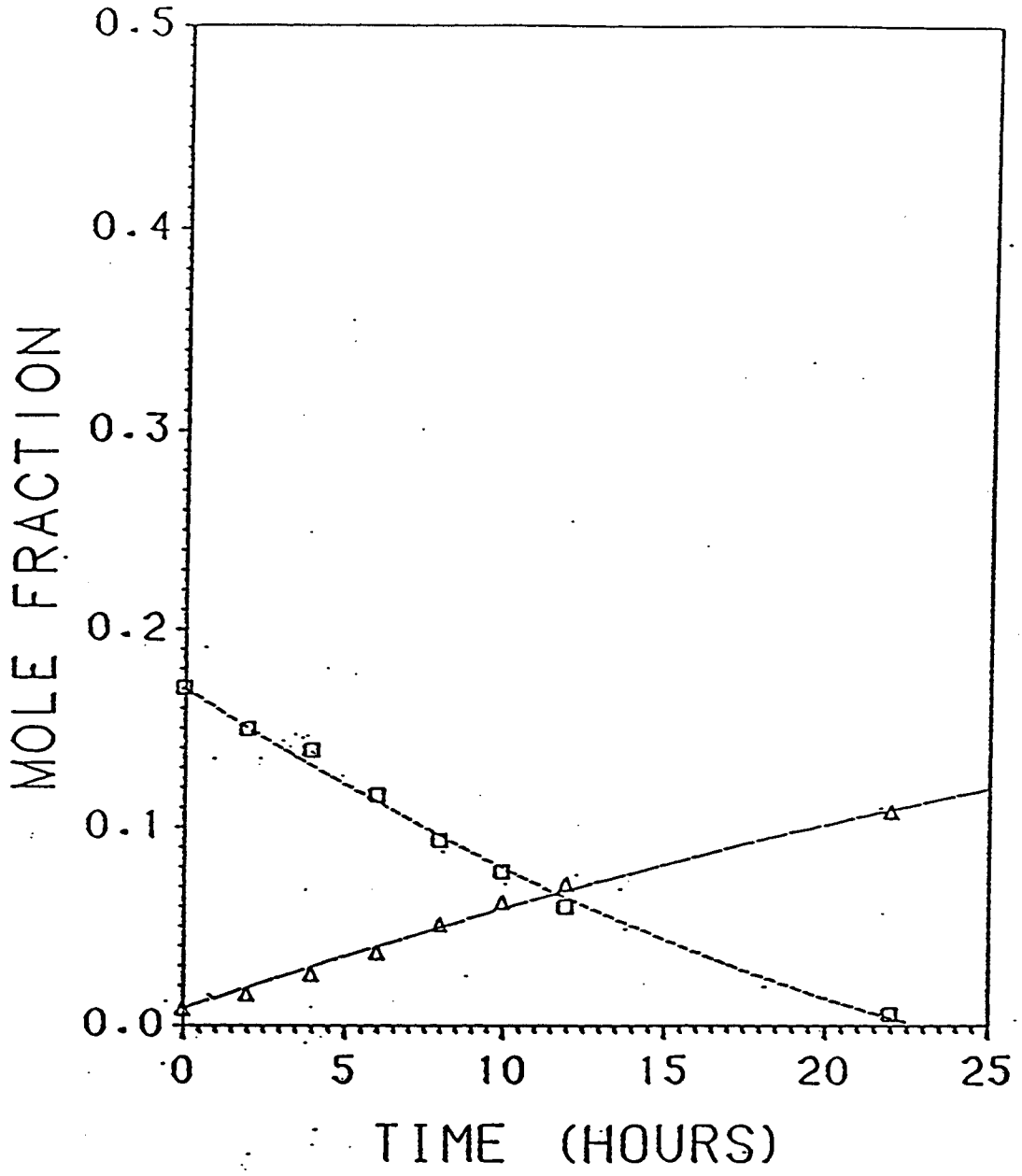

Figure 2. Carbon dioxide (Δ) and Oxygen (□) variation with time in the gas phase for mixed population of microorganisms growing on oil sample IRMCO 141 at an initial oil concentration of 5.0%. Dotted lines are the non-linear regression best fit.

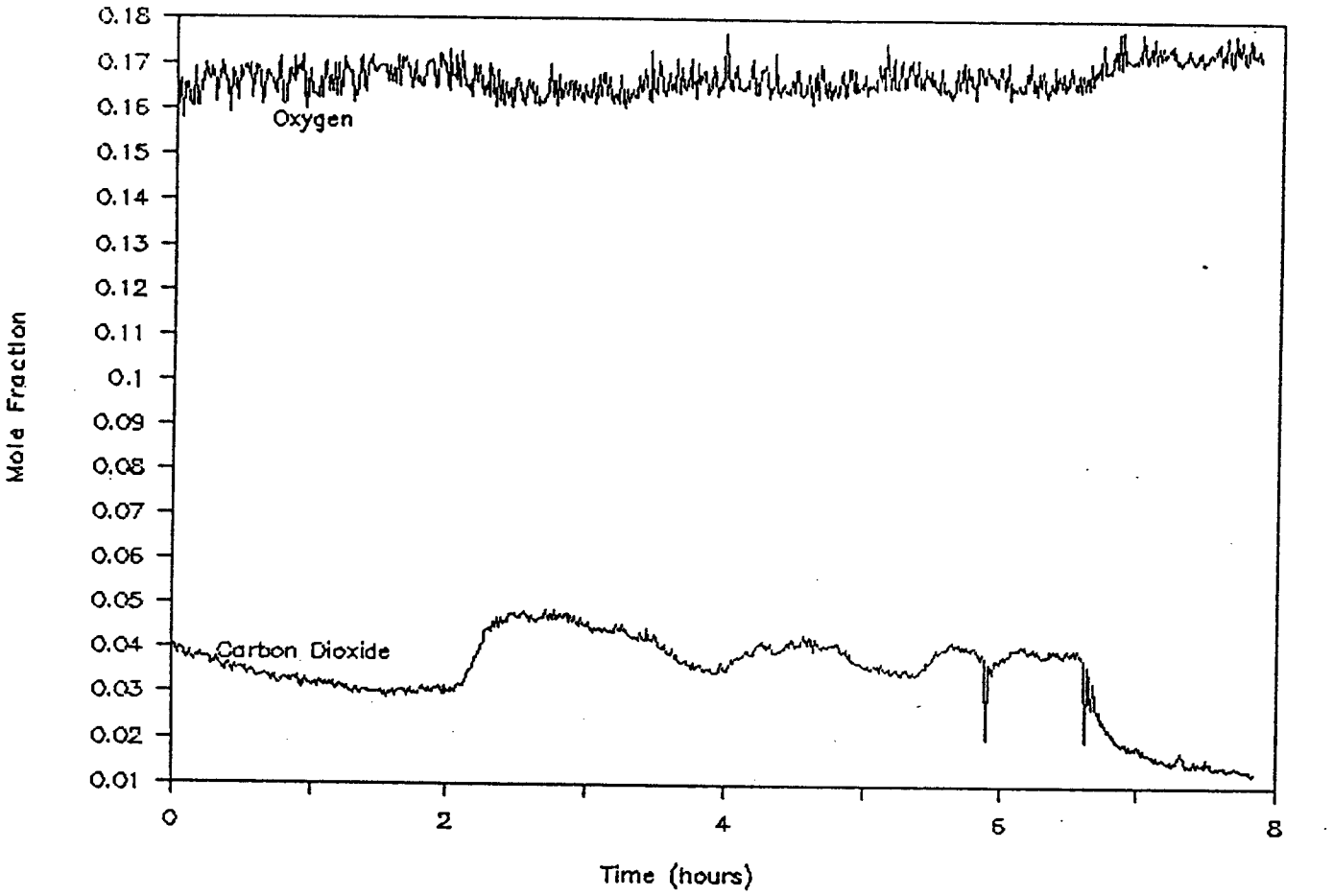

Figure 3. Yeast Fermentation off-gas analysis by quadrupole mass spectrometry with dextrose as substrate.

ENZYMATIC HYDROLYSIS OF CORN GLUTEN PROTEINS

J. E. Hardwick and C. E. Glatz
Department of Chemical Engineering
Iowa State University, Ames, IA 50011

Abstract

Corn gluten meal was hydrolyzed using Alcalase 2.4L, an alkaline protease. The effects of enzyme concentration and gluten size reduction on the hydrolysis were studied. Extent of reaction was expressed both in terms of the degree of hydrolysis (using the pH stat technique) and the concentration of soluble protein. Kinetic models were compared to the experimental results by minimizing the residual sum of squares between the model and the results. The models describe the time dependent behavior of three protein/peptide pools—insoluble protein, TCA-insoluble proteins and TCA-soluble peptides.

INTRODUCTION

Corn gluten meal is a by-product of the corn wet milling process, and contains approximately 60% protein. The major protein fractions in corn gluten meal are zein (68%), glutelin (28%) and globulins (1.2%) [1,2]. Currently, its main use is as an animal feed. The major drawback of using corn gluten meal in foods is that it is very insoluble in water [3,4]. There is, therefore, motivation to try and increase its solubility.

Enzymatic hydrolysis has been used to favorably modify the functional properties of proteins, such that the hydrolysates could be incorporated into foods for their flavor, functional and nutritional value [5]. Corn gluten meal has been hydrolyzed using alkaline microbial proteases [6]. The effect of temperature, pH and the enzyme concentration were studied.

Kinetic studies have been conducted on soluble enzyme/insoluble substrate systems using soy protein [5,6], fish protein [7], cellulose [8,9], gelatin [10], and starch [10]. Three different approaches have been used to model kinetic mechanisms. Michaelis-Menten kinetics, derived for the enzymatic hydrolysis of soluble substrates [5,8], have also been applied to insoluble substrate systems. Alternatively, a model based on adsorption of excess enzyme onto substrate surface sites, followed by subsequent hydrolysis, was used to model hydrolysis of fish protein [7], cellulose [9,10], and gelatin [10]. The hydrolysis of fish protein concentrate has also been modelled as two simultaneous linear reactions [7].

The main objectives of this study were to investigate the effects of Alcalase 2.4L dosage and size reduction of the gluten meal on the extent of hydrolysis and the concentration of soluble protein produced, and then to model the time course of the hydrolysis. A useful feature of a kinetic model is the ability to describe the appearance of the smaller peptides that can result in bitter flavors.

MATERIALS AND METHODS

Materials

Alcalase 2.4L (Novo Laboratories, Inc., Wilton, CT) is a food grade preparation of subtilisin Carlsberg in the liquid form. The activity was 2.4 AU/g. The enzyme was diluted by one to ten to reduce its viscosity for ease of addition to the reactor. The corn gluten meal was supplied by Grain Processing, Muscatine, IA. It was used as an 8% by weight protein slurry made up with deionized water (after [6]).

Analyses

Nitrogen content of the corn gluten meal was determined by micro-Kjeldahl [11] and protein content as 6.25 $\times$ N (the conversion factor for corn gluten proteins [12]). Soluble protein was determined by the biuret method [13]. Standard solutions of bovine serum albumin (Sigma Chemical Co., St. Louis, MO) were used to generate a standard curve.

Trichloroacetic acid (TCA) was used to precipitate proteins and higher molecular weight peptides from the hydrolysates. Five mL of 2.4N TCA was added to 10 mL of hydrolysate [12] and the precipitate removed by centrifugation (2.7×10^3 g for 30 min).

The particle size distribution was determined for the non-reduced and size reduced corn gluten samples by sieve analysis. A 30 g sample was placed on the coarsest (top) in a series of six 8 in. sieves and shaken in a sieve shaker for 30 min [14]. The fractions were collected and weighed. Sieve sizes of the non-reduced samples were between 1400 μm (12 mesh) and 45 μm (350 mesh), whereas for a size reduced sample, the size range was between 1180 μm (14 mesh) and 38 μm (400 mesh). Surface areas were measured by B.E.T. analysis using krypton gas as the adsorbate [15]. External surface areas were calculated by assuming that the corn gluten meal consisted of spheres of the average diameter of the sieving fraction.

Experimental Procedure

Procedure I Hydrolysis was performed on non-reduced and size reduced corn gluten. The dry corn gluten meal was pulverized using a rotating hammer mill (Micro switch, Freeport, IL). Enzyme concentrations used were between 0.375 AU/L and 0.75 AU/L.

The corn gluten slurry, containing 8% protein by weight, was agitated at 450 rpm for one hour at pH 9 and 50°C to allow for extraction of the soluble fractions. After an initial sample (15 mL) was withdrawn, the enzymatic hydrolysis began with addition of enzyme. The pH stat meter was zeroed at this point. The hydrolysis time was four hours, with samples taken at two and four hours. Concentrated hydrochloric acid was added to the samples to deactivate the enzyme. The samples were then centrifuged and the supernatants assayed for soluble protein.

Procedure II To study the time course of the hydrolysis, the procedure was essentially the same except samples were taken more frequently. 10 mL samples were taken every 10 min for samples taken during the first hour, every 15 min during the second hour, and every 30 min during the remaining two hours of the four hour hydrolysis. The enzyme was deactivated by placing the sample

in a water bath at 90°C for 15 min. The samples were centrifuged and supernatants were assayed for soluble protein before and after TCA precipitation.

Kinetic Model Development

The kinetic models considered were all based on three compartments (see Figure 1). I represents insoluble protein, while compartments S and P both represent soluble material. S is the group of high molecular weight proteins/peptides precipitated by trichloroacetic acid (TCA), and P is the low molecular weight (TCA soluble) peptide pool.

The rate expressions r_I and r_S may be written as

$$r_I = \frac{-dI}{dt} = \frac{d(S+P)}{dt} \tag{1}$$

$$r_S = \frac{-dS}{dt} = \frac{dP}{dt}. \tag{2}$$

Various kinetic expressions for both r_I and r_S were tested in different combinations as shown in Table 1.

A linear rate expression is the simplest and is a limiting case of the Michaelis-Menten expression, classically used for soluble substrates. Product inhibition was reported for enzymatic hydrolysis of soybean protein and lean meat proteins [5,16]. The Freundlich adsorption isotherm allows for enzyme adsorption to limited substrate surface sites.

RESULTS AND DISCUSSION

Effect of enzyme dosage

The rate of hydrolysis and the soluble protein concentration increased with increasing enzyme concentration (Figures 2 and 3). All enzyme concentrations demonstrated an acceleration in the rate of hydrolysis (Figure 4), followed by a decline during the later period of the hydrolysis. At the lowest enzyme concentration (0.375 AU/L), the rate of hydrolysis proceeded slowest, consequently the acceleration in the rate of the hydrolysis occurred at later times. Initially the most accessible bonds are cleaved. As a result of these cleavages further accessible bonds would be exposed, causing an acceleration in the rate of hydrolysis. The lower the enzyme concentration, the longer it takes to reach the same extent of cleavage at higher enzyme concentrations. Figure 5 shows that the increase in the rate for different enzyme concentrations occurs when a certain number of peptide bonds have been cleaved—when h reaches 0.05 mequiv/g.

Figure 4, showing rate of hydrolysis versus time, was compared to typical plots for simultaneous reaction systems. The rate of hydrolysis (dh/dt) was obtained from the pH stat values of base consumption with time. These values were first smoothed, and then the rate was calculated using Lagrange's forward, central and backward difference formulas for equally spaced points [17]. The logarithm of the rate versus time plots for typical simultaneous reaction systems [18,19,20,21] are initially curved (fast and slow reactions), followed by a linear region (slow reaction only), and therefore the corn gluten meal hydrolysis is not explained by simultaneous fast and slow bond cleavages. The system is more complicated in that each type of bond could exist in both the insoluble and the soluble pools, and the relative amounts in the pools vary throughout.

Effect of size reduction

The size of unground corn gluten was found to be mostly (74.56%) between 355 μm (44 mesh) and 180 μm (85 mesh). Pulverizing the corn gluten reduced the sample to a size between 75 μm (200 mesh) and 38 μm (400 mesh). Based on a standard deviation of $\pm 0.6\%$ in the degree of hydrolysis, the differences in the degrees of hydrolysis between non-reduced corn and size reduced corn (Figure 6) were not significant at the 90% level (t test). Likewise, the differences in the soluble protein between non-reduced and size reduced (Figure 7) were not significant. Since surface area was increased by size reduction (Table 2), it is evident that available surface area did not limit the rate of reaction. Table 2 also shows that the gluten meal had very little internal surface area. The internal surface area accessible to the enzyme will likely be even less than that measured using krypton gas as the adsorbent.

Time Course of the Hydrolysis

Initially only insoluble protein was present so that most of the hydrolysis was in the insoluble phase and produced soluble proteins and high molecular weight peptides (S). At this point, the rate of hydrolysis of I (r_I) is greater than that of S (r_S), which results in an overall increase in S. The concentrations of pools S and P for the course of the hydrolysis are shown in Figure 8 for low (0.375 AU/L) and high (0.625 AU/L) enzyme concentrations. The 10 to 20% greater reduction in I (or an increase in $(S + P)$) at the higher enzyme concentration shows up predominantly in pool P. This implies that the additional enzyme preferentially hydrolyses soluble protein.

The low rate of conversion by four hours (Figure 8) suggests that there is a hydrolysis resistant core [21]. An estimation of the content of this unreactive material was made by performing an extended hydrolysis of 48 hours. At this point 46.8% (43.26 mg/mL) remained insoluble and this was used as the value for IE in all the kinetic models studied.

Comparison of kinetic models

The expressions used to describe the kinetic models are shown in Table 1. The constants in each compartmental model were evaluated by finding the values giving the least squares fit to the experimental data of $(S + P)$ and P versus time (Levenburg-Marquardt subroutine ZXSSQ [22]).

The values of the linear model (solid lines) compared to the experimental values (symbols) are shown in Figures 9 and 10 at low (0.375 AU/L) and high (0.625 AU/L) enzyme concentrations. The linear model was able to predict the main trends of the experimental data, but it tended to overpredict the values of P towards the end of the hydrolysis. This effect was more pronounced for the higher enzyme concentrations. The linear model allows for reduction in substrate concentrations but not for bonds of different susceptibility or product inhibition, two other possible causes of decreasing rates.

The experimental values in pool S increased initially, then gradually decreased. The linear model fitted this poorly during the first fifty minutes of the hydrolysis. It did, however, predict the later times well. Values for the constants k_I and k_S were estimated for each set of experimental data. The average values of k_I and k_S over all runs were found to be $1.29 \times 10^{-2} \pm 0.18 \times 10^{-2}$ mL/mg min and $4.60 \times 10^{-2} \pm 0.79 \times 10^{-2}$ mL/mg min, respectively. The constants k_I and k_S were shown to be statistically "constant" for a small population (t distribution).

The calculated values for the simplified product inhibition model (dashed lines) are also shown in Figures 9 and 10. The calculated P values fit the experimental values much closer than the linear model during the later stages of the hydrolysis. The main weakness of this model was an underestimation of S during the first 50 min of the hydrolysis. The improved fit is reflected in the lower sums of squares at all enzyme concentrations (Table 3). The reduction in the residual sum of squares was more pronounced at higher enzyme levels where product levels, and consequently product inhibition, would be greater. The average values for k_I, k_S and K_{mP} were found to be $5.27 \times 10^{-2} \pm 4.38 \times 10^{-2}$ mL/mg min, $1.65 \times 10^{-1} \pm 1.43 \times 10^{-1}$ mL/mg min and 3.79 ± 2.36 mg/mL, respectively. Variations in these parameters between individual runs were also shown to be within the bounds of statistical error.

With the product inhibition model a second region of convergence appears in the least squares procedure. The values reported were chosen on the bases of lower sums of squares and consistency with the values of k_I and k_S from the linear model.

The two other models shown in Table 1 didn't result in any improvement over the linear and simplified inhibition models. The Michaelis-Menten/Michaelis-Menten model resulted in the same values for the constants k_I and k_S as were found for the linear model, while the constants K_{mI} and K_{mS} were found to be so large (approximately 10^{17}) that their influence in the denominator was negligible. The Freundlich adsorption/linear model also failed to represent the mechanism any better than the linear model, another indication that the hydrolysis did not seem to be limited by available surface sites.

CONCLUSIONS

The rates of hydrolysis and formation of soluble protein increase with enzyme concentration. The increase in soluble protein was accounted for by an increase in low molecular weight peptides (P). The rate of hydrolysis increases during the early stages of the hydrolysis, due to increased bond accessibility for cleavage. The eventual decline is attributed to disappearance of substrate and either product inhibition or a reduction in the susceptible bonds. Corn gluten meal does not exhibit a high internal surface area. Nevertheless, an increase in the rate of hydrolysis was not observed, even when the total surface was increased by four times. The hydrolysis was apparently not limited by the availability of surface sites at which the enzyme can bind.

Of the kinetic models studied, the linear and the simplified product inhibition models generate the best representation of the experimental data. The addition of the product inhibition term to the linear model results in improvement in the residual sum of squares of between 33 and 85%. The largest improvement is observed at the highest enzyme concentrations.

Acknowledgement

Support of this research by a grant from the Iowa Corn Promotion Board is gratefully acknowledged.

NOMENCLATURE

CGM	Corn gluten meal
e_0	Initial enzyme concentration (mg/mL)
h	Hydrolysis equivalents (mequivalents of peptide bonds per/g)
I	Insoluble substrate concentration (mg/mL)
IE	Insoluble substrate concentration, resistant to hydrolysis (mg/mL)
k_I	Reaction rate constant for insoluble pool I (mL/mg min)
k_S	Reaction rate constant for soluble pool S (mL/mg min)
K_{mi}	Michaelis-Menten constant for pool i (mg/mL)
P	Concentration of soluble low molecular weight peptides, not precipitated by TCA (mg/mL)
r_I	Rate of hydrolysis of substrate I (mg/mL min)
r_S	Rate of hydrolysis of substrate S (mg/mL min)
S	Soluble protein/high molecular weight peptides, precipitated by TCA (mg/mL)
t	Time (min)

References

[1] P. E. Neumann and J. S. Wall, *Cereal Chem.*, **61**(4), 353 (1984).

[2] J. S. Buck, C. E. Walker and K. S. Watson, *Cereal Chem.*, **64**(4), 264 (1987).

[3] C. W. Ofelt and C. D. Evans, *Ind. Eng. Chem.*, **41**(4), 830 (1949).

[4] M. H. Russell and G. T. Tsao, *AIChE Symp. Series*, **78**(218), 83 (1982).

[5] A. Constantinides and B. Adu-Amankwa, *Biotechnol. Bioeng.*, **22**, 1543 (1980).

[6] J. Adler-Nissen, *Process Biochem.*, **12**(6), 18 (1977).

[7] M. C. Archer, J. O. Ragnarsson, S. R. Tannenbaum and D. I. C. Wang, *Biotechnol. Bioeng.*, **15**, 181 (1973).

[8] J. A. Howell and D. Stuck, *Biotechnol. Bioeng.* **17**, 873 (1975).

[9] M. Mandels, J. Kostick and R. Parizek, *J. Polym. Sci.* **26**, 445 (1971).

[10] A. D. Mclaren, *Enzymologia.* **26**, 237 (1963).

[11] Association of Official Agricultural Chemists (AOAC), Official Methods of Analysis, 11th edition, AOAC, Washington, (1970).

[12] J. Adler-Nissen, *Enzymatic Hydrolysis of Food Proteins*, (Elsevier, New York, 1985).

[13] B. T. Doumas, *Clin. Chem.* **21**(8), 1159 (1975).

[14] B. A. Willis, *An Introduction to Practical Aspects of Ore Treatment*, 2nd ed. (Pergamon, New York, 1981).

[15] A. L. McClellan and H. F. Hamsberger, *J. Colloid and Interface Sci.* **23**, 577 (1967).

[16] G. M. O'Meara and P. A. Munro, *Biotechnol. Bioeng.* **27**, 861 (1985).

[17] R. H. Perry and C. H. Chilton, *Chemical Engineers Handbook*, 5th ed. (McGraw Hill, New York, 1973).

[18] G. Ronca, U. Montali, A. Lucacchini, S. Ronca-Testoni and C. A. Rossi, *Int. J. Pept. Prot. Res.* **7**, 111 (1975).

[19] U. Montali, A. Lucacchini, G. Ronca and C. A. Rossi, *Int. J. Pept. Prot. Res.* 17, 427 (1981).

[20] E. Mihalyi and J. E. Godfrey, *Biochim. Biophys. Acta* **67**, 73 (1962).

[21] E. Mihalyi and W. H. Harrington *Biochim. Biophys. Acta.* **26**, 447 (1959).

[22] International Mathematical and Statistical Libraries Inc. (I.M.S.L.), Version 2.0, Houston, Texas, (1987).

Table 1: Kinetic expressions used to model the rates r_I and r_S.

Model	Insoluble substrate r_I	Soluble substrate r_S
Linear/Linear	$k_I\, e_0\, (I - IE)$	$k_S\, e_0\, S$
Michaelis-Menten/ Michaelis-Menten	$\frac{k_I\, e_0\, (I - IE)}{1 + (I/K_{mI}) + (S/K_{mS})}$	$\frac{k_S\, e_0\, S}{1 + (I/K_{mI}) + (S/K_{mS})}$
Freundlich adsorption/Linear	$k_I\, (e_0\, (I - IE))^{2/3}$	$k_S\, e_0\, S$
Simplified product inhibition/ Product inhibition	$\frac{k_I\, e_0\, (I - IE)}{1 + (P/K_{mP})}$	$\frac{k_S\, e_0\, S}{1 + (P/K_{mP})}$

Table 2: Actual surface area of ground and unground corn gluten meal (CGM) compared to the external surface area based on perfect spheres

Size	External surface area m^2/g	Actual (B.E.T.) surface area m^2/g
Unground CGM (355–180 μm)	0.063	0.1069
Ground CGM (75–35 μm)	0.31	0.432

Table 3: A comparison of the residual sum of squares at different enzyme concentrations (AU/L) for linear and product inhibition models

Enzyme concentration (AU/L)	Residual sum of squares	
	Linear model	Product inhibition model
0.375	90.92	52.44
0.375	17.25	CP[a]
0.500	87.72	57.99
0.500	110.15	60.81
0.625	243.60	35.97
0.625	138.87	32.10
0.750	157.70	59.01
0.750	220.14	73.05

[a]Did not converge

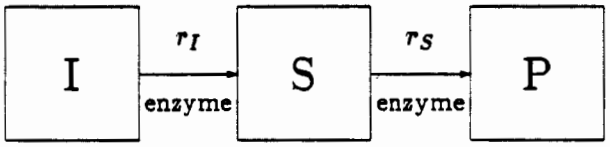

Figure 1: Illustration of the different compartments used in the kinetic modelling of the hydrolysis

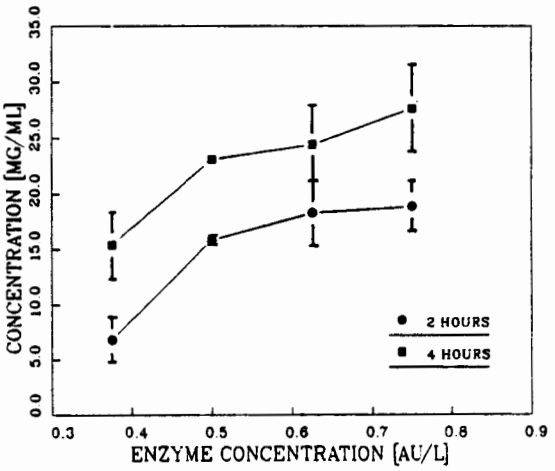

Figure 3: Variation with enzyme concentration (AU/L) of soluble protein (mg protein/mL) after 2 and 4 hours of hydrolysis. Error bars represent high and low values of two observations.

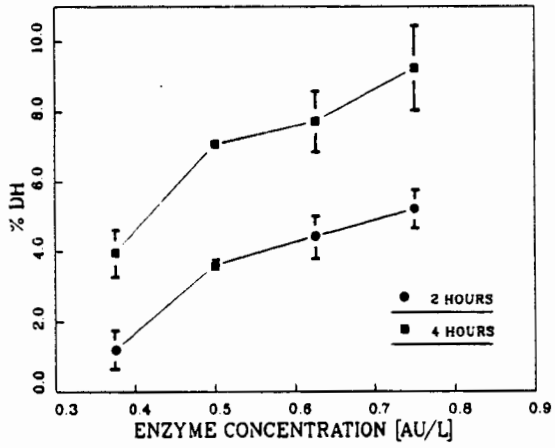

Figure 2: Variation with enzyme concentration (AU/L) of % degree of hydrolysis after 2 and 4 hours of hydrolysis. Error bars represent low and high values of two observations.

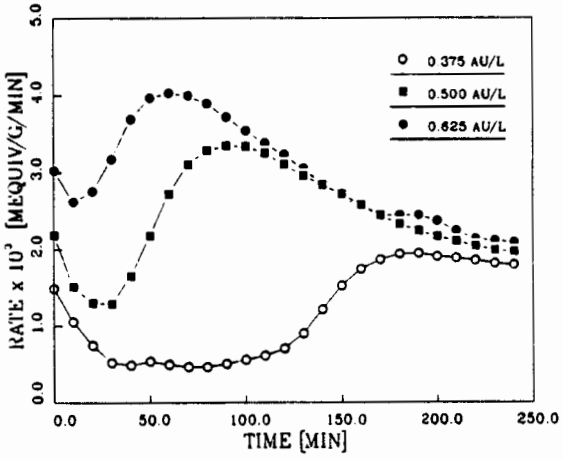

Figure 4: Variation in the rate of hydrolysis (mequiv/g/min) with time (min) at three levels of enzyme concentration (AU/L). Smoothed values of h were used to calculate the rate dh/dt.

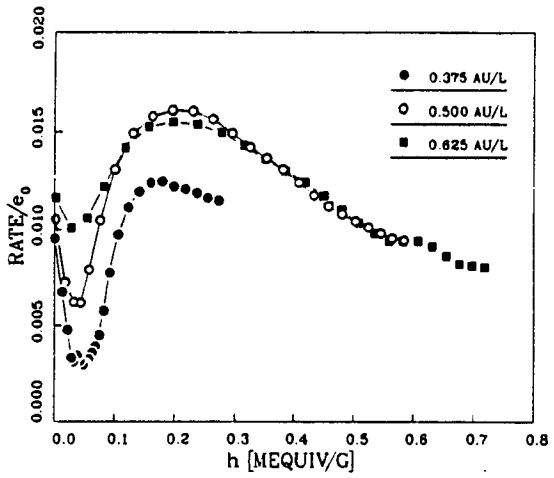

Figure 5: Variation in the rate of hydrolysis (mequiv/g/min) with the number of peptide bonds cleaved (mequiv/g) at three levels of enzyme concentration (AU/L). Smoothed values of h were used to calculate the rate dh/dt.

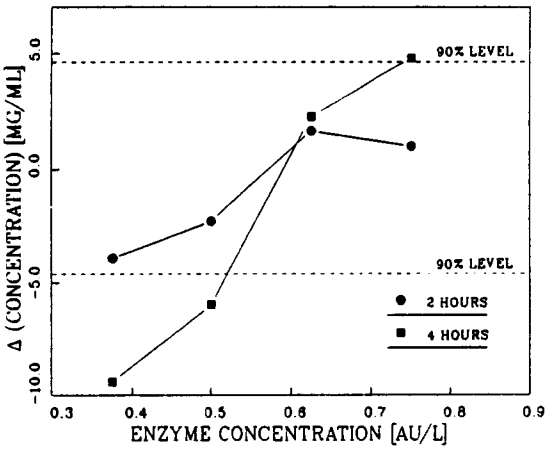

Figure 7: Difference between the amount of soluble protein for non-reduced (NR) and size reduced (SR) corn gluten meal (NR – SR) versus enzyme concentration (AU/L). 90% confidence interval is shown.

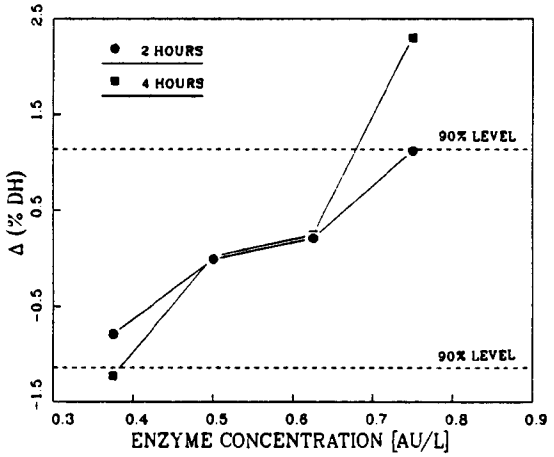

Figure 6: Difference between the degree of hydrolysis for non-reduced (NR) and size reduced (SR) corn gluten meal (NR – SR) versus enzyme concentration (AU/L). 90% confidence interval is shown.

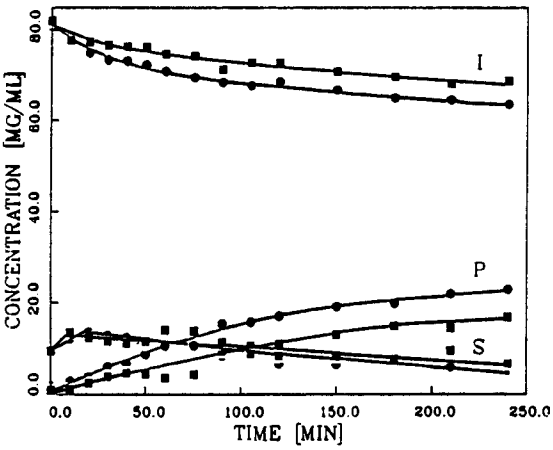

Figure 8: Experimental values of protein concentration (mg protein/mL) with time (min). ■ denotes low enzyme concentration (0.375 AU/L) and • denotes high enzyme concentration (0.625 AU/L)

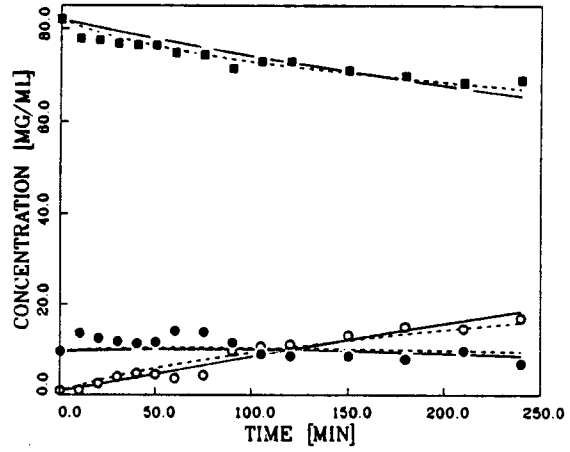

Figure 9: Comparison of the linear (—) and the simplified product inhibition model (- - -) with experimental data. Experimental data are denoted by: ■ insoluble, I; ○ soluble proteins/peptides; S, and • soluble peptides, P. Enzyme concentration 0.375 AU/L.

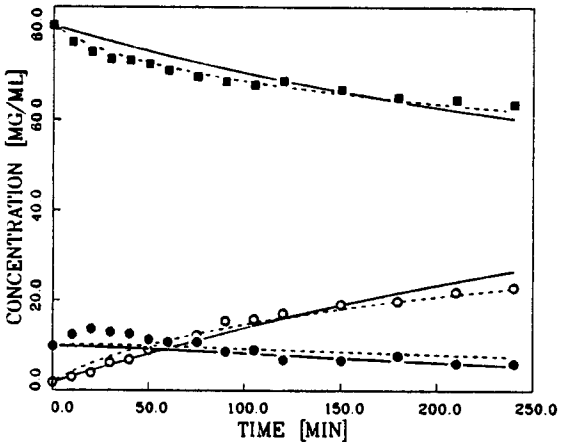

Figure 10: Comparison of the linear (—) and the simplified product inhibition model (- - -) with experimental data. Experimental data are denoted by: ■ insoluble, I; ○ soluble proteins/peptides, S; and • soluble peptides, P. Enzyme concentration 0.625 AU/L.

IMPROVED ACETONE-BUTANOL FERMENTATION ANALYSIS

Z. Buday

Department of Agricultural and Chemical Engineering
Colorado State University
Fort Collins, Colorado 80523

INTRODUCTION

In the acetone-butanol (ABE) fermentation acetone, butanol, ethanol, acetoin, acetic acid and butyric acid are produced from sugars by the bacteria Clostridium acetobutylicum. One main objective of process control of this fermentation is to maximize the butanol production. Advanced fermentation process control requires an automatic analytical system which measures the composition of the fermentation broth.

In this section the currently used methods for measuring the substrate and the products are reviewed. Quantitation of the volatile products has been conducted using gas chromatography (GC). Various methods of analysis that have appeared in the literature are tabulated in Table 1. Detailed information about the performance of those methods (resolution, LOD, stability, analysis time, etc.) have not been presented in the literature. According to the studies of Ackman (1) and the previous GC analysis experience in our laboratory, absorptive tailing of the acetic acid occurs in several of the methods, which results in a poor quantitation. Mes-Hartree et al.(2) overcame the problem by the addition of formic acid vapor to the carrier gas, which method was first described by Ackman (1). The analysis time of the GC method used in our lab was approximately 12 minutes.

The measurement of the sugar was usually done by reducing sugar analysis, e.g. using dinitrosalicylic acid reagent (DNSA), or by an enzymatic method such as glucose oxidase, or dehydrogenase coupled with hexokinase. The sugar analysis methods used in the referred studies are also tabulated in Table 1.

Schwald and Saddler (3) used high performance liquid chromatography to analyze Klebsiella pneumoniae, Candida shehatae and Clostridium acetobutylicum fermentation broths, but the resolution of ethanol, acetone and butyric acid was very poor, resulting in poor quantitation. The resolutions for butyric acid-acetone and for acetone-ethanol, defined by equation 1, were approximately 0.46 and 0.62 respectively.

$$R = \frac{2(t_1 - t_2)}{w_1 + w_2} \qquad (1)$$

When compounds are present with concentrations of different orders of magnitude a system with such resolution and without sophisticated mathematical tools cannot quantitate the compounds of lower concentration at all.

EXPERIMENTAL

The analyses were conducted using a Waters Associates 201 liquid chromatograph with R 400 differential refractometer and a Gilson 231-401 autosampling injector with 20 ul sample loop. Column temperature was adjusted by submersion in a Lauda waterbath. The solvent phase was 0.01N sulfuric acid which was filtered (0.45um) and degassed. The flowrate was adjusted to 0.7 ml/min through a Biorad Aminex HPX-87H column (300 x 7.8 mm). The samples were centrifuged and filtered (0.45um).

A Hewlett-Packard 9836 computer with a Hewlett-Packard 3497A Data Acquisition and Control Unit was used to integrate the chromatogram and to calculate the concentrations. The software, which was written by the authors in PASCAL acquired the refractometer signal for specified time intervals after the injections. The baseline was determined, baseline correction was performed and the peaks were integrated by the trapese rule (4). With the given slopes of the calibration curves the concentrations of the respective compounds in broth samples were calculated.

Chromatographic standards were obtained as follows: Ethanol: Eagle Mfg. Co., Wellsburg, W.Va.; acetone, acetic acid, butyric acid, D-xylose, D-galactose and L-arabinose from Fisher Scientific Co., Fairlawn, N.J.; butanol and acetoin: J. T. Baker Chemical Co., Phillipsburg, N.J.; D-dextrose: Mallinckrodt, Paris, Ky.; D-mannose and D-cellobiose: Sigma Chemical Co., St. Louis, Mo.

RESULTS AND DISCUSSION

Optimal operating temperature

Operation of an HPLC column at less than ambient temperature is not usual, because of the elevated pressure drop and peak broadening. In our case the best resolution of the compounds of interest was achieved at 14°C. Studies at lower temperatures were not conducted because the pressure drop (1300 psi) was close to the allowed maximum (1500 psi) according to manufacturer recommendations. Chromatograms of the standard solutions were determined at various temperatures between 14°C and 60°C. The chromatograms can be seen in Figure 1; the retention times and the pressure drops across the column are tabulated in Table 2. At all temperatures except 14°C, unsatisfactory resolution of the overlapping peaks was obtained. This problem did not exist at 14°C where even the worst resolution (ethanol-acetoin), defined by equation 1, was between 1 and 1.2. The retention time of the ethanol decreased and that of the acetoin increased with decreasing temperature.

The change of the retention times with temperature is caused by the temperature dependence of the distribution coefficients governing

the equilibrum between the stationary and the mobile phases. The distribution coefficients change with temperature according to equation 2.

$$\frac{d \ln K}{dt} = \frac{Hm}{RT^2} \qquad (2)$$

The column operation is based on several mechanisms; for each compound, several distribution coefficients determine the retention time. An "average distribution coefficient" and an "average heat of absorption" can be defined for each. The inversion of the elution pattern of the ethanol and the acetoin is caused by the different signs of their "average heat of absorption". Hm was positive for the ethanol and negative for the acetoin.

Linearity

Using 14°C as operating temperature seven-point calibration curves were obtained. The concentration ranges and correlation coefficients are listed in Table 3. Correlation coefficients were estimated according to (5). Linearity was excellent for the possible concentration ranges of the measured compounds in the ABE fermentation broth.

Reproducibility

To evaluate the reproducibility of the system response, a standard solution was injected 5 times. The standard deviations of the normalized peak areas were estimated according to (5) and are tabulated in Table 3. The standard deviations were less than 2%, which is considered as good reproducibility.

Stability of the system parameters

Over a 2 week period of operation, recalibration of the system was not necessary and the retention times stayed constant.

Limit of detection

The limit of detection (LOD) is defined by the concentration, when the signal to noise ratio was equal to 2.0. The LOD's for the compounds of interest are tabulated in Table 3.

Measurement of fermentation samples

The system was evaluated by analyzing samples of a continuous fermentation of C. acetobutylicum. The fermentation was conducted in a 5 1 Chemap CFT fermentor at 37°C and pH 5 with 150 rpm stirring rate, using 3 1 constant volume of complex medium (6). Continuous flow began at 8 hr with a dilution rate of 0.2 hr^{-1}. The oscillatory behavior of the products may be typical of the transient phase of the continuous fermentation. The concentration profiles of the substrate and the products can be seen in Figure 2.

Retention times of various sugars

A very important fermentation of C. acetobutylicum growth on hemicellulose hydrolysate (2). The measurement of the various sugars, in addition to the measurement of the products, would be an improvement over the existing system. In its present state the system exhibits some resolution of the important sugars, but the resolution is not satisfactory for good quantitation. The resolution may be improved, (e.g. by addition of a satellite column and/or modification of the solvent system) and good quantitative analysis may possibly be achieved. The retention times (in minutes) of various sugars under conditions which gave the best resolution of the products are as follows: Cellobiose (7.73), dextrose (8.73), mannose (9.70), xylose (9.73), galactose (9.76) and arabinose (10.93).

CONCLUSIONS

An HPLC based analytical system was developed to measure the components of ABE fermentation broth (dextrose, acetic acid, ethanol, acetoin, acetone, butyric acid, butanol) which gives complete chemical information in 31 minutes. Resolution, reproducibility, linearity, stability were excellent. These features make the system a reliable and convenient tool for those studying fermentations producing any of the above products. With some minor development (i.e. automatic sample filtration) the computer coupled system would be appropriate as the sensor for an automatic control system. Such a system is appealing considering the importance of a fully automated scheme for the monitoring of a fermentor and the serious deficiency of the appropriate sensors (10). Possibly the system can be further improved to give adequate quantitation of mixed sugar substrates.

In this study the chromatographic column was operated at lower than ambient temperature. In the study of Schwald and Saddler the temperature has been varied between 50 and 85°C in order to optimize the resolution (3). This is an example showing that adjustment of the column temperature to less than ambient is usually not considered as an option, because of the extended peak broadening and pressure drop. The finding that the resolution can be dramatically improved by cooling the column, may be useful information to those working with HPLC based analytical systems to monitor fermentations.

REFERENCES

1. Ackman, R. G. J. Chrom. Sci. 1972. 10: 560-565.
2. Mes-Hartree, M. and Saddler J. N. Biotechnol. Letters. 1982. 4: 247-252.
3. Schwald, W. and Saddler J. N. Enzyme Microb. Technol. 1988. 10: 37-41.
4. Carnahan, B. L., Luther, H. A. and Wilkes, J. O. Applied Numerical Methods p 71. John Wiley & Sons, Inc., 1969, New York.
5. Bailey, N.T.J. Statistical Methods in Biology. pp 16 & 82. John Wiley & Sons, Inc., New York; 1959.

6. Doremus, M. G., Linden J. C. and Moreira, A. R. Biotechnol. Bioeng. 1984. 27: 852-860.
7. Monot, F. and Engasser, J. M. Biotechnol. Letters. 1983. 4: 213-218.
8. Gottschal, J.C. and Morris, J. G. Biotechnol. Letters. 1981. 9:525-530.
9. Bahl H., Andresch, W. and Gottschalk, G. European J. Appl. Microbiol. Biotechnol. 1982. 15: 201-205.
10. Wang, N. S. and Stephanopoulos, CRC Crit. Rev. Biotechnol., 1984, 1, 1-103.

Notation:

R - resolution
t - retention time
w - peak width
K - distribution coefficient
Hm - heat of absorption
T - temperature
P - pressure drop across the column

Table 1. Gas chromatographic and sugar measurement methods currently used for determination of ABE Fermentation products and substrates

Column packing	Carrier gas	Tailing	Sugar measurement	Ref.
Chromosorb W-AW with 10% AT-1000	He	yes	glucose oxidase	6
PORAPAK Q	N_2	yes	hexokinase	7
10% of diethylene glycol adipate on diatomite C	N_2	?	glucose oxidase	8
CHROMOSORB 101	N_2	yes	dehydrogenase	9
CHROMOSORB 101	He saturated with formic acid	no	DNSA	2

Table 2. Retention times in minutes of the components of ABE fermentation broth and pressure drops across the column as functions of temperature on an HPX-87H column with flowrate of 0.7 ml/minute.

Temp. °C	Glucose	Acetic acid	Ethanol	Acetoin	Acetone	Butyric acid	Buta-nol	ΔP (psi)
14	8.73	14.66	16.66	18.13	20.20	22.06	29.32	1300
20	8.80	14.53	17.13	17.93	20.13	21.86	30.27	1100
30	8.82	14.40	17.53	17.53	19.80	21.53	31.26	1000
40	8.86	14.20	18.06	17.26	19.53	21.00	31.61	800
50	8.93	14.00	18.33	16.93	19.13	20.33	31.51	600
60	9.00	13.86	18.66	16.53	18.66	19.73	31.13	500

Table 3. Standard curves for components of ABE fermentation broth and standard deviations of normalized peak areas at given concentration in parenthesis.

	Concentration ranges(g/l)	Correlation coefficients	Limit of detection (g/l)	Standard deviation @ (g/l)
dextrose	0-50	0.999	0.03	0.0063(10)
acetic acid	0-4	0.998	0.09	0.0196(1)
ethanol	0-4	0.999	0.08	0.0162(1)
acetoin	0-4	0.999	0.09	0.0186(1)
acetone	0-6	0.998	0.10	0.0172(1)
butyric acid	0-8	0.999	0.10	0.0143(2)
butanol	0-8	0.999	0.08	0.0195(2)

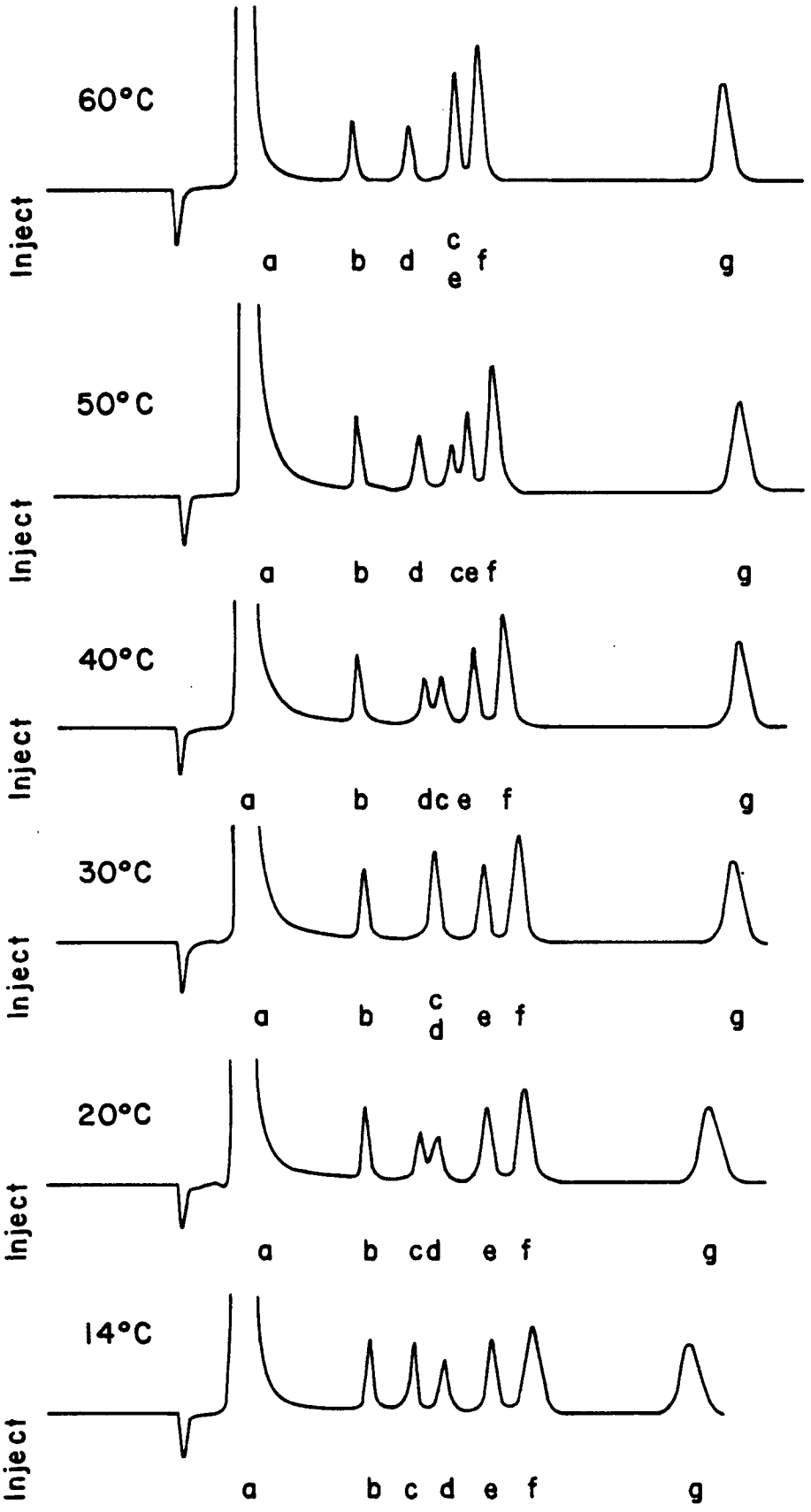

Figure 1. Chromatograms of a standard solution with flowrate 0.7 ml/min. taken at different temperatures. a. dextrose 20.0 g/l; b. acetic acid 2.0 g/l; c. ethanol 2.0g/l; d. acetoin 2.0g/l; e. acetone acid 1; f. butyric 4.0g/l; g. butanol 4.0g/l.

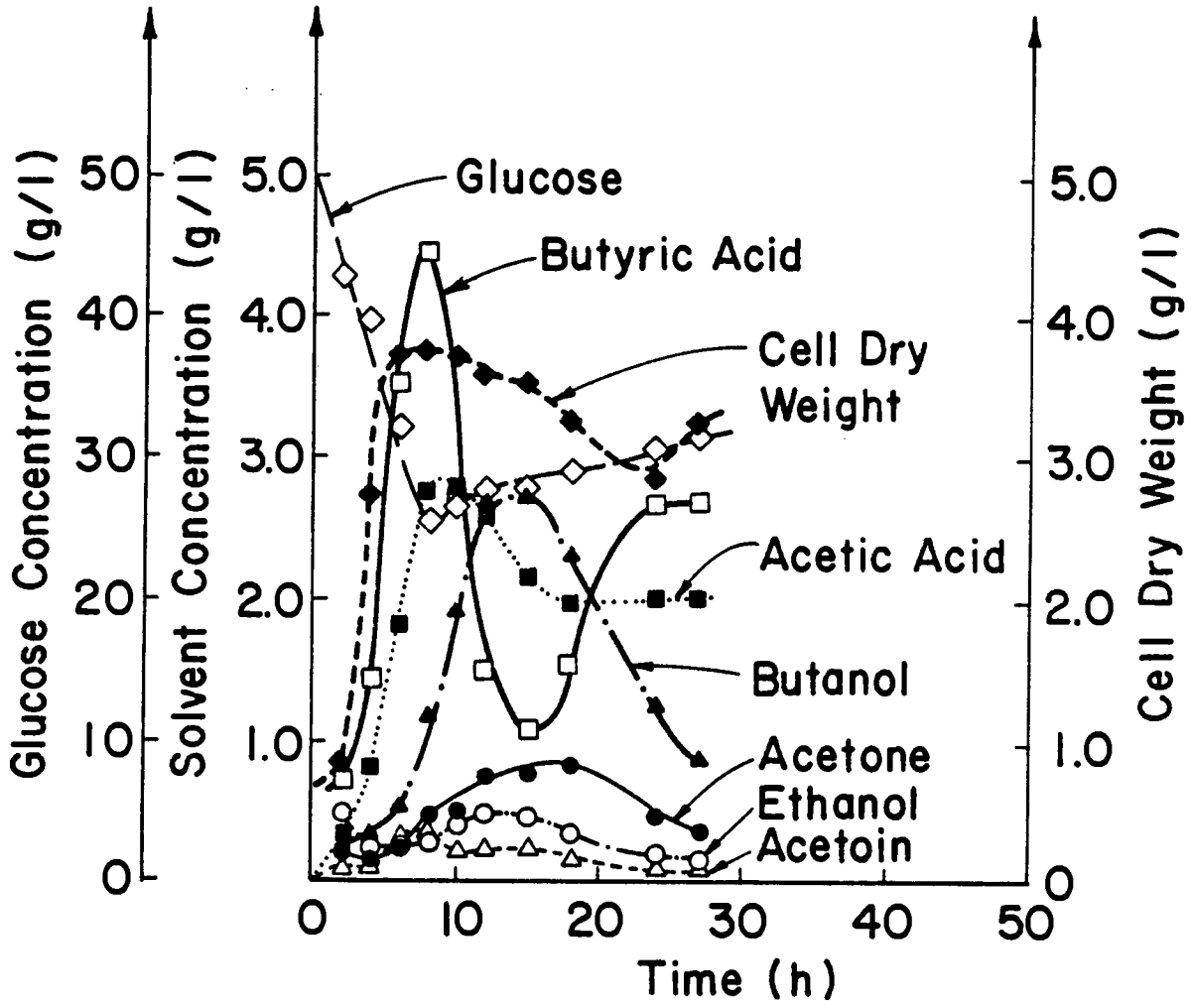

Figure 2. Concentration profiles of the substrate and products in a continuous ABE fermentation monitored using the described method.

ON–LINE STATE IDENTIFICATION FOR BATCH FERMENTATION

by D. A. Gee and W. F. Ramirez

Dept. of Chemical Engineering, University of Colorado, Boulder, CO 80309–0424

Introduction

Beer fermentations are typically run in a batch format where the wort and yeast are placed in a fermentor at the beginning and the batch is allowed to run its course from there. The only control on the process is generally the fermentor temperature. Fermentation is terminated when the mixture reaches a designated specific gravity, which experience has shown to be the desired final condition. During the course of the process, very little is known of what is actually happening inside the fermentor other than what can be discerned from monitoring the temperature and periodic specific gravity measurements. If specific gravity measurements should happen to show that the fermentation is going too slowly, one typical industrial compensation technique is to raise the temperature to increase the rate of fermentation. This compensation is done without any knowledge of the source of the problem. Varying the temperature in this way, while perhaps changing the rate of fermentation, has a tendency to alter the flavor and aroma profile of the final beer, often unfavorably. It would therefore seem preferable to have a better knowledge of what is actually happening inside the fermentor so that a problem could be traced to its cause and compensated for correctly.

The problem is how can we obtain more information about the fermentation when our measurements are incomplete (temperature, specific gravity, and perhaps CO_2 evolution rate). Significant improvements cannot be made unless we make use of our knowledge of the process itself through the use of a mathematical model. A process model, when coupled with measurements and an appropriate estimation technique such as a Kalman filter, becomes a very powerful and valuable tool for elucidation of the fermentation process. In this paper, the application of a Kalman filter for state estimation of beer fermentation is studied using the three simple measurements listed above. A similar application has recently been reported by Rajab et al. for a baker's yeast fermentation and their results were very promising.[1] Wang and Stephanapoulos have also applied an adaptive Kalman-Bucy filter to the fermentation of glucose by *S. cerevisiae* with excellent results.[2]

Theory—The Process Model

The model of beer fermentation used here is that of Engasser,[3] and Gee and Ramirez[4] described previously. This model is admittedly simplistic in its scope, but proves to be a valuable tool when coupled with the Kalman filter algorithm. Glucose, maltose, and maltotriose are the three fermentable sugars considered present in the wort (fructose can be modeled as glucose). The model equations describing the yeast growth and substrate uptake are given by:

$$\frac{dG}{dt} = -\mu_1 X \tag{1}$$

$$\frac{dM}{dt} = -\mu_2 X \tag{2}$$

$$\frac{dN}{dt} = -\mu_3 X \tag{3}$$

$$\frac{dX}{dt} = (\mu_1 Y_{XG} + \mu_2 Y_{XM} + \mu_3 Y_{XN})X - K_X \tag{4}$$

where the specific growth rates are given by

$$\mu_1 = \frac{\mu_{GM} G}{K_G + G} \tag{5}$$

$$\mu_2 = \frac{\mu_{MM} M}{K_M + M} \cdot \frac{K'_G}{K'_G + G} \tag{6}$$

$$\mu_3 = \frac{\mu_{NM} N}{K_N + N} \cdot \frac{K'_G}{K'_G + G} \cdot \frac{K'_M}{K'_M + M} \tag{7}$$

and:

$$K_X = \begin{cases} 0 & E < E_{threshold} \\ K_D & E \geq E_{threshold} \end{cases} \tag{8}$$

Yeast growth on maltose is inhibited by glucose and growth on maltotriose is inhibited by both glucose and maltose as has been observed.[3] This model differs from that discussed previously in the CO_2 production and yeast growth equations.

A CO_2 production curve for a typical beer fermentation is shown in Figure 6. This figure demonstrates the need for both a mass transfer term in the CO_2 dynamic equation (Eq. 10) and a yeast "deactivation" (due to flocculation and ethanol inhibition) term in the biomass equations (Eqs. 4 and 8).

During the initial part of the fermentation (0–40 hrs), sugars are metabolized to CO_2 at a high rate by the yeast. However, this does not show up in the CO_2 evolving from the fermentor because the yeast and media must become saturated with CO_2 before the flowrate of CO_2 from the tank becomes a true indicator of metabolic activity. Therefore, this effect must be taken into account by any mathematical model of this process and is included in our model in the form of a simple mass transfer term. The equations describing carbon dioxide in the system are:

liquid phase

$$\frac{dC_l}{dt} = \begin{cases} K_{GL}(C_{sat} - C_l) & C_l < C_{sat} \\ 0 & C_l = C_{sat} \end{cases} \tag{9}$$

gas phase

$$\frac{dC_g}{dt} = [Y_{CG}\mu_1 + Y_{CM}\mu_2 + Y_{CN}\mu_3]X - K_{GL}(C_{sat} - C_l) \tag{10}$$

In biological systems, CO_2 is known to be produced in the liquid phase as an ionic species. Based on this, CO_2 evolution during fermentation should be non-existent until the liquid phase saturates, after which CO_2 should be evolved at the same rate it is produced in the cells. However, we have not observed this in our fermentations. Figure 6 shows a typical CO_2 evolution curve for a fermentation. If the liquid were becoming fully saturated before CO_2 was evolved as a gas, we would have seen no CO_2 evolution until saturation were complete after which we should have seen an immediate increase in CO_2 evolution to a level such as that shown at 40 hrs in Figure 6. However, this is not the case. What we do observe seems to be more indicative of the CO_2 being produced in the gas phase and undergoing mass transfer to the liquid phase as the bubbles travel through the vessel. This runs counter-current to the knowledge that CO_2 is produced in the liquid phase. To explain this behavior, we have postulated that, since our system is agitated only by CO_2 evolution, during the first part of fermentation the cells and liquid in a close neighborhood (boundary layer) become quickly saturated with CO_2. Therefore, in the boundary layer, the CO_2 produced by the cells causes the evolution of an equal amount of CO_2 gas to satisfy the saturation limitation. The gas bubbles thus formed then travel through the unsaturated liquid as they rise in the vessel and mass transfer takes place between the two phases. In this way, the system approximates what would be seen if the CO_2 were produced in the gaseous phase in the first place, and this explains the behavior seen in Figure 6. For this reason, the CO_2 has been modeled in equations (9) and (10) as if it were actually produced as a gas in the cellular metabolic pathways.

In the latter part of fermentation (t > 120 hrs in Figure 6) the evolution of CO_2 shows a sudden sharp decrease. We have postulated that this decrease is caused primarily by ethanol inhibition of the yeast activity. The ethanol threshold concentration at which this activity decline begins appears to be fairly consistent for our yeast strain and has a value of 960 mols/m^3. At this point the yeast activity begins to decline at a fairly constant rate for 40 hours at which point it seems to stabilize at a constant value which is 10% of its original (pre-inhibition) value. For greatest simplicity, we have modeled this as a linear decline in the effective yeast concentration of slope K_D which lasts until 90% of the effective yeast concentration has been lost and then the deactivation constant (K_D) is set to zero as the yeast continues to maintain a minimal activity level. Mathematically, this deactivation model

is expressed as shown in equations (4) and (8) above.

The fermentation temperature and ethanol production rate are modeled as:

$$\frac{dT}{dt} = \frac{1}{\rho C_p}\left[H_{FG}\mu_1 + H_{FM}\mu_2 X + H_{FN}\mu_3 X - u(T - T_c)\right] \tag{11}$$

$$\frac{dE}{dt} = \left[Y_{EG}\mu_1 + Y_{EM}\mu_2 + Y_{EN}\mu_3)\right] X \tag{12}$$

The rate constants μ_{iM}, K_i, and K_i' were assumed to follow an Arrhenius type temperature dependency.

$$\mu_{iM} = \mu_{io}\exp(-E\mu_i/R(T + 273.15)) \quad i = G, M, N \tag{13}$$

As discussed by Gee and Ramirez[4], the model can be simplified to contain only four state variables by direct integration of equations (4) and (12) which yield the following:

$$X = X_0 + Y_{XG}(G_0 - G) + Y_{XM}(M_0 - M) + Y_{XN}(N_0 - N) - K_X t \tag{14}$$

$$E = E_0 + Y_{EG}(G_0 - G) + Y_{EM}(M_0 - M) + Y_{EN}(N_0 - N) \tag{15}$$

Equations (1)–(3), (5)–(11) and (14)–(15) comprise the model of beer fermentation. The parameters of this model were fit previously[4] and are summarized in Table 1. The carbon dioxide yield values were obtained from Harrison and Grahams' balanced overall reaction for yeast fermentation as quoted by Williams.[5]

Kalman Filter Equations

The discrete Kalman filter was developed in the early 1960s and results were obtained using this discrete formulation before the continuous formulation. The pioneering work in this area was done by Kalman[6] and others.[7,8]

The filter assumes a model of the form:

$$\boldsymbol{y}(n+1) = \boldsymbol{F}\boldsymbol{y}(n) + \boldsymbol{\Gamma}\boldsymbol{u}(n) + \boldsymbol{w}(n) \tag{16}$$

with a measurement model of:

$$\boldsymbol{z}(n) = \begin{cases} \boldsymbol{H}\boldsymbol{y}(n) + \boldsymbol{v}(n) & \text{for the linear filter} \\ \boldsymbol{h}(\boldsymbol{y}(n)) + \boldsymbol{v}(n) & \text{for the extended filter} \end{cases} \tag{17}$$

where $\mathbf{w}(n)$ and $\mathbf{v}(n)$ are Gaussian white noise with variances given by:

$$\mathrm{Var}(\boldsymbol{w}(n)) = \boldsymbol{Q}\,, \quad \mathrm{Var}(\boldsymbol{v}(n)) = \boldsymbol{R}$$

Based on this model, the filter is derived using discrete variational calculus based on a quadratic performance functional and is given by the following equations:[9]

Optimal State Estimate:

$$\hat{\boldsymbol{y}}_{k+1} = \bar{\boldsymbol{y}}_{k+1} + \boldsymbol{P}_{k+1}\boldsymbol{H}^T\boldsymbol{R}^{-1}(\boldsymbol{z} - \boldsymbol{L}(\boldsymbol{y})) \tag{18}$$

Predicted Estimate:

$$\bar{\boldsymbol{y}}_{k+1} = \boldsymbol{F}\hat{\boldsymbol{y}}_k + \boldsymbol{\Gamma}\boldsymbol{u}_k \tag{19}$$

Predicted Covariance

$$\boldsymbol{M}_{k+1} = \boldsymbol{F}\boldsymbol{P}_k\boldsymbol{F}^T + \boldsymbol{Q} \tag{20}$$

Updated Covariance (from a Riccati transformation):

$$\boldsymbol{P}_{k+1} = \boldsymbol{M}_{k+1} - \boldsymbol{M}_{k+1}\boldsymbol{H}^T(\boldsymbol{H}\boldsymbol{M}_{k+1}\boldsymbol{H}^T + \boldsymbol{R})^{-1}\boldsymbol{H}\boldsymbol{M}_{k+1} \tag{21}$$

where:

$$\boldsymbol{P}_0 = \mathrm{Var}(\boldsymbol{y}(o) - \boldsymbol{y}_0) \tag{22}$$

and:

$$\boldsymbol{L}(\boldsymbol{y}) = \begin{cases} \boldsymbol{H}\boldsymbol{y}_{k+1} & \text{for the linear Kalman filter} \\ \boldsymbol{h}(\boldsymbol{y}_{k+1}) & \text{for the extended Kalman filter} \end{cases} \tag{23}$$

Equations (18) through (21) make up the discrete Kalman filter.

with which to compare these estimates although they seem physically realistic. Notice the large jumps in the maltose and maltotriose concentrations at approximately 70 hrs. These jumps are the result of the input of the

Discussion of Simulation Results

With the model in the form of eqn. (16), simulations were run to determine the effectiveness of this observable estimator[10] using measurements of temperature, specific gravity, and CO_2 evolution rate. The results for one of these simulations are shown in Figures 1-3. This simulation was run with high initial estimates (10 mols/m^3 higher than actual) given for the three sugars.

Figure 1 gives the results of the sugar estimation. As seen, the estimator brought all three sugars in close to their actual values rapidly and maintained them there. Notice that it was not able to converge on the exact values, but could only approach them closely. This is a result of the non-uniqueness of the filter used. We are using three independent measurements to estimate four state variables. Therefore, the estimator cannot be expected to converge on a unique solution, but does well in following the system behavior as closely as it does.

Figures 2 and 3 show comparisons between the true measurements and the estimates of those measurements. As shown in Figure 2, the total fermentable sugars converged rapidly on the measurement and followed it closely throughout the fermentation. Note that the estimated versus measured temperature curves are not shown. This is because the estimate followed the true value so well as to make the two indistinguishable on a plot.

In Figure 3, the estimate of the CO_2 evolution rate is offset by a fairly constant amount greater than the measurement for most of the fermentation. This is due to the fact that the biomass estimate calculated from equation (14) is based on the initial estimated sugar concentrations. In this case, where all three sugars were estimated high initially, there is a bias upward in the biomass concentration throughout the fermentation. Since the biomass concentration is highly involved in the various reaction rates during the fermentation, those rates are all accelerated above their true values in the estimator and this results in a high bias in the CO_2 evolution rate which cannot be corrected by the estimator (because the estimator cannot adjust the initial sugar estimates, nor the biomass estimate to alleviate the error).

On-Line Identification

The results of the simulations showed the Kalman filter to be very promising for estimating fermentation process states. Based on this, software was developed to implement this filter on-line in our laboratory.

The fermentation temperature was measured using a type K thermocouple inserted in the fermentor thermowell. The resulting signal was amplified 100 times and was then sent to a Data Translation DT-2801 board where it was again amplified by a factor of eight before A/D conversion was performed (overall amplification = 800X).

Carbon dioxide production was measured by a Tylan FM-360 mass flowmeter calibrated for a CO_2 flow range of 0-2 standard liters per minute (SLM) with an accuracy of ± 0.02 SLM. This flowmeter put out a 0-5 VDC signal proportional to the flowrate which was converted to a digital signal by the Data Translation board with no amplification.

The specific gravity of the beer was measured off-line using a hydrometer. The beer was degassed by agitation before this measurement was made. Corrections were made for temperature. The measurement value was then entered into the computer for use by the filter.

Typical brewer's wort and yeast (*S. carlsbergensis*) were used for the fermentation. The equipment was cleaned and sterilized using a 25 ppm solution of Rapidyne and water. The yeast was aerated for one hour prior to pitching and the wort and yeast together were aerated for four hours after pitching to ensure oxygen availability for yeast growth throughout the fermentation. The fermentation was run isothermally at a temperature of 12.5°C.

Discussion of On-Line Results

The results of the on-line identification run are shown in Figures 4-6. These figures give results for individual sugar estimation, total sugars estimation, and CO_2 estimation, respectively. As in the simulation, the estimated and measured temperature curves were indistinguishable, and, therefore, a plot is not included.

The sugar estimates (Figure 4) display the expected dynamic behavior with glucose being exhausted first and maltose being utilized more rapidly than maltotriose. There were no measurements, on- or off-line, available

with which to compare these estimates although they seem physically realistic. Notice the large jumps in the maltose and maltotriose concentrations at approximately 70 hrs. These jumps are the result of the input of the first specific gravity measurement. This was the first point at which the estimator had more to go on than merely the measured CO_2 evolution rate and system temperature. We can see from the total sugars plot (Figure 12) that it corrects itself nicely by bringing the total sugars to the correct concentration. Had more specific gravity measurements been made and entered prior to 70 hours, both the individual sugar estimates and the total sugar estimate would have shown a series of small jumps similar to those resulting from later measurements. The estimator would then have been able to remain on track without relying solely on the CO_2 evolution rate and temperature measurements.

In Figure 5, the total sugars estimate is shown to agree quite well with the measurements given by the points on the graph. Although the estimate decreases initially more rapidly than it should, the first measurement brings it back into line nicely, and the trend in the estimate agrees quite well with the measurements from there on.

Figure 6 gives the comparison between the measured and estimated CO_2 evolution rate. As shown, the mass transfer term included in the model allows the estimator to follow the initial fermentor saturation phase very well. Had this term not been included in the model, the estimator would still have tried to imitate the measured signal and, in doing so, would have caused the other estimates to be in error. As it is, the estimator is able to follow the CO_2 signal quite well without causing the other estimates (such as the sugars) to get off track. Notice the jump in the estimate at approximately 70 hrs. This, again, is due to the first specific gravity measurement available for use by the estimator. As shown, the CO_2 estimate continues to follow the measurement fairly well after this jump, but is never able to completely recover its earlier accuracy.

Conclusions

The method of Kalman filtering as applied to a model of batch beer fermentation using simple measurements of temperature, CO_2 evolution rate, and specific gravity has shown promising results in simulations. The filter can be used in conjunction with these measurements to yield a much better picture of what is actually happening during the process. Sugar, ethanol, and yeast concentrations can be discerned fairly well using this technique. When given a good initial estimate of the sugar and yeast concentrations, the estimator does an excellent job at identifying the fermentation state for all time. Due to non-uniqueness, the filter performance is somewhat corrupted for bad initial state estimates, although it has been shown to improve these estimates over the course of the fermentation.

References

1. Rajab, A., M.-N. Pons, P. Dantigny, and J. M. Engasser, "Extended Kalman Filtering with Physiological Modeling Applied to Baker's Yeast Fermentation," personal communication.
2. Wang, N.S. and G. Stephanopoulos, "A New Approach to Bioprocess Identification and Modeling," *Biotech. Bioeng. Symposium No. 14*, John Wiley and Sons, NY, 635-656 (1984).
3. Engasser, J. M., I. Marc, M. Moll, and B. Duteurtre, "Kinetic Modeling of Beer Fermentation," EBC Congress, 579-586 (1981).
4. Gee, D. A. and W. F. Ramirez, "Optimal Temperature Control for Batch Beer Fermentation," accepted for publication in *Biotech. Bioeng.* (1987).
5. Williams, L. A., "Heat Release in Alcoholic Fermentation: A Critical Reappraisal," *Amer. J. Enol. Vitic.* **3**(3), 149-153 (1982).
6. Kalman, R. E., "A New Approach to Linear Filtering and Prediction Problems," *Trans. A.M.E., J. Basic Engr.* **82**, 34-45 (March, 1960).
7. Ho, Y. C. and R. C. K. Lee, "A Bayesian Approach to Problems in Stochastic Estimation and Control," *IEEE Trans. Aut. Control* **AC-9**, 333-339 (1964).
8. Lee, R. C. K., *Optimal Estimation, Identification, and Control*, M.I.T. Press, Cambridge, MA (1964).

9. Franklin, G. F. and J. D. Powell, *Digital Control of Dynamic Systems*, Addison-Wesley, Reading, MA, 260-262 (1980).

10. Sage, A. P. and C. C. White, *Optimum Systems Control*, Prentice Hall (1977).

11. IMSL Software Library, Integration Routine DGEAR.

Nomenclature

C	–	carbon dioxide concentration, mol/m^3
C_p	–	heat capacity, J/kg/K
C_{sat}	–	effective solubility of CO_2, mols/m^3
E	–	ethanol concentration, mol/m^3
E_{μ_i}	–	parameter activation energy, J/mol
$\boldsymbol{F}$	–	state coefficient matrix
G	–	glucose concentration, mol/m^3
$\boldsymbol{\Gamma}$	–	control coefficient matrix
$\boldsymbol{H}$	–	measurement matrix
H_{FS}	–	heat of fermentation for substrate, J/mol
K_D	–	yeast deactivation constant
K_S	–	Michaelis constant for substrate, mol/m^3
K_{GL}	–	effective mass transfer coefficient for evolution of CO_2(g), hr^{-1}
K'_S	–	inhibition constant for substrate, mol/m^3
K_X	–	the death/deactivation term in the biomass equation, mols/m^3/hr
$\boldsymbol{M}$	–	predicted state covariance matrix
M	–	maltose concentration, mol/m^3
μ_S	–	specific rate of substrate uptake, 1/hr
$\mu_{S,max}$	–	maximum specific rate of substrate uptake, 1/hr
μ_{io}	–	Arrhenius frequency factor, 1/hr
N	–	maltotriose concentration, mol/m^3
$\boldsymbol{P}$	–	state covariance matrix
$\boldsymbol{Q}$	–	state noise variance matrix
$\boldsymbol{R}$	–	measurement noise variance matrix
R	–	the gas constant
ρ	–	density, kg/m^3
t	–	time, hr
T	–	temperature, °C
T_c	–	coolant temperature, °C
$\boldsymbol{u}$	–	control vector
$\boldsymbol{v}$	–	measurement noise
$\boldsymbol{w}$	–	state noise
X	–	biomass concentration, mol/m^3
$\boldsymbol{x}$	–	state vector
Y_{CS}	–	yield of CO_2 per mole substrate
Y_{ES}	–	yield of ethanol per mole substrate
Y_{XS}	–	yield of biomass per mole substrate
$\boldsymbol{y}$	–	deviational state vector
$\boldsymbol{z}$	–	deviational measurements

Table 1 – Model Parameters

Parameter	Glucose	Maltose	Maltotriose
Y_{Ei}	1.92	3.84	5.76
Y_{Ci}	1.94	3.88	5.82
Y_{Xi}	0.134	0.268	0.402
H_{Fi}, KJ/mol	-91.2	-226.3	-361.3
$\ln(\mu_{io})$, $\ln(\mathrm{hr}^{-1})$	35.77	16.40 .	10.59
$E_{\mu i}$, Kcal/mol	22.6	11.3	7.16
$\ln(K_{io})$, $\ln(\mathrm{mol/m^3})$	-121.3	-19.15	-26.78
E_{Kio}, Kcal/mol	-68.6	-14.4	-19.9
$\ln(Kio')$, $\ln(\mathrm{mol/m^3})$	23.33	55.61	
E'_{Kio}, Kcal/mol	10.2	26.3	

$$\rho = 1040 kg/m^3 \qquad V = 0.23 m^3$$

$$C_p = 4016 J/Kg \cdot^\circ C \qquad K_p = 10$$

$$C_{sat} = 400 mol/m^3 \qquad K_{GL} = 0.07 hr^{-1}$$

Table 2 – Estimator Matrices

$$\boldsymbol{h} = \begin{bmatrix} \frac{\partial R_c}{\partial G} & \frac{\partial R_c}{\partial M} & \frac{\partial R_c}{\partial N} & \frac{\partial R_c}{\partial T} \\ 1 & 1 & 1 & 0 \\ 0 & 0 & 0 & 1 \end{bmatrix}^*$$

$$\boldsymbol{Q} = \begin{bmatrix} 10. & 0 & 0 & 0 \\ 0 & 0.11 & 0 & 0 \\ 0 & 0 & 0.0013 & 0 \\ 0 & 0 & 0 & 1. \end{bmatrix}$$

$$\boldsymbol{R} = \begin{bmatrix} 1 & 0 & 0 \\ 0 & 1 & 0 \\ 0 & 0 & 0.25 \end{bmatrix}$$

*where R_c =dC/dt

Figure Legends

Figure 1 – Simulation Results – Sugar Estimates – Curves are: (a) true glucose, (b) estimated glucose, (c) true maltose, (d) estimated maltose, (e) true glucose, (f) estimated maltriose. Initial Estimates were G = 14.4 g/l, M = 78.7 g/l, N = 25.2 g/l (10 mol/m^3 higher than actual initially)

Figure 2 – Simulation Results – Total Fermentable Sugars – Curves are: (a) measurement, (b) estimated, same conditions as Figure 1

Figure 3 – Simulation Results – Carbon Dioxide Evolution – Curves are: a) measurement, (b) estimated, same conditions as Figure 1

Figure 4 – On–Line Results – Sugar Estimates – Curves are: (a) glucose estimate, (b) maltose estimate, (c) maltotriose estimate

Figure 5 – On–Line Results – Total Fermentable Sugars – Points are measurements, the curve is the estimate

Figure 6 – On–Line Results – Carbon Dioxide Evolution – Curves are: (a) measurement, (b) estimate

FIGURE 1 – SUGARS TRUE VS ESTIMATED

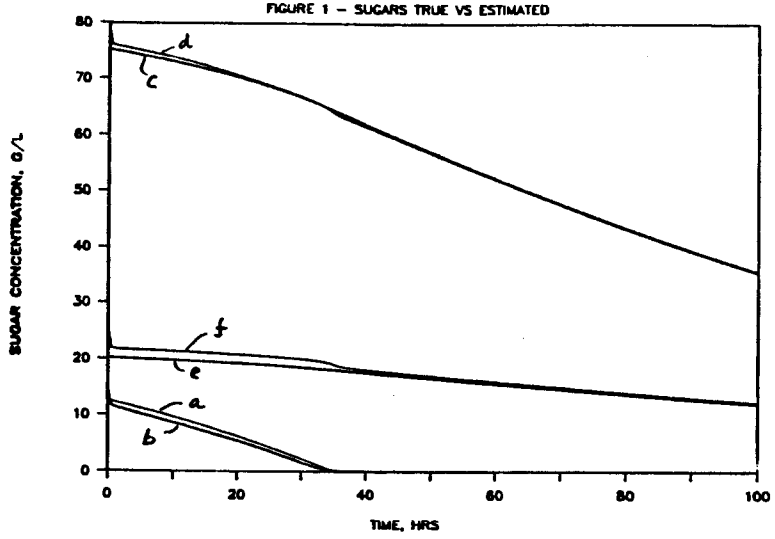

FIGURE 2–TOTAL SUGARS TRUE VS ESTIMATED

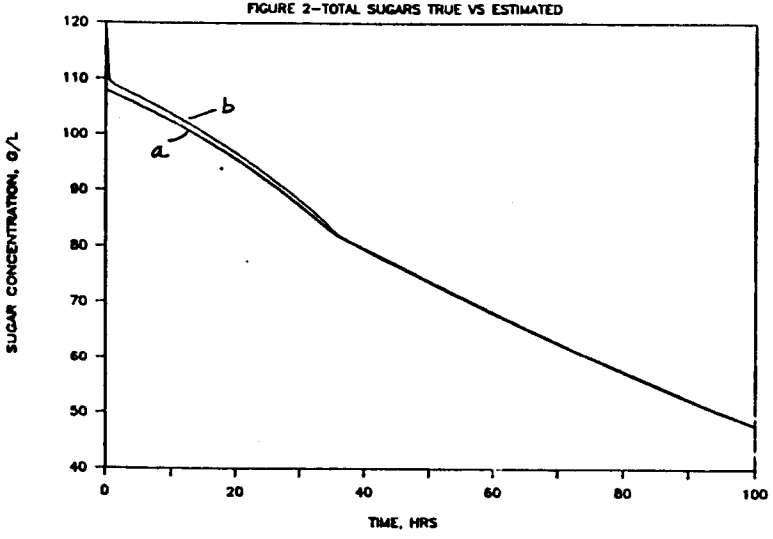

FIGURE 3–CO2 EVOLUTION MEAS VS ESTIMATE

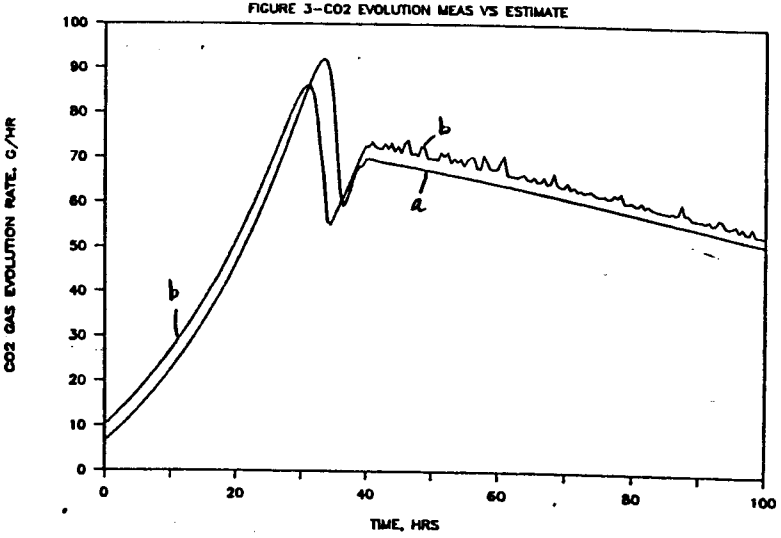

FIGURE 4 – ON–LINE SUGAR ESTIMATES

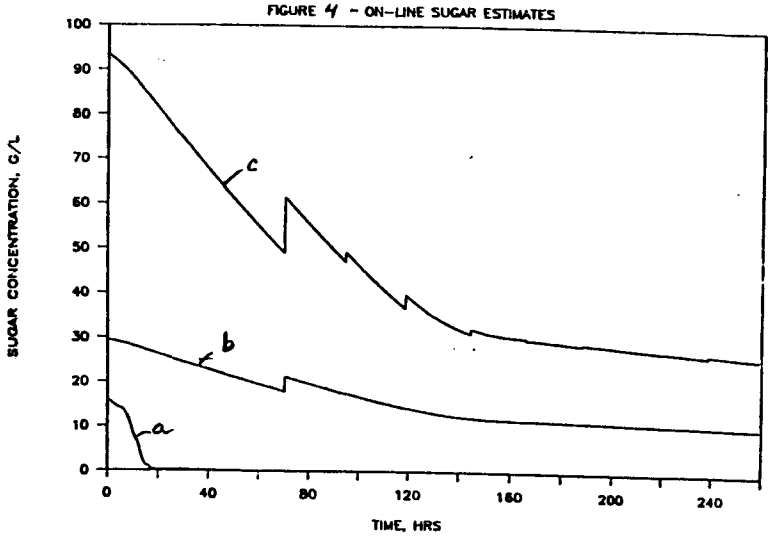

FIGURE 5 –TOTAL SUGARS MEAS. VS EST.

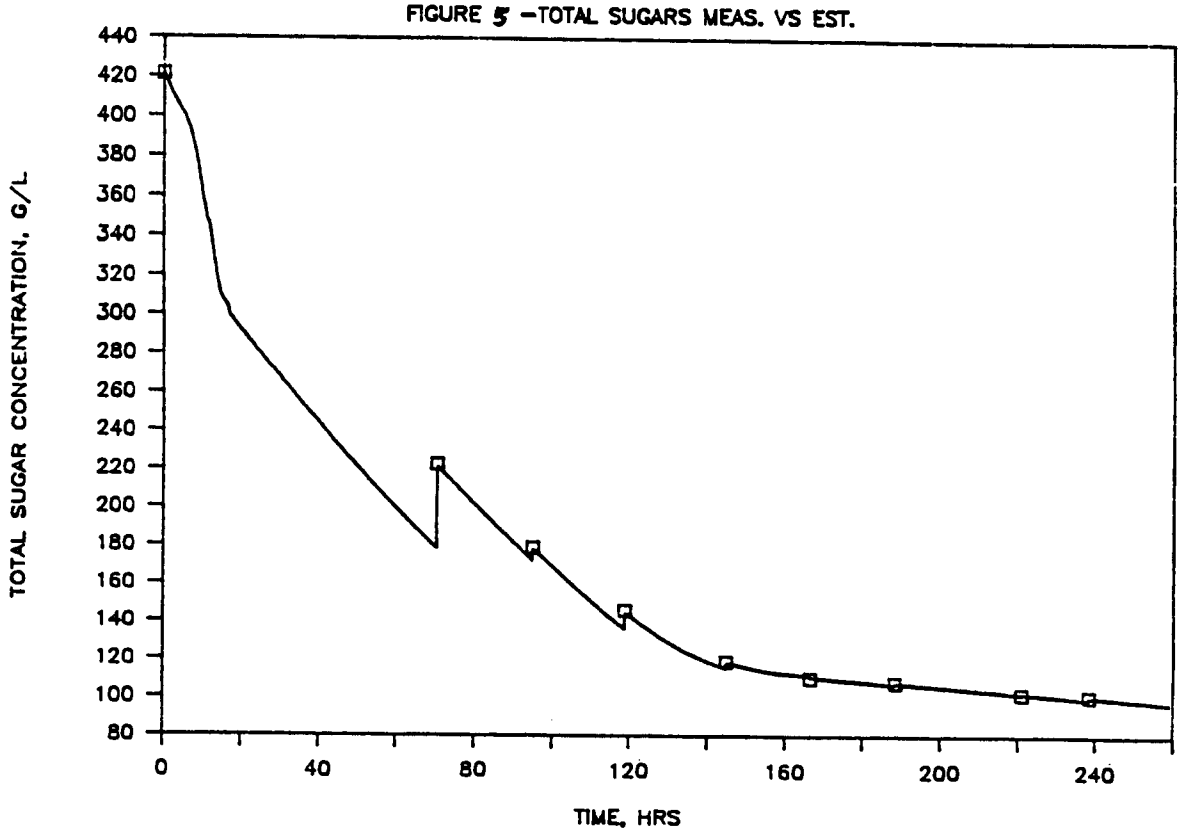

FIGURE 6 –CARBON DIOXIDE MEAS. VS EST.

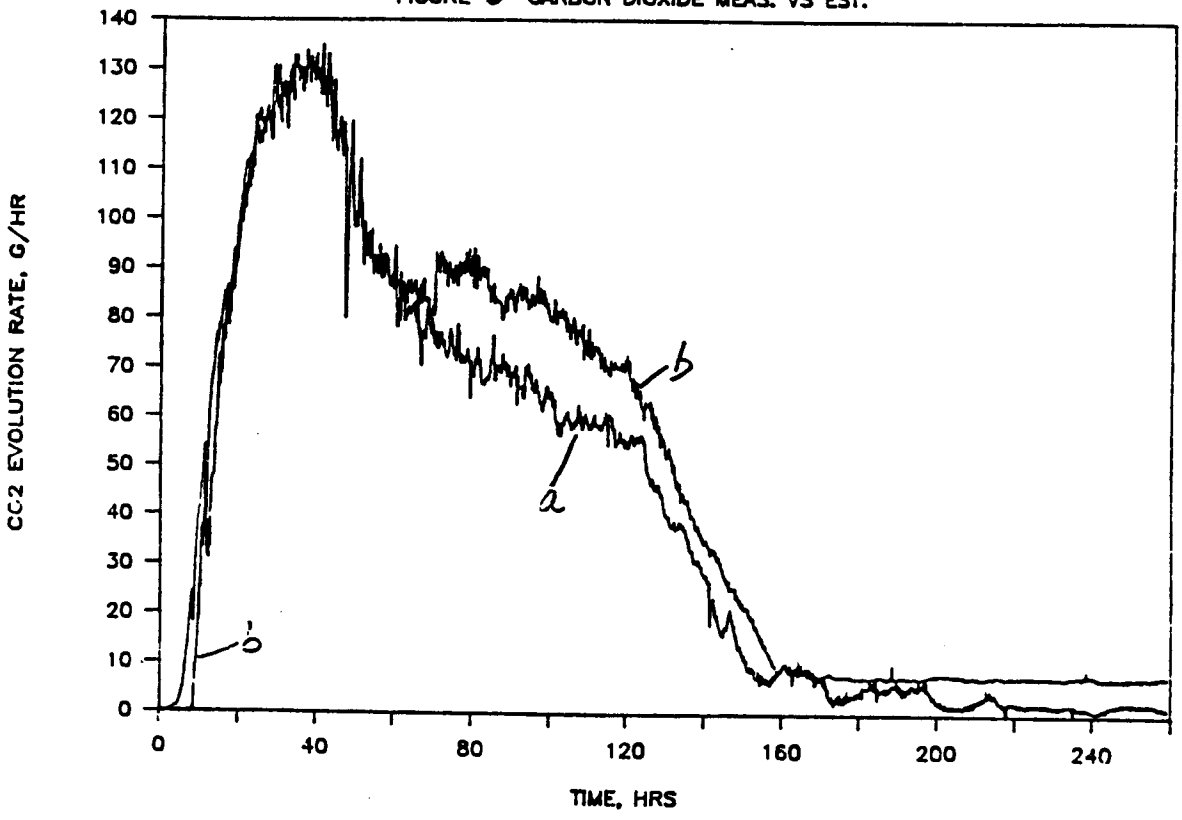

Role of spargers in Air-lift reactors

Peter U. Sohn and Rakesh K. Bajpai

Department of Chemical Engineering
University of Missouri-Columbia

Several researchers [1,2,3,5,6] have investigated the hydrodynamic behavior of air-lift reactors and have proposed correlations to describe relationships among hydrodynamic variables (gas hold-up and liquid circulation velocity) and the operating variable (gas flow rate). However, the dependency of hydrodynamic behavior on the sparger type and size has not been investigated in detail. Therefore, this article will focus on how the sparger type and its size affect gas hold-up and liquid velocity in an air-lift reactor.

In order to investigate these, a spherical sintered sparger (diameter 25.4 mm), four different flat sintered spargers (diameters 10 mm, 21 mm, 40 mm, and 63 mm), and three different perforated plate spargers (diameters 25.4 mm, 47.6 mm, and 60.3 mm) have been used. An external loop air-lift reactor has been employed for these studies and its details are given in reference[8]. The diameter of the riser column was 76.2 mm.

Results and discussions

1. Gas hold-up behavior for different sparger types and sizes

Figure 1 is a typical plot showing gas hold-up behavior with increasing gas flow rate. The abscissa is the superficial gas velocity which is defined as the volumetric gas flow rate divided by the cross sectional area of the riser column. The ordinate is gas hold-up, defined as fraction of the volume in the riser column occupied by gas phase. The lines are drawn to emphasize trends of gas hold-up behavior for different types of spargers. Here, two almost same size spargers (diameters of 63 mm and 60.3 mm) but with different type (sintered and perforated) were used. It can be observed from figure 1 that, in the bubbly flow regime[4] which occurs at low gas flow rates, gas hold-up for both types of spargers increases linearly with increasing gas flow rate, but with different slopes which is a measure of the effect of sparger type on bubbles formed. However, at high gas flow rates, gas hold-up for both types of spargers are same. It

is probably because, at high gas flow rates where the churn-turbulent flow regime[4] prevails, the effect of sparger type on bubble sizes diminishes due to the vigorous coalescence and redispersion which is usually dependent on the column itself.

Figure 2 shows again gas hold-up behavior for different gas flow rates for another set of experimental data. Here, two sintered disk spargers with different sizes (diameters of 63 mm and 21 mm) were used. The transition from the bubbly flow regime to the churn-turbulent flow regime is obvious for a 63 mm sparger, but the distinction of flow regimes is not very visible for a 21 mm sparger. In fact, even at low gas flow rates, the churn-turbulent flow regime still prevails. Therefore, it can e said that the transition of flow regimes is decided by the sparger size. Also, it possibly changes the profiles of gas hold-up in the riser and it will be mentioned in a later section.

2. Macroscopic energy balance and drift flux model

Sohn, Preckshot, and Bajpai[7] proposed two hydrodynamic relationships among gas flow rate, gas hold-up, and liquid circulation velocity based on the macroscopic mechanical energy balance equation and the drift flux model[9]. In this section, it will be discussed whether the effect of the sparger size and type on the hydrodynamic behavior of air-lift reactors can be incorporated with the proposed relationships by Sohn et al. or not and how it can be done.

[A] Macroscopic mechanical energy balance model

$$\alpha = K J_1^2 \qquad \text{Eq. (1)}$$

where α represents a gas hold-up, K is a measure of the resistance to fluid circulation per unit height, and J_1 is the superficial liquid circulation velocity which is defined as the volumetric flow rate of the liquid divided by the cross sectional area of the riser.

Figure 3 and 4 show gas hold-up behavior against increasing liquid flow rates. Each line represents different restriction orifices, which result into various resistances to the flowing fluid. It can be observed that, from linear relationships between the gas hold-up and the liquid circulation rates for different type of spargers, the macroscopic mechanical energy balance is independent on the sparger types employed. Same type of phenomena were observed when different size of spargers were used[8]. It is because, when a reactor with a large ratio of the riser diameter

to the downcomer diameter is used, the coefficient, K, in equation (1) results mostly from the downcomer section of the reactor where two phase flow hydrodynamics does not play an important role.

[B] Drift flux model

For the bubbly flow and the churn-turbulent flow regime

$$\frac{J_2}{\alpha} = C_o(J_1 + J_2) + V_\infty(1 - \alpha)^n \qquad \text{Eq. (2)}$$

n = 2 for small bubbles in a reactor
n = 0 for large bubbles in a reactor

where J_2 is the superficial gas velocity, C_o is the distribution parameter to account for the nonuniformity of the total gas-liquid velocity and the gas hold-up, V_∞ is the bubble rise velocity, and n is an empirical parameter which changes value depending on the bubble size.

The drift flux model for two phase flow, which focuses the attention upon the relative motion of the dispersed phase with respect to that of the overall gas-liquid system, accounts for the sparger effect by including terms such as the bubble rise velocity and the distribution parameter. The distribution parameter, C_o, which can be represented as equation (3), is a measure of the nonuniformity of total gas-liquid profile and gas hold-up profile in the riser column.

$$C_o = \frac{\overline{\alpha(J_1 + J_2)}}{\overline{\alpha}\,\overline{(J_1 + J_2)}} \qquad \text{Eq. (3)}$$

The bubble rise velocity depends mainly upon the bubble size distributed from the sparger. Thus, the bubbly flow regime experimental data for two types of spargers with relatively same size (a sintered sparger with a diameter of 63 mm and a perforated plate sparger with a diameter of 60.3 mm) are plotted according to the drift flux model in Figure 5 assuming n=2. It can be noticed that both lines have almost same slopes but have different intercepts. These intercepts represent the individual bubble rise velocity from two different types of spargers.

Therefore, it can be said that different type of spargers with different size of pore diameter will result into distinctive bubble rise velocities.

It is also suspected that the relative size of the sparger to column diameter changes the profiles of the gas phase inside the column, which eventually changes the value of C_o. Therefore, the bubbly flow regime experimental data for sintered disk spargers with diameters of 21 mm and 63 mm are plotted according to the drift flux model in figure 6. It can be observed that the slopes for two lines are different enormously with the same intercepts, which is the bubble rise velocity. These slopes represent the distribution parameter. Therefore, it can be said that the effect of the sparger size may be analyzed with the distribution parameter in the drift flux model.

The relationship of C_o against the relative sparger size have been extensively investigated experimentally. Figures 7 and 8 show some of the results obtained for the bubbly flow and the churn-turbulent flow regimes, respectively, for sintered spargers. It can be seen from both figures 7 and 8 that, in the bubbly flow regime, the distribution parameter, C_o, decreases as the fractional aerated area increases and it remains around 1.2 at a high aeration fraction. However, in the churn-turbulent flow regimes, C_o seems to remain constant at around 1.7 even though the fractional aerated area changes. This may be the result of the fact that, at high gas flow rates as in the churn-turbulent flow regimes, the bubble swarm characteristic is not dependent upon the sparger but is dependent only upon the flow condition and the column diameter.

In the case of perforated spargers, almost the same phenomena were found to prevail. Table 1 listed the C_o values and their respective ratios of the aerated area of the sparger to the column area. The C_o values in the bubbly flow regime follow the same trend as for the sintered sparger (see Figure 7). The C_o values in the churn turbulent flow regime were around 1.7 (see Figure 8).

The results obtained here were deduced from the data for viscosities of solutions ranging from 0.9 to 1.6 cp. Therefore, these findings are valid for newtonian solutions with low viscosity.

Literature cited

1 Bello, R. A., C. W. Robinson, and M. Moo-Young, Biotech. and Bioeng., vol 27, pp 369 (1985)

2 Bello, R. A., C. W. Robinson, and M. Moo-Young, Can. J. Chem. Eng., vol 62, pp 573 (1984)

3 Chisti, M. Y. and M. Moo-Young, Chem. Eng. Commun. vol 60, pp 195 (1987)

4 Hewitt, G. F., Handbook of Multiphase systems, McGraw Hill

Book Company, ed. by Hetsroni (1982).
5 Hsu, Y. C. and M. P. Dudukovic, Chem. Eng. Sci., vol 35, pp 135 (1980)
6 Lee, C., Proceedings of 16th Annual Biochemical Engineering Symposium, Kansas State University, pp 65 (1986)
7 Sohn, P., G. W. Preckshot, and R. K. Bajpai, Proceedings of 17th Annual Biochemical Engineering Symposium, Iowa State University, April, (1987).
8 Sohn, P., Ph.D. Dissertation, University of Missouri-Columbia, (1988)
9 Zuber, N. and J. A. Findlay, J of Heat Transfer (Trans. of ASME), vol 87, pp 453 (1965)

Table 1 : The relation between C_o and the ratio of the aerated area of perforated spargers to the riser diameter

Media	D_s/D_u	C_o	Flow regime
Tap water	0.333	1.68	Churn-turbulent
	0.625	1.09	Bubbly
	0.791	1.21	Bubbly
20.1 wt% glycerine soln.	0.333	1.48	Churn-turbulent
	0.625	1.00	Bubbly
	0.791	1.17	Bubbly

* Glycerine solution have been made by mixing Pure glycerine and distilled water

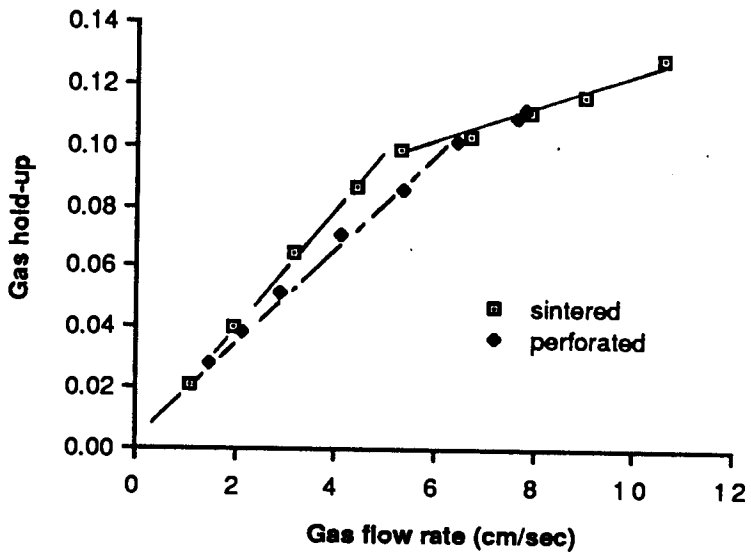

Figure 1

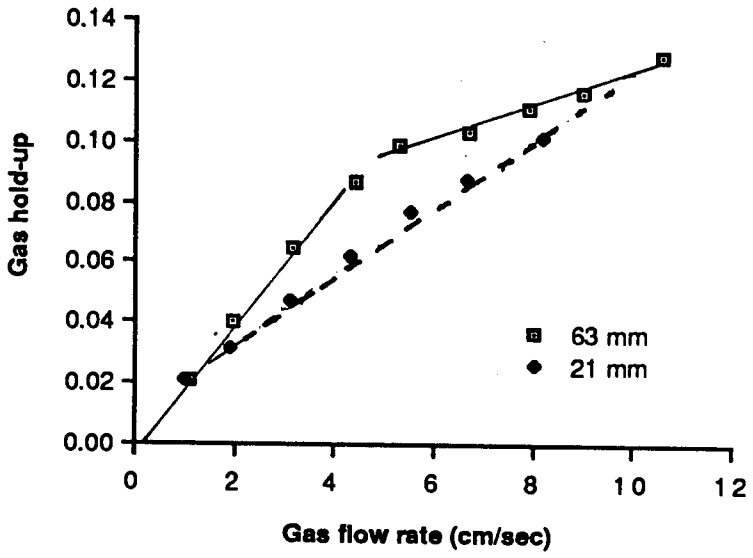

Figure 2

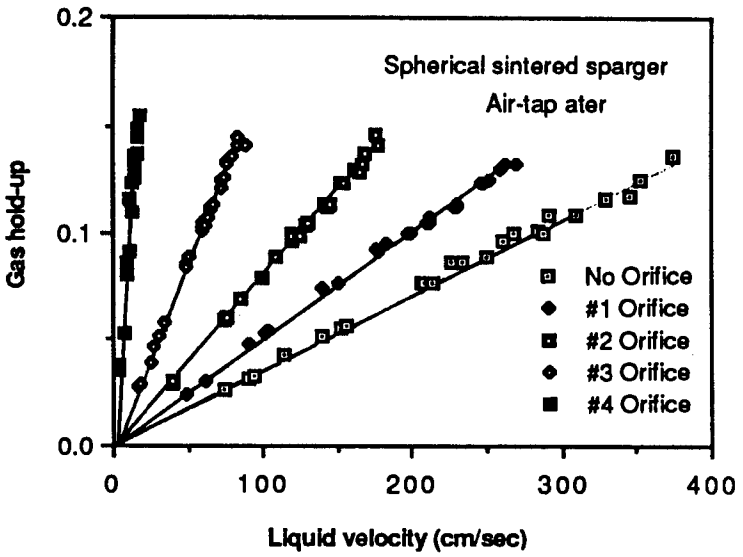

Figure 3

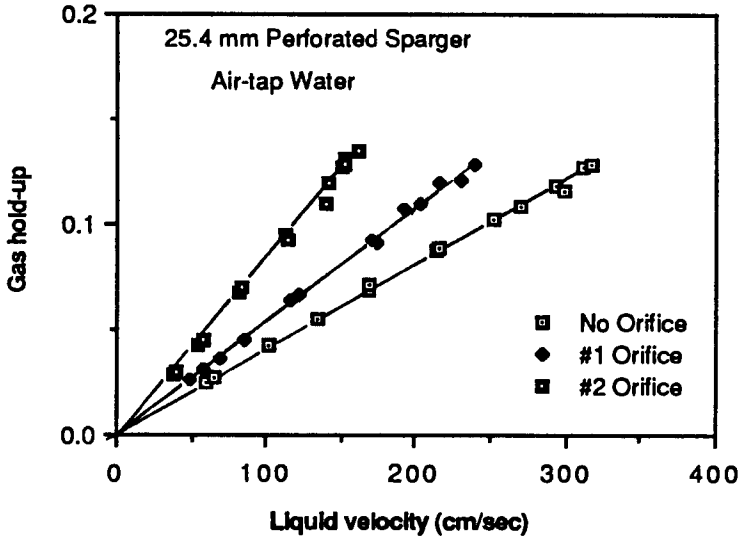

Figure 4

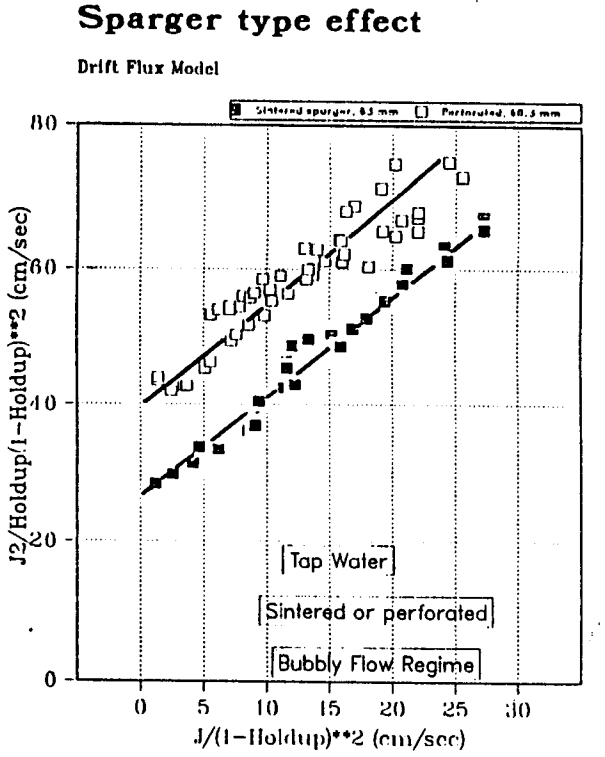

Figure 5

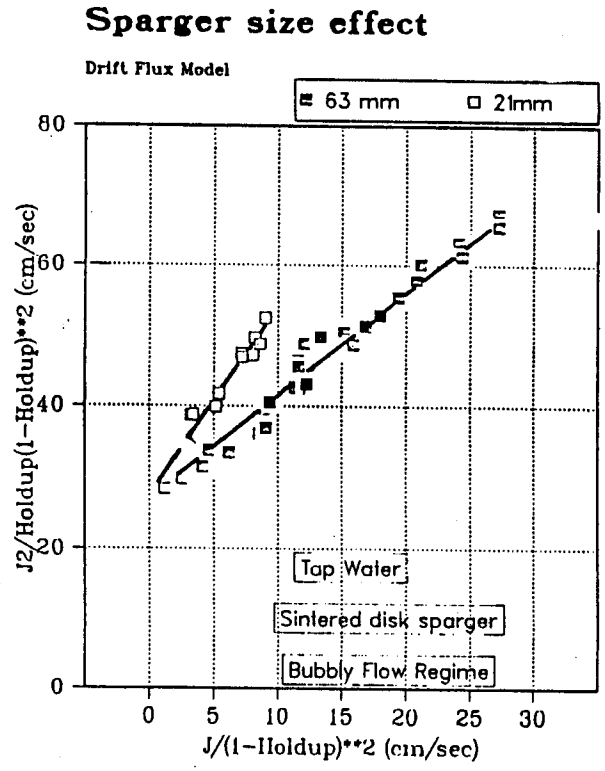

Figure 6

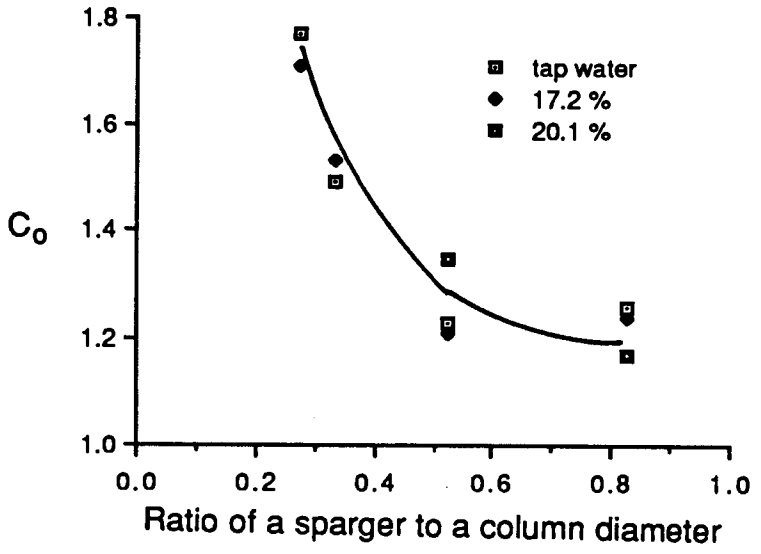

Figure 7

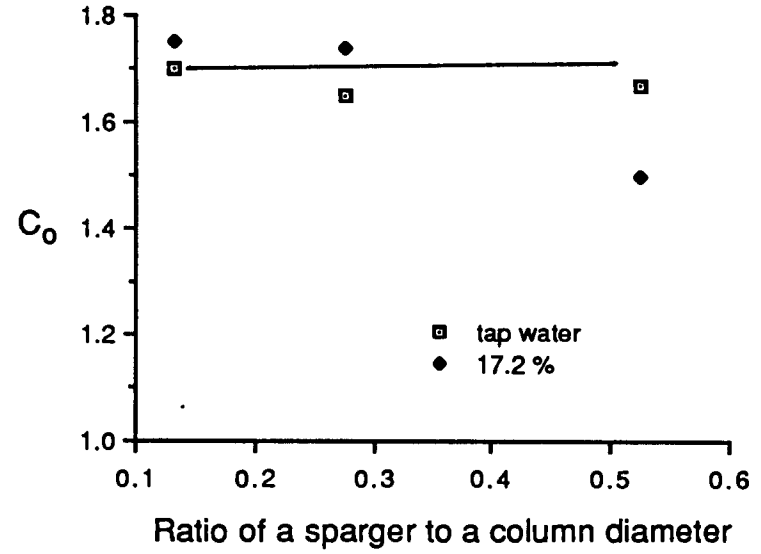

Figure 8

THE INTERACTION OF MICROCARRIERS AND TURBULENCE WITHIN AN AIRLIFT FERMENTER

G. Travis Jones

Department of Chemical Engineering
Durland Hall
Kansas State University
Manhattan, Kansas 66506

Introduction

Airlift reactors are increasingly being used in the large scale cultivation of animal [1-3], plant [4], and insect cells [5]. The shear sensitivity of these cells is of major concern whenever culturing within a fermenter. Croughan et. al. [6] have shown that for a stirred tank the most important parameter to be measured with respect to loss of viability for anchorage dependent cells (ADC) grown upon microcarriers is the turbulent energy dissipation rate (ϵ). Limited understanding exists of the interaction of laden microcarriers and turbulence resulting in the loss cell viability. The purpose of this research is to gain an understanding of the interaction of microcarriers and the turbulence present within an airlift fermenter.

Mixing within an airlift loop reactor is accomplished by the sparging of air into the bottom of the column and allowing degassed liquid at the top of the column to return to the bottom (see Fig. 1). The use of air to both provide oxygen and mixing within the column avoids the moving seal present in stirred tank reactors though which contaminating microorganisms may enter. Therefore, a number of advantages are present in the use of airlift fermenters; simple construction, low initial costs, good oxygen transfer, reduced power consumption and low hydrodynamic shear.

While sparger aeration is the simplest method of providing oxygen and agitation to a fermenter there are indications that mammalian and insect cells are susceptible to damage by bubbles [7,5]. Nevertheless, it is unclear whither damage to the cell is occurring due to turbulent shear, gas-liquid interfacial effects or a combination of these two phenomena. Most researchers in this area have suggested that the loss of viability is due to turbulent shear encountered in a fermenter [6,8]. Handa et. al. [7] have investigated gas-liquid interfacial effects on hybridoma viability within a bubble column. Not only was the aggitation rate found to be important but, bubble size and the addition of surface active polymers also affected cell viability. A decrease in the Sauter mean bubble diameter was found to be more detrimental to the cells, yet the addition of surfactants had a protective effect.

Hinze [9] has noted that the behavior of discrete particles within a turbulent flow field depends upon the concentration of particles and particle size with respect to the turbulent eddy size

scale. High particle concentrations result in entity interactions through collisions and effects on fluid flow near the particles. The motion of particles relative to the fluid (i.e. lag) may result in an increase in the dissipation of energy. At low concentrations the particles may be regarded as being alone in the turbulent flow field. If the particle is small relative to the microscale of turbulence it will follow the turbulent fluid motions; whereas, a larger particle (e.g. on the order of a characteristic integral length scale) will follow only the large scale turbulent motions.

Theory

The Reynold's decomposition [10] is commonly used in the study of turbulence based upon the Navier-Stokes equations. For a statistically stationary flow the local instantaneous velocity u_i is decomposed into a mean flow component U_i and a velocity fluctuation u_i' about the mean. Typically U_i is a time-averaged quantity and $\overline{u_i'}$ is the standard deviation about the mean more commonly known as the root-mean-square (RMS) velocity fluctuation. Dissipation of turbulent energy has been shown to correlate with the loss of cell viability within stirred tank reactors [6]. Specifically, the turbulent dissipation rate is defined as

$$\epsilon = 2\nu \overline{s_{ij}s_{ij}}$$

$$= \frac{\nu}{2} \overline{\left(\frac{\partial u_i'}{\partial x_j} + \frac{\partial u_j'}{\partial x_i} \right)^2} \qquad (1)$$

where ν is the kinematic viscosity of the fluid, s_{ij} is the fluctuating rate of strain, the i,j subscripts refer to the Eulerian coordinate axis and the overbar denotes a time averaged quantity [10]. Accurate measurement of ϵ is difficult and requires special equipment, nonetheless, estimates can be made using Taylor's large-scale inviscid estimate

$$\epsilon = A\overline{u_i'}^3/\ell \qquad (2)$$

where A is a constant to be determined and ℓ is the integral length scale that is characteristic of the system being studied.

The size of dissipative eddies, η, is determined by the dissipation rate, ϵ, and the kinematic viscosity, ν, as

$$\eta = \left(\frac{\nu^3}{\epsilon} \right)^{1/4} \qquad (3)$$

Estimates can also be made of the dissipative eddy velocity

$$v = (\nu\epsilon)^{1/4} \tag{4}$$

The relative size and velocity of a turbulent eddy with respect to a particle is an important aspect of the fluid-particle phenomena.

Order of magnitude estimates of time averaged shear stress can be made using ϵ, nevertheless, these estimates are of limited value. The resulting estimate is a time averaged value of shear stress and may include spatial averaging; whereas, local instantaneous values of shear stress may be much greater. In order to estimate the time average shear rate it is necessary to assume the turbulence is isotropic. Therefore, the small scale turbulent motions are independent of any orientation and a potential estimate of shear stress is [11]

$$\mu \overline{\frac{\partial u_1}{\partial x_1}} = \sqrt{\frac{\epsilon\mu^2}{15\nu}} \tag{5}$$

For example, for water with $\epsilon = 1000\ cm^2s^{-3}$ the size of the dissipative eddies would be $\eta \sim 56\ \mu m$ with a velocity ~ 1.8 cm/s and the time averaged shear stress $\sim 0.08\ Nm^{-2}$. A potential order of magnitude estimate of the instantaneous shear might assume the formation of an eddy 10 μm from the surface of a microcarrier. This distance and the previous estimate of eddy velocity would give a shear stress of $1.8\ Nm^{-2}$, a result two orders of magnitude greater than the time averaged quantity. However, there are a number of potential length scales that could be used to evaluate the local instantaneous shear stress.

For comparison, mammalian cells are typically 20 ± 10 μm in diameter and microcarrier diameters are on the order of 180 μm. Thus, for the above example the eddy would entrain the cells, however, it would impact the surface of the microcarrier resulting in either a dynamic pressure force or a shear force on an immobilized cell. Reported shear stresses that cause the loss of viability are: $1.5\ Nm^{-2}$ for pupal ovaries of the fall army-worm Spodoptera frugiperda [5]; $0.6\ Nm^{-2}$ for human embryonic kidney cells [12]; 0.01 to $0.1\ Nm^{-2}$ for red blood cells [13]. Endothelial cells exposed to an average shear stress of $0.33\ Nm^{-2}$ (pulsatile flow) lose viability [14]; however, at a steady shear stress of $0.5\ Nm^{-2}$ this cell line remained stable [15]. It should be noted that the values of shear stress at which viability loss waa observed for the above case is for laminar flow.

Experimental Procedure

The airlift column used in these studies was an 151 cm tall and 15 cm diameter acrylic plastic cylinder with a vertical baffle along its axial length and is shown in Figure 1. Four optically flat viewing ports along its length allow the use of back-scatter laser-Doppler velocimetry (LDV) to determine local liquid velocities. Air was sparged into the column through a sieve plate with 38 holes 1.6 mm in diameter. Polymer microspheres from Duke Scientific Corp. (cat. no. 434) with diameters ranging from 100 to 500 μm were used to model microcarriers in the fermenter. The measuring apparatus consisted of a TSI 9100-5 model laser-Doppler velocimeter using a 350 mm front lens and a Nicolet 4094A digital recording oscilloscope. Powder aluminum metal was used as the seed particles for LDV measurements to be made.

The LDV system used is commonly known as a dual beam-or-fringe type of system [16]. A single component of the velocity vector is measured when a particle passes through the fringe pattern resulting in the reflected light having a frequency directly proportional to the particle's velocity. Light scattered by a particle passing through the measurement volume was reflected back along the axis of the laser and the detected signal amplified by a photomultiplier mounted atop the receiving optics assembly. Each recorded data set of 15,872 points was transferred to a Zenith 158 computer via RS-232 interface and analyzed using an algorithm written to determine the Doppler burst frequencies present within the data set. Four concentrations of microcarriers were studied; 0 g/l, 5 g/l, 10 g/l, and 15 g/l.

The program was written in BASIC and designed to detect and evaluate the characteristic frequency of suspected Doppler bursts within the data set. A single pass of a five point digital filter

$$V_i = (V_{i-2} + 2V_{i-1} + 3V_i + 2V_{i+1} + V_{i+2})/9 \qquad (6)$$

was used to reduce the noise present within the recorded data. Peaks were detected on the following basis: 1) positive and negative differences between the preceding and succeeding two points respectively from the point under consideration; 2)evaluating the first derivative using

$$V'_i = (V_{i+9} + V_{i+6} + V_{i+3} - V_{i-3} - V_{i-6} - V_{i-9})/36 \qquad (7)$$

and noting a sign change from positive to negative for the derivative. In both cases a minimum amplitude between peaks is required for the peak to be considered as a possible candidate. The first method detected high frequency Doppler bursts and the second method detected low frequency bursts. Approximately equidistant peak separation in the same time region is required for a verified burst. Since there is variation between peak separations within Doppler bursts the current separation, t_i, is divided by ten and two is added to give a separation range to determine if the subsequent peak is considered to be within the burst; that is,

$$t_i - (t_i/10 + 2) < t_{i+1} < t_i + (t_i/10 + 2)$$

Suspected Doppler bursts must have at least four detected peaks to be recorded. The peak separations of a verified burst are averaged and multiplied by the time interval between data points and inverted to arrive at the burst frequency.

Results and Discussion

Figure 2 displays a cumulative probability distribution for velocity for four concentrations of microcarriers at 25 C and at 0.63 fractional height above the sparge plate. Where fractional height is in relation to the entire column height. The distributions given are for the upflow side at a specific gas rate of 2.6 cm/s. From this figure it is seen that the distributions are similar with the greatest variation occurring at the end regions which will result in differing values of RMS velocity.

Figure 3 displays the mean liquid velocities based on the ensemble average in relation to the fractional height above the sparge plate. The lines denote the averaged values of the mean velocities for the different microcarrier concentrations. If the case of no microcarriers present is disregarded, it can be seen that as the particle concentration increases the average velocity decreases. This decrease suggests an increase in the effective viscosity of the liquid phase. Analysis of variance performed on this data indicates that no significant differences exist between the mean velocities when all are considered together.

Figure 4 displays the RMS velocities based on the ensemble standard deviation in relation to the fractional height above the sparge plate. The lines denote the averaged values of the RMS velocities for specific concentrations of microcarriers. From this figure it is seen that the addition of microcarriers may increase the RMS velocity, however, an analysis of variance indicates that no significant difference exist for the addition of microcarriers. The use of Taylor's inviscid estimate of ϵ would show that the addition of microcarriers has increased the overall dissipation of energy on the upflow side assuming that A and ℓ are the same for all concentrations. An approximation of the integral length, ℓ, that has been proposed is the Sauter mean bubble diameter [11].

Conclusions

The presence of microcarriers within the airlift reactor may promote an increase in the turbulent dissipation of energy based upon Taylor's inviscid estimate of dissipation. Measurements of the effects that the presence of microcarriers has on the Sauter mean bubble diameter is needed to provide an integral length scale such that Taylor's large-scale inviscid estimate of ϵ can be used. Hydrodynamic modeling of the interaction of microcarriers and turbulence is needed to better understand the magnitude and frequency of shear stresses occurring on the surface of a microcarrier.

References

[1] Katinger, H. W.-D., and W. Scheirer, Developments in Biological Standardization 42:111 (1979).

[2] Birch, J. R., P. W. Thompson, K. Lambert, and R. Boraston, Large-Scale Mammalian Cell Culture, J. Feder and W. R. Tolbert, Ed., Academic Press, New York (1985).

[3] Birch, J. R., Chemtech, 17:378-381 (1987).

[4] Kong, I. C., R. D. Sjolund, and R. A. Yoshisato, Proceedings of the 17th Annual Biochemical Engineering Symposium, P. J. Reilly, Ed., Iowa State University (1987).

[5] Tramper, J., J. B. Williams, D. Joustra, and J. M. Vlak, Enzyme Microb. Technol., 8:33-36 (1986).

[6] Croughan, M. S., D. I. C. Wang, and J.-F. Hamel, Paper 7e, A.I.Ch.E. Annual Meeting, Chicago, IL (Nov., 1985).

[7] Handa, A., A. N. Emery, and R. E. Spier, Developments in Biological Standardization 66:241-253 (1987).

[8] Cherry, R. S., and E. T. Papoutsakis, Proceedings of the World Congress III of Cheimical Engineering Tokyo 1986, 1:805-808 (1986).

[9] Hinze, J., Turbulence, McGraw-Hill, New York (1975).

[10] Tennekes, H., and J. L. Lumley, A First Course In Turbulence, MIT Press, Cambridge, Massachusetts, (1972).

[11] Jones, G. T., Proceedings of the 17th Annual Biochemical Engineering Symposium, P. J. Reilly, Ed., Iowa State University (1987).

[12] Stathopoulos, N. A., and J. D. Hellums, Biotech. Bioeng. 27:1021 (1985).

[13] Chein, S., Blood Cells, 3:71 (1977).

[14] Eskin, S. G., L. T. Navarro, W. O'Bannon, and M. E. DeBakey, Second US-USSR Joint Symposium on Circulatory Assistance and Artificial Heart (Sept., 1981).

[15] Dewey, C. F., S. R. Bussolari, M. A. Gimbrone, and P. F. Davies, J. Biomech. Eng. 103:177 (1981).

[16] Durst, F., A. Melling, and J. H. Whitelaw, Principals and Practices of Laser-Doppler Anemometry, Academic Press, New York (1981).

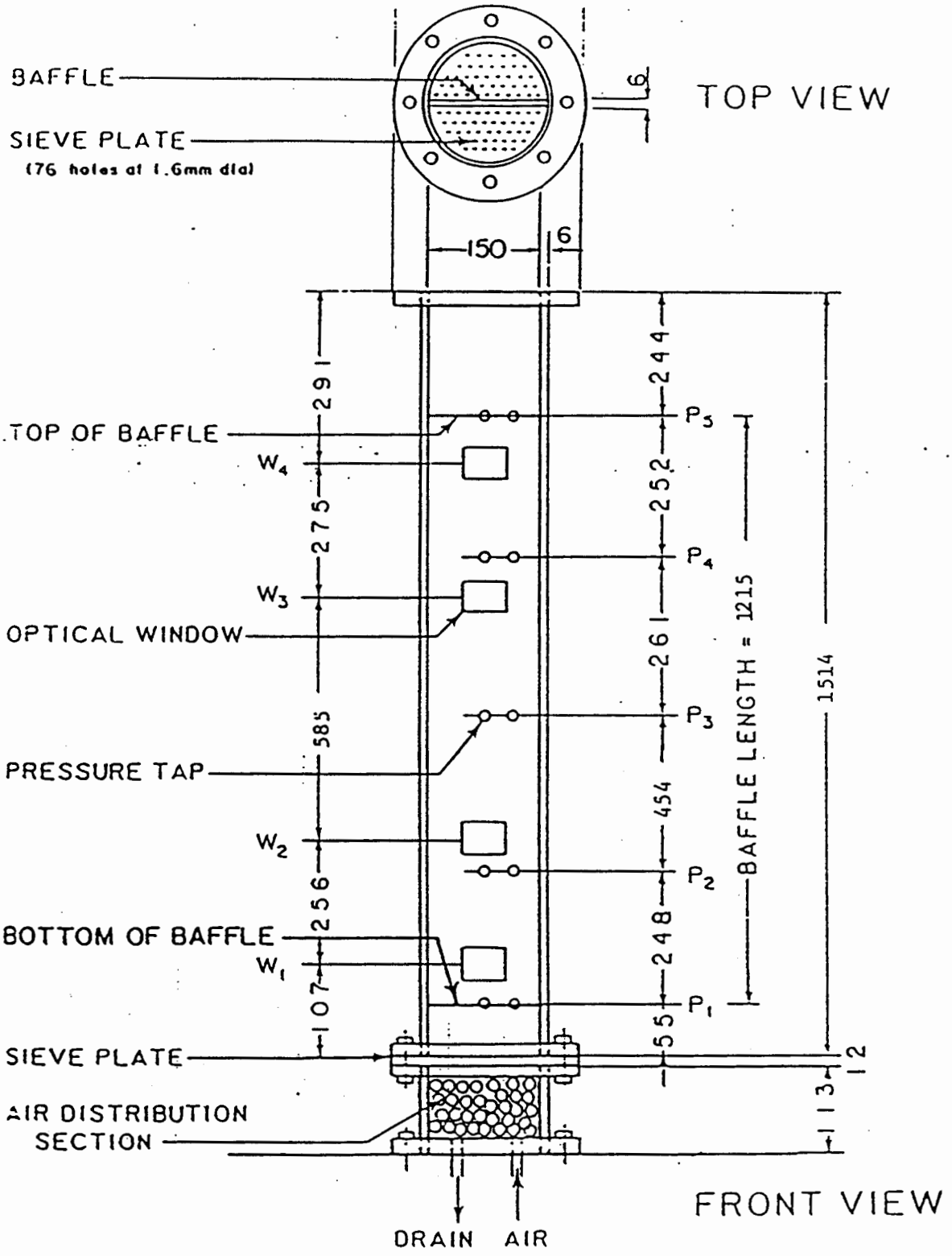

Figure 1. Acrylic plastic airlift column used in the experiments (all dimensions are in millimeters).

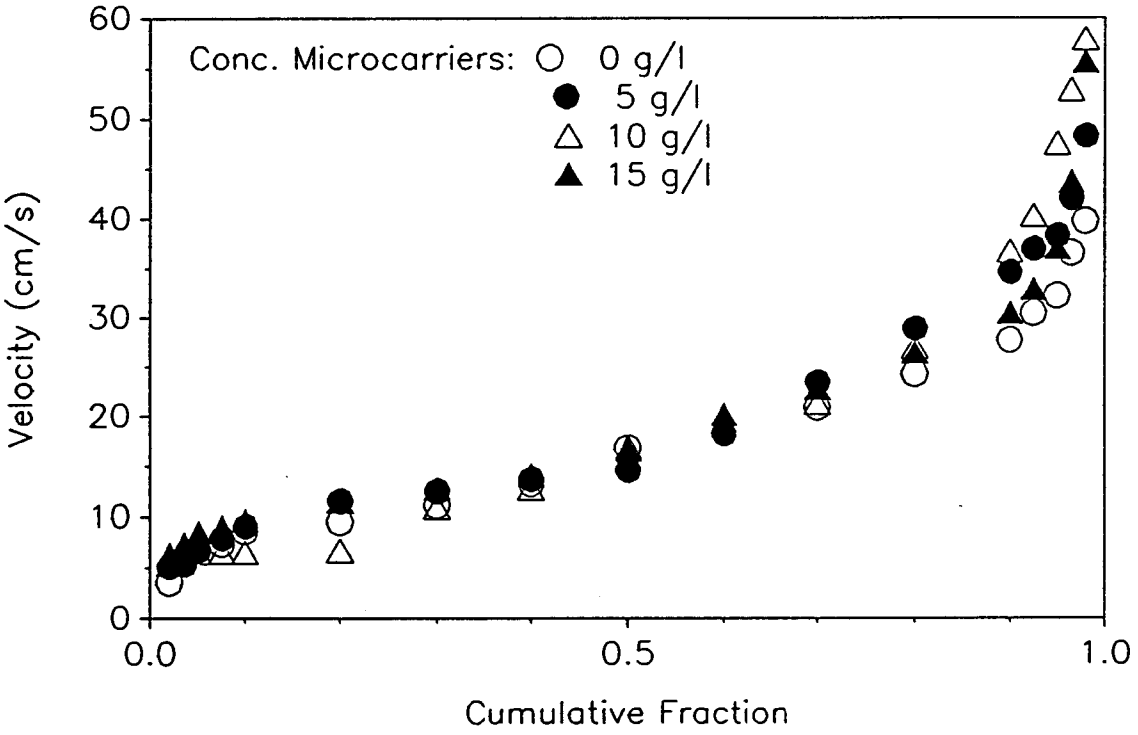

Figure 2. **Cummulative frequency distribution for the velocity occurring at a fractional height of 0.63 above the sparge plate on the upflow side for a specific gas rate of 2.6 cm/s.**

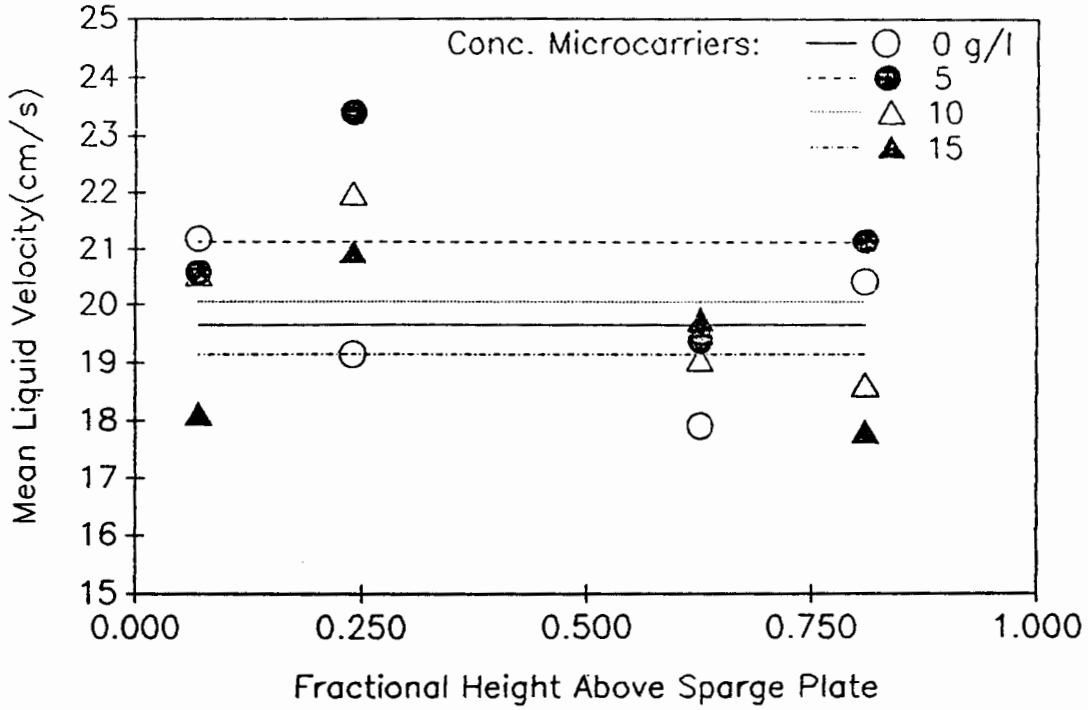

Figure 3. **Mean velocity of the liquid phase on the upflow side of the column for a specific gas rate of 2.6 cm/s with different concentrations of microcarriers present.**

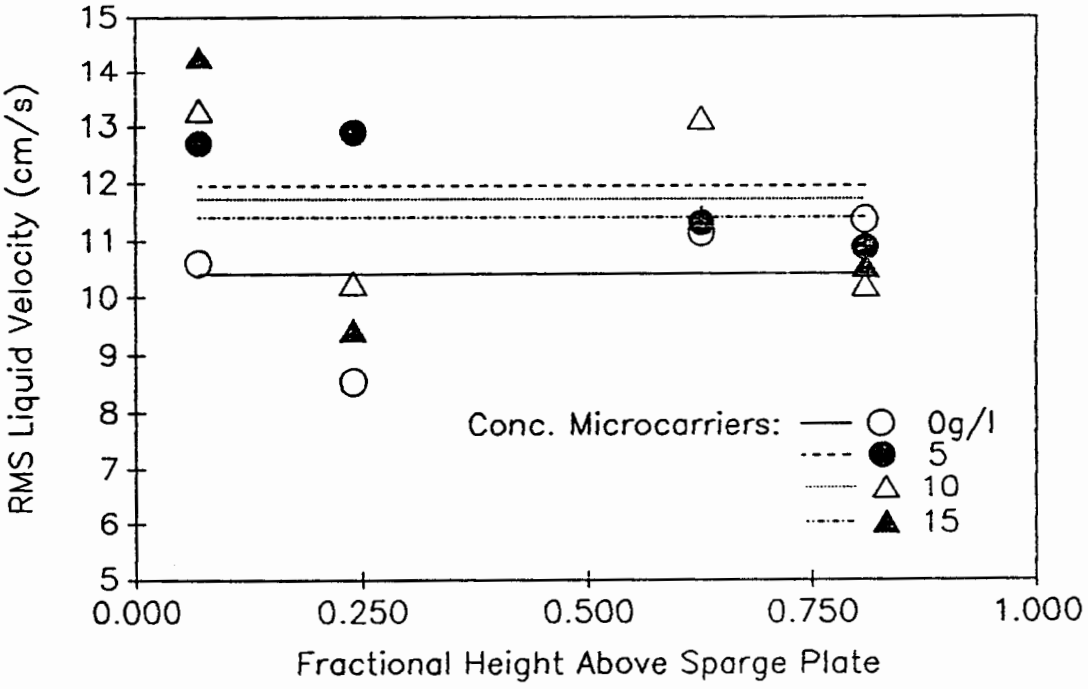

Figure 4. **RMS velocity of the liquid phase on the upflow side of the column for a specific gas rate of 2.6 cm/s with different concentrations of microcarriers present.**

OXYGEN DIFFUSION IN THE INTER-FIBER GEL/CELL MATRIX OF NMR-COMPATIBLE HOLLOW FIBER BIO-REACTORS

S.L. Hanson, B.E. Dale, and R.J. Gillies*
Department of Agricultural and Chemical Engineering
*Department of Biochemistry
Colorado State University
Fort Collins, CO 80523

ABSTRACT

The problem of adequate oxygen supply to immobilized mammalian cells in hollow fiber bio-reactors must be solved to achieve optimal cell growth. Proper characterization of oxygen transfer in the inter-fiber gel/cell matrix of hollow fiber bio-reactors is essential for the design and operation of such reactors. To accurately estimate the oxygen concentration profile in the inter-fiber space, the diffusion coefficient of oxygen and its relationship to cell density and percent solids in the gel matrix is being investigated.

INTRODUCTION

Since the early part of this century mammalian cells 'in vitro' have been successfully cultured and studied on a small scale[1,5]. Within the last twenty years, industry has become increasingly interested in some of the important and valuable products that can be produced by mammalian cells[2]. Examples of these products are listed in Table 1.

As these original bench scale processes are scaled-up many problems are being encountered. Foremost of these is adequate oxygen transfer to the cells[7]. This problem is experienced mainly because of the low solubility of gases in aqueous mediums. The maximum oxygen concentration is only 0.254 mM in water at 25°C and 1 atmosphere, and with high cell densities required for large-scale processes the problem of low oxygen concentrations is exacerbated as the cells rapidly deplete what little oxygen is available. The problem can be further complicated if the cells are immobilized. Cell immobilization can create an increased diffusion path length which causes the cells to see even less oxygen than if they were freely suspended[2].

Even on the bench level the problem of decreased oxygen availability due to immobilization has been encountered. Chresand, Dale, and Gillies[4] have developed a nuclear magnetic resonance (NMR) compatible hollow fiber bio-reactor (HFBR) for on-line analysis of mammalian cells. This

TABLE 1[7]

List of Potential Products from Mammalian Cell Cultures	
Group 1:	Cells as End Products
	Artificial skin
	Artificial organs
	Beta-islet cells (pancreas)
	Hepatocytes (liver)
	Bone Marrow
	Lymphocytes
Group 2:	Cell-derived Products
	Growth factors
	Nerve growth factor
	Epidermal growth factor
	Blood factors
	Monoclonal antibodies
	Interferons
	Proteases (Urokinase, act.)
	Vaccines
	Hormones
	Human growth hormone
	Insulin
	Calcitonin
	Parathyroid hormone

TABLE 2

Diffusion Coefficients of Oxygen In Various Gels Used For Immobilization

$D_{O_2} \times 10^5$ (m^2/sec)	Immobilization Gel	Method	Ref.
2.11	Ca-Alginate	1	1
0.68	Ba-Alginate	1*	8
1.92	Agar	2*	16

Methods:
(1) Effectiveness Factor - the diffusion coefficiant is estimated from the effectivveness factor of the overall reaction.
(2) A special diffusion apparatus measures directly the uptake of oxygen by the gel and the diffusion coefficient is then calculated.

*Partition Coefficient assumed equal to 1.0

bio-reactor is a prototype of the original cartridge design of Knazek developed in 1972[10]. The difference is that the cells are immobilized in the extra capillary space (ECS) of this reactor instead of just growing attached to the outside of the fibers as was Knazek's original design. The immobilization increases the surface area available for cell attachment and allows for high cell densities to be reached.

Using this reactor, these investigators have obtained global cell densities on the order of 7×10^7 cells/ml. However, the problem of axial and radial gradients in the cell population has been observed. This behavior is believed to arise due to inadequate oxygen transfer in the inter-fiber gel/cell matrix. Since the nature of NMR analysis requires homogeneous conditions these cellular gradients must be overcome to achieve true NMR compatibility.

Optimal reactor design plays an important part in making this bio-reactor homogeneous. Since it is believed oxygen is the limiting substrate the correct oxygen concentration profiles are necessary for adequate design. To obtain these profiles the diffusion coefficient of oxygen through the gel/cell matrix must be known.

Oxygen diffusion coefficients through aqueous mediums have been widely studied and are very abundant in the literature. However, reports of diffusion coefficients of oxygen in gels is very limited. Table 2 lists the available data and how they were obtained for oxygen diffusion in gels commonly used for cell immobilization. There is clearly a need for further investigation into this subject.

The objective of the research presented in this communication is to characterize oxygen transfer, with respect to dissolved solids in the gel, into the inter-fiber gel/cell matrix of these NMR-compatible hollow fiber bio-reactors described above so that an accurate oxygen concentration profile may be obtained and the reactors optimized with respect to oxygen diffusion.

MATERIALS AND METHODS

Cell Membrane Integrity. Twenty microliters of ^{35}S was added to a 250 milliliter spinner flask containing Erlich Ascites Tumor (EAT) cells grown in Eagles Modified Medium (SMEM) with 10% Fetal Bovine Serum (FBS) (Gibco) to a density of 2.9×10^5 cells/ml. After an incorporation time of 17 hours two 25 milliliter aliquots of the labeled cells were harvested, spun down, and washed twice in 10 ml Hanks Balanced Salt Solution (HBSS). One of the pellets was re-suspended in 10 ml of HBSS and the other was fixed for one hour with 1% glutaraldehyde. The glutaraldehyde was neutralized with 100 mM ammonium chloride and then these fixed cells were re-suspended in 10 ml of HBSS. Fifty microliters of tritiated leucine was added to each suspension and at specific time points a 0.5 milliliter aliquot was taken, the cells separated, and counted on a liquid scintillation counter (Beckman LS 78,000).

The Diffusion Chamber. The chamber used for measuring oxygen diffusion is shown schematically in Figure 1. It was machined out of polymethylmethacrylate or Plexiglass (Regal). The bottom portion of the diffusion chamber contained the gel matrix. The dimensions of this gel chamber were critical to the success of the experiment. The matrix had to be tall and thin so its integrity was maintained under vigorous stirring at the matrix/bath interface, but also wide enough so that no meniscus formed when the gel hardened so as to ensure a planer interface between gel and bath. The bath was contained in the upper portion of the chamber and a stir bar was placed on the lip between the gel matrix and the bath to allow stirring. The chamber was encased in a water jacket for temperature control. The chamber cap, shown in Figure 2, had a hollowed out center where the YSI 5331 Oxygen Probe fit. A good seal was ensured between the cap and the probe by the membrane o-ring. To keep the chamber free of oxygen during the experimental preparation a second cap was constructed with two ports to allow a nitrogen purge. An o-ring seal between the cap and the body of the chamber rendered the chamber hermetic.

Oxygen Measurements. The gel was either a 2%-6% agar gel or a 1% gel/EAT cell matrix. Both were made with Bacto Difco Agar and a 0.01% Sodium Azide solution as the aqueous phase. The stirred bath was also a 0.01% Sodium Azide solution that had been saturated with air. The agar was measured out, heated to a boil, and purged for approximately 15-20 minutes with

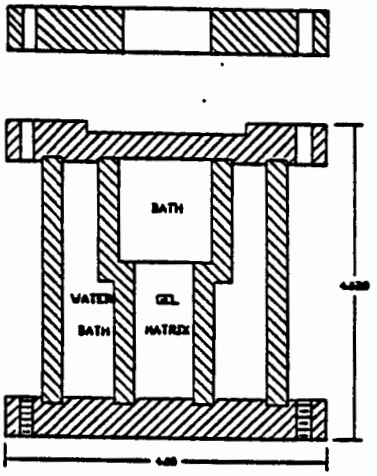

FIGURE 1 DIFFUSION CHAMBER BODY

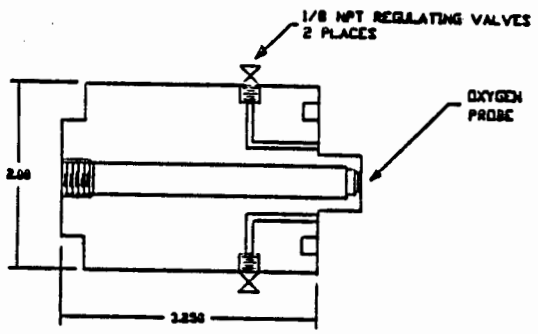

FIGURE 2 DIFFUSION CHAMBER CAP

nitrogen. A vacuum was then drawn to remove any bubbles which would later be voids in the hardened gel, and further remove any dissolved oxygen from the gel. If a gel/cell matrix was desired EAT cells were grown in spinner flasks to a density of approximately 4 x 10^5 cells/ml, harvested and fixed for one hour with a 1% glutaraldehyde solution. The cells were then re-suspended in HBSS that had been purged with nitrogen and de-gassed and then this mixture was added to an equal volume of 2% agar treated as described above. Thirteen milliliters of the liquid agar was pipetted into the lower gel matrix chamber and allowed to polymerize under a nitrogen purge. The whole apparatus was then placed inside the anaerobic chamber to ensure further removal of oxygen. After approximately 24 hours the diffusion chamber was removed from its anaerobic environment and thermal equilibrium established. The experiments were carried out at either 25°C or 37°C.
The second cap was then exchanged with the cap housing the oxygen probe and the chamber sealed. Aerated water at the same temperature as the gel was introduced into the chamber through a port in the cap, the port sealed off, and the stir bar started. The oxygen tension measurement was registered on a YSI Biological Oxygen Monitor (model 5300) and recorded on a Houston Instruments Microscribe Recorder over a period of approximately 2-3 hours. The difference between the initial and final oxygen tension was used to determine the diffusion coefficient, and probe consumption was negligible over the time of these experiments. To determine the partition coefficient the above procedure was repeated except the experiment was allowed to continue until equilibrium had been established between the bath and gel. Equilibrium was usually reached in 10 to 18 hours.

Probe Drift. The particular oxygen probe used in this set of experiments exhibited quite a bit of probe drift and was very sensitive to stirring conditions. To determine what portion of the apparent change in oxygen concentration could be attributed to probe drift and what was actual diffusion into the gel an oxygen tension measurement of a standard salt solution was measured before and after the diffusion experiment. Care was taken to make sure the standard solution was measured at the same temperature and the same stir rate for both the initial and final standardization measurements.

RESULTS AND DISCUSSION

Theory

As mentioned earlier, the NMR-compatible HFBRs, shown schematically in Figure 3, must exhibit uniform conditions to be used to obtain accurate NMR scans. This reactor is modeled as diffusionally limited[4] and oxygen is the suspected limiting substrate. A cross section of an individual hollow fiber, Figure 4, shows the expected relative radial concentration gradients in the reactor. The hypothesis is this drop in concentration causes the cells farther from the fiber edge to see little oxygen and consequently not grow as densely as the cells closer to the fibers. By optimizing the fiber spacing the radial oxygen concentration decrease seen by the cells can be minimized while not greatly reducing the area available for cell growth.

The inter-fiber region, or cell annulus, is represented by the following continuity equation:

$$\frac{D_a}{r}\frac{\delta}{\delta r}\left(r\frac{\delta C}{\delta r}\right) = V \qquad (1)$$

with

$$D_f\frac{\delta C}{\delta r} = D_a\frac{\delta C}{\delta r} \quad \text{at} \quad r = R_o$$

$$\frac{\delta C}{\delta r} = 0 \quad \text{at} \quad r = MP$$

where D_a = the diffusion coefficient of the limiting substrate (oxygen) through the cell annulus
V = the consumption term -- dependent upon cell density
D_f = substrate diffusion through the fiber
R_o = the hollow fiber edge
MP = the midpoint between fibers

V is assumed zero order rate (maximum rate) of consumption. The corresponding boundary conditions reflect continuity of

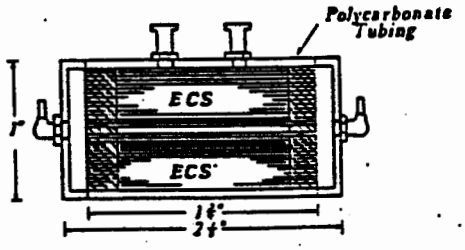

FIGURE 3. NMR-compatible hollow fiber bio-reactor.

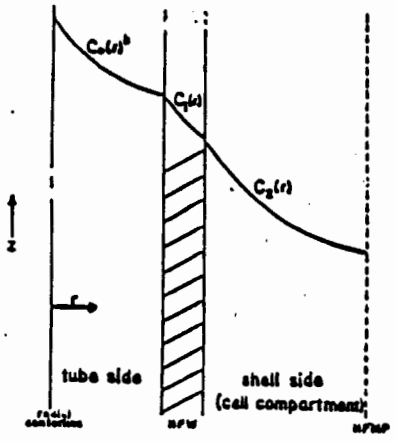

FIGURE 4. Predicted relative concentration gradients in a single hollow fiber.

flux at the fiber wall, and account for the symmetry between adjacent fibers respectively. The necessity for a correct diffusion coefficient of oxygen through the cell annulus is obvious from these equations.

To determine this value a stirred bath experiment detailed by Crank[5] was employed. This experimental protocol assumes a sheet, x, of uniform thickness, l, initially free of the solute of interest, $C_s = 0$. The sheet is in contact with a well stirred bath of uniform concentration, C_b, and volume equal to a. If the bath is well stirred that the change in solute concentration in the bath is only time dependent, and is determined by the fact that the total amount of solute remains constant as diffusion proceeds. Therefore, we can calculate the diffusion coefficient through the sheet if we assume Fickian diffusion, equation 2, applies,

$$\frac{\delta C}{\delta t} = -Do_2 \frac{\delta^2 C}{\delta x^2} \qquad (2)$$

with

$C_s = 0$ at $t = 0$
$C = C_b$ at $x = 0$
$dC/dX = 0$ at $x = 1$

and add a balance on the bath, equation 3, expressing the fact that the rate the solute leaves the bath is equal to the rate at which it enters the sheet over the surface at x = 0.

$$\frac{a*C_b}{\alpha*t} = Do_2 \frac{\delta C}{\delta x} \qquad (3)$$

Then, by the use of a LaPlace transform we can obtain an expression which relates the solute concentration in the sheet

at time t , M_t, to the amount of solution in the sheet after infinite time , M_∞, to the effective diffusion coefficient of the solute through the sheet. This relationship is shown below as equation 4

$$\frac{M_t}{M_\infty} = 1 - \sum_{n=1}^{\infty} \frac{2*\alpha*(1+\alpha)}{1+\alpha+\alpha^2 q_n^2} \exp(-D*q_n^2*t/l^2) \qquad (4)$$

where q_ns are the non-zero positive roots of

$$\tan q_n = \alpha * q_n$$

and $\alpha = a/l*K$ where K = the partition coefficient between sheet and bath.

The value for the desired diffusion coefficient can then be easily obtained by the use of numerical analysis.

To determine the necessary values for equation 4 a special diffusion apparatus was designed. It was modeled after the apparatus developed by Chresand et al[3] which they used to successfully find the diffusion coefficients of glucose and lactate through a gel/cell matrix. The apparatus and the necessary modifications are described in the Materials and Methods section of this paper.

It was necessary to ensure the chamber was hermetic and that no head space was present during the experiment or erroneously large or small oxygen concentration changes would be recorded. Sodium Azide was used in the aqueous phase through out the chamber due to an interesting problem encountered with the plexiglass material. Apparently, plasticizers leached out of the plastic and bacteria present in the chamber consumed these organics and subsequently consumed the oxygen. This created huge oxygen concentration drops in the chamber when only distilled water was present. The Sodium Azide killed the bacteria and a straight base line was obtained.

Cell Membrane Integrity. To uncouple reaction from diffusion the cells were fixed with 1% glutaraldehyde. Glutaraldehyde cross links the primary amines of the cell proteins[9] and effectively shuts off metabolic activity. The uptake rates of the leucine by fixed and non-fixed cells were studied to determine if the fixing procedure disrupted the cell membrane integrity. The results, shown in Figure 5, demonstrated active diffusion of the acetate into the non-fixed cells and passive diffusion into the fixed cells. If the cell membranes had been broken we would have seen a very rapid increase in the amount of leucine in the cells as the molecule passed freely through the cell membrane to reach equilibrium.

Partition Coefficient. Using the equation

$$K_{gel/bath} = C_{gel\infty} / C_{bath\infty} \qquad (5)$$

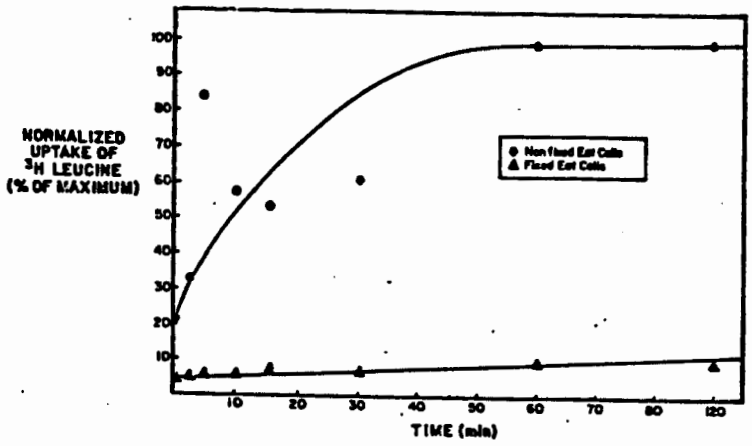

FIGURE 6. ³H Leucine uptake by fixed and non-fixed EAT cells.

the partition coefficient between the gel and the bath was obtained. For the oxygen/1% agar system, $K_{gel/bath}$ = 0.64, with a standard deviation[13] of + or - 0.06 around the mean, indicating the oxygen favored the aqueous solution over the agarose gel. This is understandable if one remembers how insoluble oxygen is in water. The added hindrance of the agarose gel, although it is 99% water, could conceivably exclude the oxygen to a greater extent than the water.

Diffusion Coefficient. The diffusion coefficient in a 1% agar gel at 25°c was 3.3 x 10^{-4} cm^2/sec, with an error[6] of 30%. This is contradictory to what would be expected for oxygen diffusion in a gel. The theoretical expression for diffusion through a gel is given by Lauffer[11] and relates the effective diffusion coefficient to the volume fraction, ϕ, of solids in the gel. This expression is shown in equation 6,

$$\frac{D_e}{D} = \frac{1 - a\phi}{1 - \phi} \qquad (6)$$

where 'a' is the coefficient of obstruction. For a gel considered to be made up of randomly oriented rods 'a' is equal to 5/3. This is the value Lauffer suggests for agar gels[17]. The value obtained from our system was more than an order of magnitude greater that the diffusivity of oxygen through pure water at the same temperature, D_{O_2} in pure water at 25°C equals approximately 2.6 x 10^{-5} cm^2/sec (this value varies from source to source), making the right hand side of equation six greater than one. This contradicts Lauffer's discoveries.
A possible explanation would be if there was some type of reaction occurring to facilitate diffusion through the gel. In the case of facilitated diffusion equation 6 in not valid.

To determine the extent of the gel/solute interaction the activation energy of diffusion, E_D, can be used. This is found from equation 7,

$$E_D = \frac{R*T_1*T_2}{T_2 - T_1} \ln \left(\frac{D_2}{D_1} \right) \qquad (7)$$

which requires the diffusion coefficient at two different temperatures. Activation energies of diffusion are usually on the order of 4 to 5 kcals/mole at temperatures of 25°C[12]. Chemical reactions have activation energies on the order of 30 kcals/mole. Consequently, a significant interaction between gel and solute can be assumed if E_D is greater than 5 kcal/mole. At 37°C, however, the diffusion coefficient obtained was 4.4×10^{-4} cm^2/sec which gives us an activation energy of diffusion equal to approximately 4 kcals/mole. With the error included into both terms there is no real difference between the two values which would lead to an E_D of much less than 5 kcal/mole. This seems to discredit our findings.

CONCLUSIONS

It is the belief of this investigator that the failing lies in the system. The data obtained are contradictory, both to prior theory and each other. A number of failings can be cited: (1) the pre-treatment of the agar may be changing the structure of the agar and altering the apparent D_{o2}. (2) The assumption that the pre-treatment satisfies the boundary conditions, i.e. initial concentration of oxygen equal to zero, may not be true, and the extent to which the oxygen is removed may vary from run to run. (3) The oxygen probe, which is where the majority of the error emanates, is notoriously unstable[14]. In the period of time it takes to reach a steady-state value the initial oxygen tension value is lost. By changing the starting oxygen tension value by 2 percentage points the apparent diffusion coefficient can be changed by as much as 50%.

A better design would be a dynamic system which would allow the measurement of the appearance of oxygen through a slab of un-treated gel instead of the disappearance of oxygen into a gel that has been treated to remove the oxygen. This would eliminate the sources of error now plaguing these measurements.

Although this research project did not produce the desired results, the data that was obtained should be useful in future studies of this nature.

REFERENCES

1. Adlercruetz, Patrick, Biotechnology and Bioengineering, 28:223-232 (1986).
2. Bailey, James E., and Ollis, David F., Biochemical Engineering Fundamentals, McGraw-Hill Book Company, 2nd ed., 1986.
3. Chresand, Thomas J., Dale, Bruce E., Gillies, Robert J., and Hanson, Shari L., A Stirred Bath Technique for Diffusivity Measurements in Cell Matrices, Biotechnology and Bioengineering, in press (1988).
4. Chresand, T.J., Gillies, R.J. and Dale, B.E., Optimum Fiber Spacing in A Hollow Fiber Bio-reactor, Colorado State University, unpublished data.
5. Crank, J., The Mathematics of Diffusion, 2nd ed., Clarendon Press, 1975.
6. Day, R.A. Jr., and Underwood, A.L., Quantitative Analysis, 2nd ed., Prentice-Hill, Inc., 1967.
7. Glacken, M.W., Fleischaker, R.J., and Sinsky, A.J., Annals New York Academy of Science, 413:355-371 (1983).
8. Hiemstra, H.,Dijkhuizen, L., and Harder, W., Eur. J. Appl. Microbiol. Biotechnol., 18:189-196 (1983).
9. Johnson, T.J., J. Electron Micros. Tech., 2:129 (1985).
10. Knazek, R.A., Gullino, P.M., Kohler, P.O. and Didrick, R.L., Science, 178:65-67 (1972).
11. Lauffer, Max A., Biophysical Journal, 1:205-213 (1961).
12. Longsworth, L.G., Journal of Physical Chemistry, 58:770 (1954).
13. Miller, Irwin, and Frend, John E., Probability and Statistics for Engineers, 3rd ed., Prentice-Hall, Inc., 1985.
14. Murphy, V.G., Barr, R.E., and Hahn A.W., Oxygen Transport To Tissue - II, Plenum Press, 69-76 (1976).
15. Pollack, R., (editor), Readings In Mammalian Cell Cultures, Cold Springs Harbor Laboratory, 1975.
16. Sato, K., and Toda, K., J. Ferment Technol, 61:239-245 (1983).
17. Schantz, E.J., and Lauffer, M.A., Biochemistry, 1(4):658-663 (1962).

Characterization of Ca-alginate gel beads formation

Horngtwu Su, Rakesh K. Bajpai, and George W. Preckshot
Department of Chemical Engineering
The University of Missouri-Columbia
Columbia, MO 65201

Introduction

In a number of bioprocesses, formation of the desired product can be effectively decoupled from growth of the cells. In such cases, immobilization of the biocatalyst is often practiced to improve the yield and the volumetric productivity of the processes. Immobilization is commonly achieved by injecting a suspension of cells in an appropriate gelling agent (such as aqueous solution of sodium alginate[1], κ-carrageenan[2], and chitosan[3]) through a nozzle into a suitable salt solution. The suspensions are generally non-Newtonian in nature. Sizes of the beads, thus formed, depend upon the design of the nozzle system, operating parameters, and the rheological properties of the solution/suspension being injected.

For a number of applications, beads of diameters as small as 1 mm are suspected to encounter mass transfer limitations[4]. For the encapsulation of animal cells, spherical beads in the size range of 100 - 300 μm are desirable[5]. These can be obtained by use of smaller nozzle diameters which unfortunately results into extremely small liquid flow rates and significantly increased frequency of the nozzles. Rehg *et al.*[6] used a two-fluid atomizer design for formation of small alginate beads. This report describes a two-fluid atomizer design and quantitative characterization of sizes of beads formed with it.

Materials and Methods

Chemicals and reagents

High purity Sodium Alginate (Keltone KTHV, lot#35256A) was obtained from KELCO, Clark, New Jersy. The alginate powder was dry autoclaved at 250^{0}F for 20 minutes and then slowly dissolved in distilled water at concentration levels of 1% (w/v) and 1.5% (w/v). The alginate beads were harden by reaction with 0.1 M $CaCl_2$ (Sigma, St. Louis, Missouri).

Experimental Set-up

The two-fluid atomizer system for injection formation of beads is shown in Figure 1. It consists of a pressure tank for holding liquid solution or suspension, an extrusion nozzle, and a collection vessel. A detailed schematics of the extrusion nozzle is shown in part A of Figure 1. The nozzle assembly is made of brass parts which can be easily assembled or disassembled for cleaning or replacement of the hypodermic needles. The whole assembly can be sterilized and a quick-connector has been used on the solution side in order to permit sterile connections to the cell suspensions. The length of the bottom tube (a) was adjusted such that its end corresponded to the tip of the needle. This design permitted use of

needles of different lengths as well as formation of a manifold of several needles.

22 gauge (o.d. 710 μm, i.d. 424 μm, length 1") and 25 gauge (o.d. 445 μm, i.d. 302 μm, length 1.5") hypodermic needles were used in this work. Needles of smaller diameters were found to clog easily. The tips of the needles were not flattened as flattening caused wider size distributions and formation of a significant number of non-spherical beads. Flow rates of the alginate solutions through the nozzle assembly were varied by adjusting pressure in the pressure-tank. Air was blown concentrically around the needle and its flow rate was monitored with a rotameter. The air flow rate as well as the pressure in the pressure-tank were carefully controlled as operating parameters.

The distance between the tip of the needle and the surface of $CaCl_2$ solution in the collection vessel was found to be crucial for the shape of the beads. The distance was kept proportional to the gas velocity, e.g., 8" for gas velocity of 29.8 m/min, and 6" for gas velocity of 23.8 m/min to insure that uniform spherical beads formed. Since the beads are dispersed in a conical pattern from the nozzle, larger distances require use of a big trough as collection vessel. The collection vessel used in this work was a 3 liter glass beaker.

All the experiments were conducted in a controlled environment at 20^0C. The beads were allowed to harden in $CaCl_2$ solution for one hour before their distributions were measured under a microscope fitted with a micrometer. Sizes of at least 100 beads were measured for each operating condition. As beads were allowed to stay longer in $CaCl_2$ solution , agglomerates were formed. Upon transfer into isotonic solutions, these agglomerates quickly dispersed into individual beads without affecting their size distribution.

Rheological Properties

Dry autoclaving of alginate powder results into changes in the rheological properties of alginate solutions. Therefore, the rheological properties of alginate solutions were estimated by using the present set-up as a capillary viscometer. Flow rates were measured for different values of pressure drops across the capillary and these data were fitted into the following expression for flow of power law fluids through capillary:

$$Q_1 = (\Delta p)^{1/m} \, [1/(2Lk)]^{1/m} \, [m/(3m+1)] \, R^{(3m+1)/m} \, \pi \qquad (1)$$

The 1% and 1.5% solution were found to follow power law model very well. For 1% solution, the flow index (m) was 0.67 and the consistency index (k) was 5.32 $g \cdot s^n/cm$. For 1.5% solution, these values were 0.62 and 18.4 $g \cdot s^n/cm$, respectively.

The Reynold's numbers of alginate solutions were also obtained by the power law model:

$$Re_1 = 2^{3-m} \, [m/(3m+1)]^m \, (d_n{}^m \rho v^{2-m})/k \qquad (2)$$

Results and Discussion

Bead size distributions were measured for different combinations of gas velocities (23.8 - 32.8 m/min), liquid flow rates (0.5 - 14.1 mL/h), needle sizes (22 and 25 gauge), and alginate concentrations (1% and 1.5% w/v). These were used to calculate the average bead diameters and standard deviations. These results are presented in Table 1. Several distributions were repeatedly measured and excellent reproducibility of data was confirmed. Figure 2 show some typical bead size distributions for different operating conditions. The qualitative nature of the results clearly shows in Figure 3 that the average bead diameter is very sensitive to gas velocity, it is not affecting by liquid flow rate, and the nozzle diameter has only a moderate influence. The bead size is one to two order of magnitudes smaller and the standard deviations are comparable to those made by Hulst *et al.*[7]

The average bead diameters have been plotted in Figures 3a, 3b, and 3c as a function of gas flow rates. The measurements for 1.5% alginate solution show a linear reduction in bead diameter with increasing gas velocity. The data for 1% alginate solution have a complex dependence on gas velocity. Unlike the experience of Rehg *et al.*[6], an attempt to explain these data with the help of Nukiyama and Tanasawa[8] correlation for two fluid atomizer was not successful. The gas velocities in the present work were many fold higher than those used by Rehg *et al.*[6] which may be the primary reason for failure of the correlation. The other attempt to make a dimensionless plot of ln Re_l vs. ln (d_b/d_n) as shown in Figure 4 was also not successful. In order to find a better dimensionless correlation which may be able to explain this phenomenon, the surface tensions of alginate solution at different concentration levels are also needed to be studied in the future work.

Conclusions

A two-fluid atomizer has been shown to be capable of producing small alginate beads in the range of 50 - 500 μm mean diameter. The distributions are as narrow as those obtained with other comparable methods producing considerably larger beads. These can be further narrowed by superimposing vibrational resonance upon two-fluid atomization, as suggested by Haas[10].

Nomenclature

d_b	average diameter of beads, μm.
d_n	external diameter of needle, μm.
k	consistency index of solution, $g \cdot s^n/cm$.
L	length of the nozzle, cm.
m	flow index of solution, dimensionless.
Δp	pressure drop across the nozzle, $g \cdot cm/s^2$.
R	internal radius of the nozzle, cm.
Re_l	Reynold's number of alginate solution, dimensionless.

Q_l liquid flow rate, cm^3/sec (cm^3/h when so stated).

v_g gas velocity around the nozzle at 20^0C and 1 atm, m/min.

ρ density of alginate solution, g/cm^3.

References

1. P. Brodelius and K. Mosbach, Adv. Appl. Microbiol., 28. 1 (1982).
2. P. Brodelius and K. Nilsson, FEBS Lett., 122, 312 (1980).
3. T. Tosa, T. Sato, T. Mori, K. Yamamoto, I. Takata, Y. Nishida, and I. Chibata, Biotechnol. Bioeng., 21, 1697 (1979).
4. D. Ryu, H. S. Kim, and H. Taguchi, J. Ferment. Technol., 62, 255 (1984).
5. A. Prokop, personal communication.
6. T. Rehg, C. Dorger, and P. C. Chau, Biotechnol. Lett., 8, 111 (1986).
7. A. C. Hulst, J. Tramper, K. van't Riet, and J. M. M. Westerbeek, Biotechnol. Bioeng., 27, 870 (1985).
8. S. Nukiyama and Y. Tanasawa, Trans. Soc. Mech. Engr. (Japan), 5, 18, 68-75 (1939). In 'Chemical Engineers Handbook', edited by R. H. Perry and C. H. Chilton, 18-58-67 (1973).
9. P. A. Haas, AIChE J., 21, 383 (1975).

TABLE 1

Alginate Conc. (w/v)	Needle size (gauge)	Vg (m/min)	Q_l (cm^3/h)	Average diameter µm	Standard deviation µm
1.0	22	32.8	0.5	38.6	7.1
		29.8		59.1	6.7
		26.8		88.4	6.0
		23.8		423.0	11.1
1.0	22	32.8	4.7	66.7	7.6
		29.8		82.4	7.7
		26.8		104.0	7.7
		23.8		442.0	17.0
1.0	22	32.8	11.0	63.9	9.6
		29.8		86.4	10.1
		26.8		107.0	7.6
		23.8		439.0	15.5
1.0	25	32.8	1.3	56.9	6.0
		29.8		62.6	6.4
		26.8		311.0	11.1
		23.8		402.0	8.4
1.0	25	32.8	2.2	49.6	6.2
		29.8		60.6	9.7
		26.8		328.0	11.5
		23.8		406.0	8.7
1.0	25	32.8	3.3	48.1	6.7
		29.8		63.7	12.2
		26.8		282.0	15.1
		23.8		401.0	9.0
1.5	22	32.8	6.5	150.0	11.1
		29.8		309.0	13.4
		26.8		447.0	13.5
		25.3		540.0	15.4
		23.8		609.0	7.6
1.5	25	32.8	14.1	103.0	9.3
		29.8		252.0	15.1
		26.8		377.0	13.2
		25.3		423.0	15.1
		23.8		541.0	11.5

Titles of Figures

Figure 1 - Experimental set-up

Figure 2 - Bead size distribution:
(a) - 22 gauge nozzle, gas velocity = 32.8 m/min, liquid flow rate = 0.5 cm^3/h, concentration = 1% w/v.
(b) - 22 gauge nozzle, gas velocity = 29.8 m/min, liquid flow rate = 6.5 cm^3/h, concentration = 1.5% w/v.
(c) - 25 gauge nozzle, gas velocity = 23.8 m/min, liquid flow rate = 1.3 cm^3/h, concentration = 1% w/v.
(d) - 25 gauge nozzle, gas velocity = 23.8 m/min, liquid flow rate = 14.1 cm^3/h, concentration = 1.5% w/v.

Figure 3(a) - Average bead diameter as a function of gas flow rate, 22 gauge, concentration = 1% w/v.
3(b) - Average bead diameter as a function of gas flow rate, 25 gauge, concentration = 1% w/v.
3(c) - Average bead diameter as a function of gas flow rate, concentration = 1.5% w/v.
3(d) - Average bead diameter as a function of liquid flow rate, 22 gauge, concentration = 1% w/v.

Figure 4 - Dimensionless diameter as a function of liquid Reynold's number. Closed symbols are for 22 gauge needle and open symbols are for 25 gauge needle.

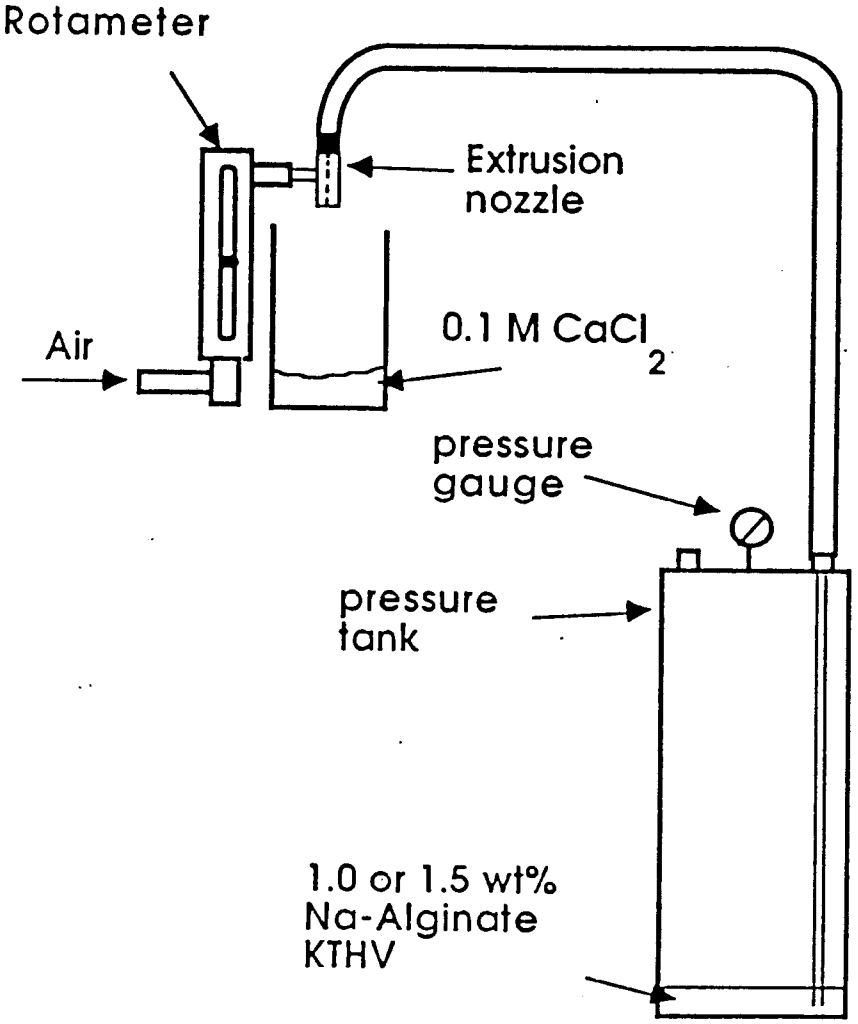

FIGURE 1

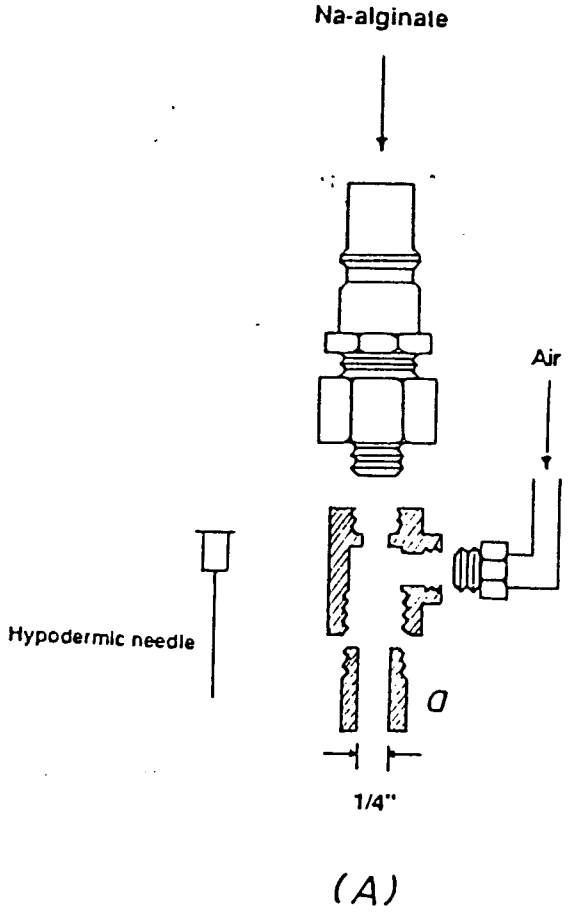

Design of extrusion nozzle

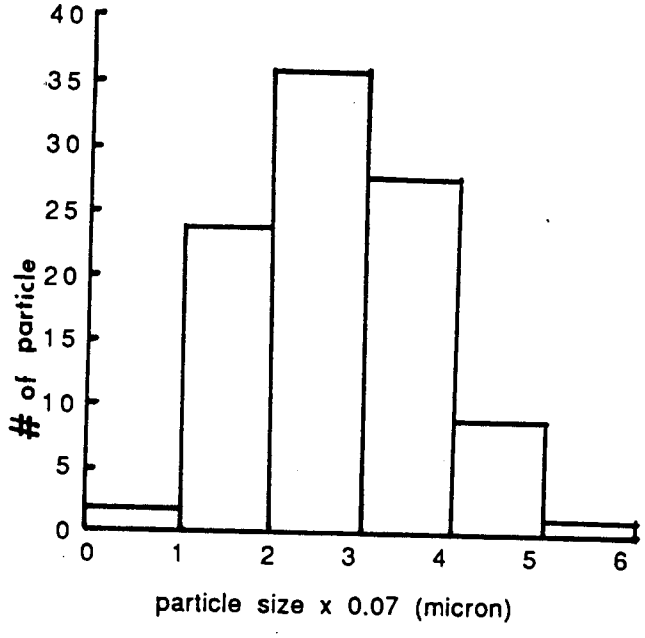

(a)

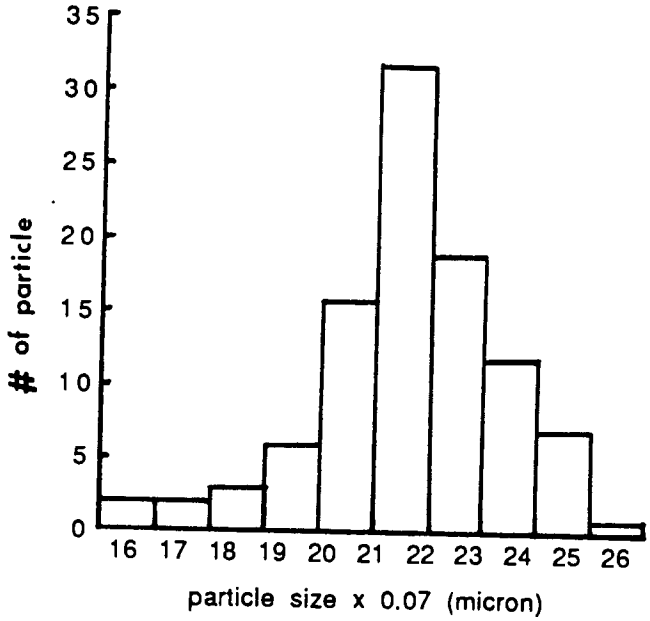

(b)

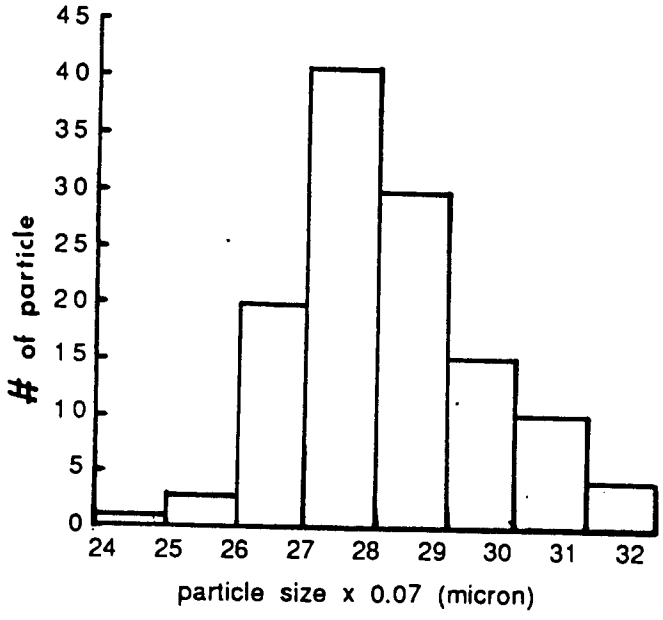

(c)

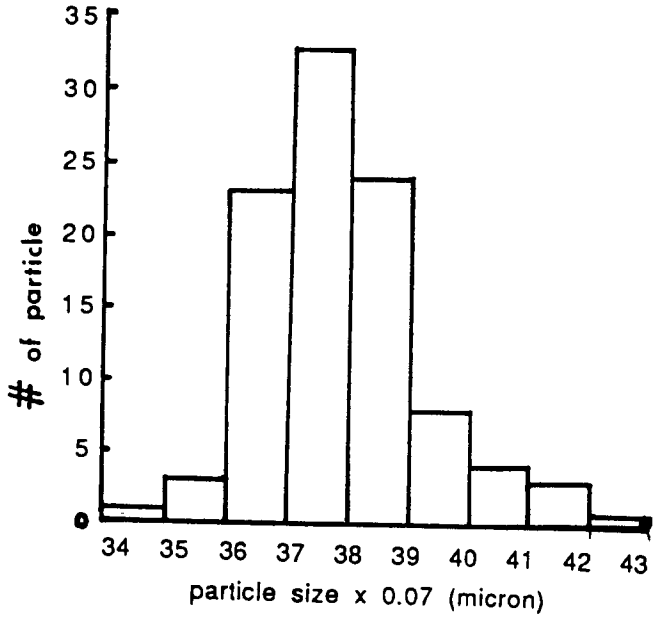

(d)

FIGURE 2

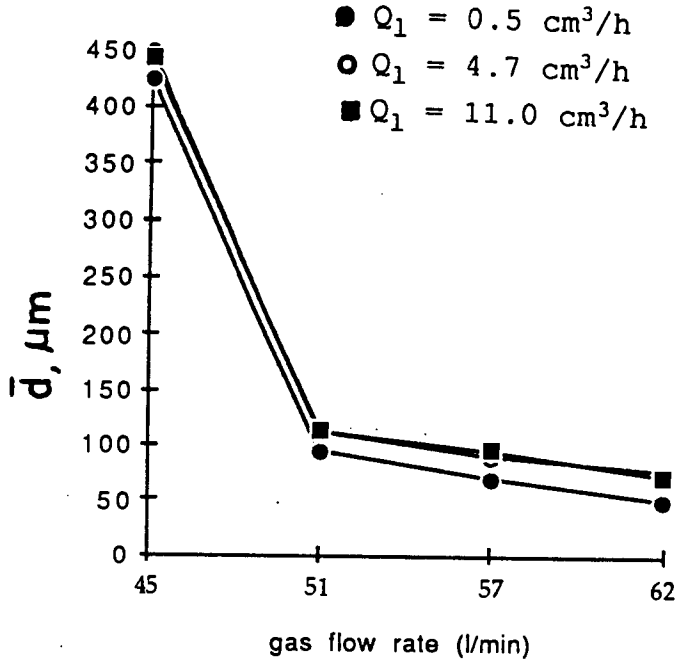

(a)

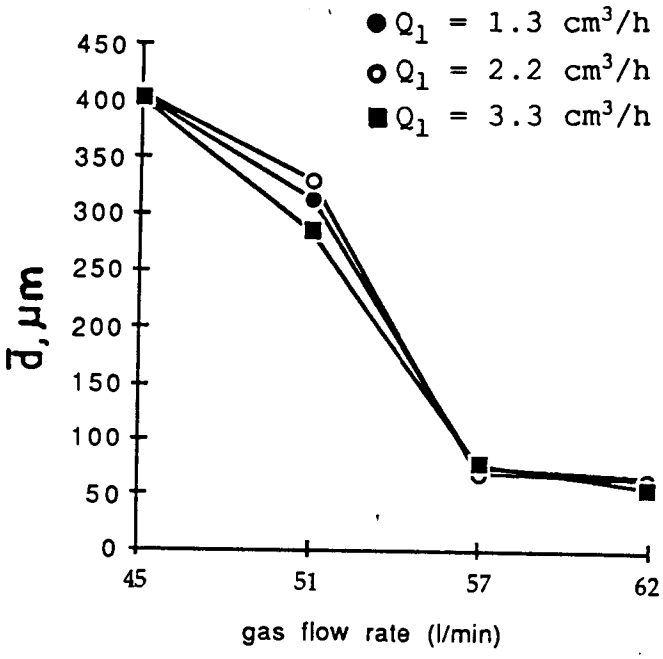

(b)

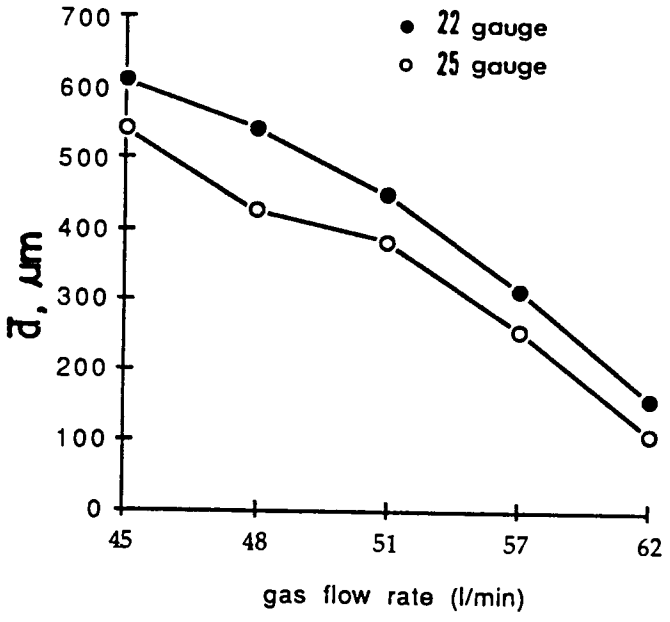

(c)

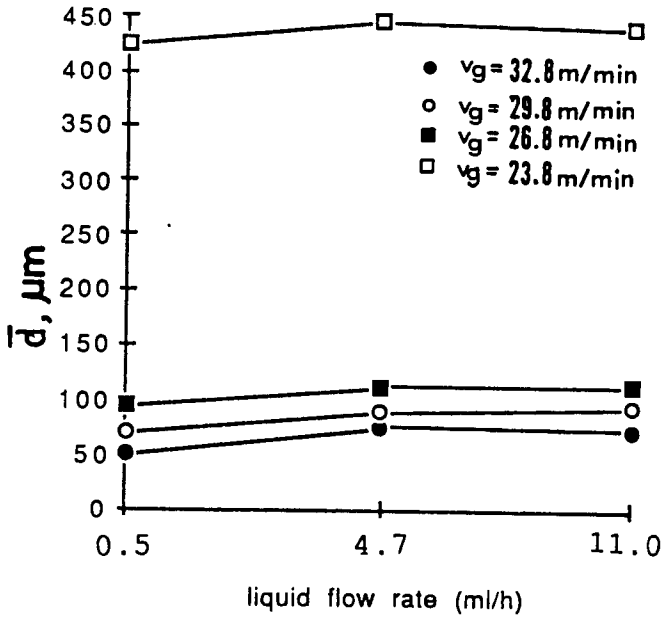

(d)

FIGURE 3

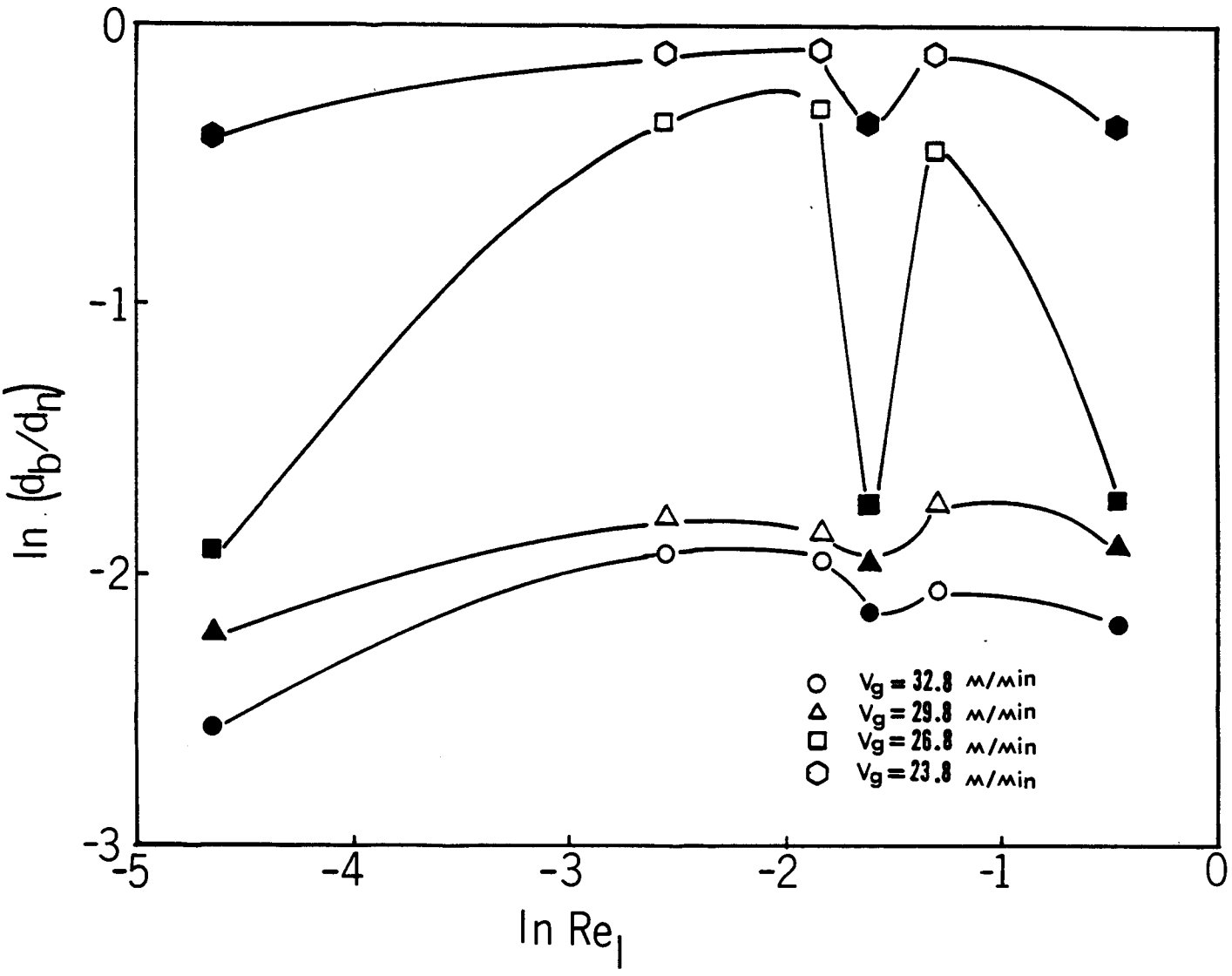
0
-1
-2
-3
-5
-4
-3
-2
-1
0
ln (d_b/d_n)
ln Re_l
V_g = 32.8 m/min
V_g = 29.8 m/min
V_g = 26.8 m/min
V_g = 23.8 m/min

FIGURE 4

Metabolic Effects of Chloramphenicol Resistance in the Recombinant Host/Vector System: *E. coli* RR1[pBR329]

William E. Bentley, Dana C. Andersen, Dhinakar S. Kompala and Robert H. Davis
Department of Chemical Engineering
University of Colorado
Boulder, Colorado 80309-0424

June 2, 1988

Abstract

The growth rate of plasmid-bearing, recombinant cells is generally lower than that of the plasmid-free host. The severity of the growth rate differential depends on the plasmid copy number and the extent of non-indigenous protein expression which, in turn, depend on the growth rate of the cell. This paper describes the experimental elucidation of the metabolic load placed on bacteria by the induction of protein expression. Our plasmid content results, which indicate that the plasmid copy number monotonically increases with decreasing growth rate, are consistant with the literature on ColE1-like plasmids. More significantly, we have experimentally quantified the reduction in growth rate brought about by the induced expression of chloramphenicol-acetyl-transferase (CAT). The functional dependence of growth rate on protein translation is media independent and previously undocumented. This work provides an important step in the development of comprehensive, metabolically structured, bioreactor models capable of predicting optimal conditions for the maximization of product yield.

I. INTRODUCTION

In order to maintain stable recombinant bacterial continuous cultures, one must overcome the inherent instability resulting from the competitive disadvantage of plasmid-bearing cells. The growth rate of bacterial cells with plasmids suffers in comparison to the growth rate of bacteria without plasmids because of the additional strain placed on the hosts by plasmid replication, rDNA transcription, and plasmid-encoded mRNA translation. This "growth rate differential" exacerbates the segregational instability brought about by uneven partitioning of plasmids to the daughter cells and can yield an unproductive bioreactor in only a few generations.[1]

Recent genetic advances, however, have provided controllable promoters (e.g. λ_{PL}, *lac*UV5, and *tac*) which, when inserted upstream of the product gene, facilitate the regulation of product expression.[2-4] Furthermore, insertions near the replication origin of R1-like plasmids have provided the first steps towards copy number control.[5,6] Further work might eventually yield a plasmid construct where both copy number and cloned gene product (cgp) expression are tightly controlled and, thus, so is the growth rate differential between plasmid-free and plasmid-bearing cells. Thus, reaction systems can be designed for product yields at previously unattainable levels. In order to optimize bioreactor productivity, researchers must integrate appropriate experimental data with reactor models and incorporate our full knowledge of the *independent* metabolic effects of protein expression and plasmid replication. Furthermore, these metabolic effects must be differentiated

from plasmid segregation. Currently, most modelling efforts have included overly simplistic expressions for the growth rate of recombinant cells relative to plasmid-free cells and consequently do not account for the dynamic influences of plasmid replication, mRNA translation, and plasmid segregation (Lauffenburger, 1986; Dibiasio and Sardonini, 1986; Stephanopoulos and Lapidus, 1988; Seressiotis and Bailey, 1987). Further analyses with these models was deemed unwarranted until more detailed models are available, based on experimental data, which simulate the metabolic dynamics associated with cgp expression[7]. Many researchers have noted the importance of these phenomena and therefore, recognize the need for comprehensive experimental results.[7-14] Only after these results become available, can a more advanced mathematical analysis be utilized.

The primary objective of this study was to determine, quantitatively and independently, the effects that protein expression and plasmid replication have on recombinant cell growth. This will be coupled with our previously reported modelling work in order to develop optimal operating conditions and reactor configurations which maximize the total product yield. Our lumped metabolic model is currently the only model capable of accommodating these metabolic dynamics while predicting behavior at a bioreactor's scale.[15,16]

We designed a simple set of experiments which successfully revealed the influence of foreign protein expression on the recombinant cell growth rate. By introducing an antibiotic for which resistance is plasmid-encoded, bacteria are forced to increase expression of the resistance proteins by inducing translation activity. According to our model predictions, an increase in foreign protein expression should be accompanied by a drop in growth rate. We have grown our recombinant strain in two media (M9 - a minimal medium and LB - a rich medium), added chloramphenicol at various levels, and consequently altered the growth rate. For each culture, the maximum specific growth rate, the specific CAT activity (nmoles/ min mg total protein), and the plasmid content per cell were measured. These are the minimum number of experimental quantities necessary to describe the effect that protein expression has on the cell.

II. Materials and Methods

A. Culture Conditions

E. coli RR1, purchased from Bethesda Research Laboratories, was transformed with the plasmid, pBR329 (tet^r, cam^r, amp^r), also from BRL. Experiments were performed in shake flasks controlled at 37°C in a New Brunswick Scientific G24 Environmental Incubator Shaker. Media (M9 and LB) were prepared according to Maniatis *et al.*[17] Chloramphenicol (Sigma) was added such that final concentrations were from 0 to 300 μg/ml.

B. Growth Rate Measurements

Optical density (absorbance at 600 nm) was measured in the linear range (0.05 to 0.25 OD units) on a Beckman DU-50 Spectrophotometer.

C. Chloramphenicol-Acetyl-Transferase (CAT) Activity

CAT assays were performed spectrophotometrically according to Rodriquez and Tait[18], with slight modification, at 37°C. The best precision was obtained when all reagent volumes were doubled and cell extract volumes were quadrupled. Total protein content was measured according to Rodriguez and Tait using BioRad protein assay dye reagent concentrate.

D. Plasmid Content

Plasmid DNA was harvested by the boiling method (Holmes and Quigley[19]), and separated from RNA and chromosomal DNA by 1.0% agarose gel electrophoresis in TPE buffer (Maniatis *et al.*). Gel loading buffer was 40% sucrose and 0.25% bromophenol blue. Gels were run at 10 mA overnight using a Hoefer Scientific Instruments Mini-gel with an EC452 power supply from E-C Apparatus Corporation. Gels were stained in 100 μg/ml ethidium bromide (Fisher Scientific) for one half hour, then destained in ddH_2O (double distilled) for one hour. Gels were then illuminated using a Spectroline TX-302 UV Transilluminator and photographed with a Polaroid DS-34 camera using positive/negative Polaroid 665 film. Negatives were scanned (λ = 580 nm) using a Beckman DU-50 spectrophotometer with a gel-scanning densitometer attachment. A photograph of one gel is duplicated below.

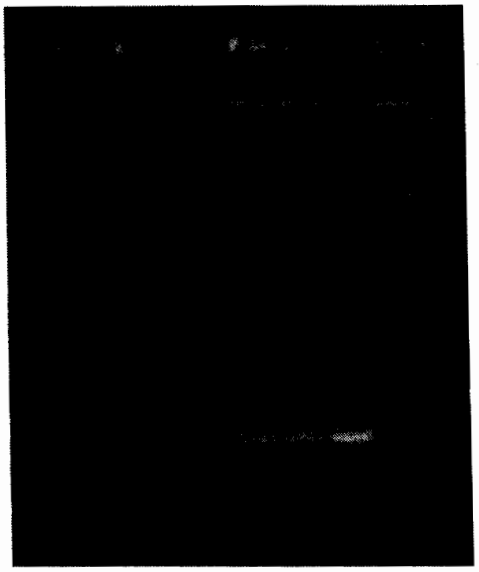

Lane 1 2 3 4 5 6 7 8
decreasing growth rate ----→

III. RESULTS AND DISCUSSION

A. Dynamic Growth Response from Chloramphenicol Spike

Each of four flasks containing 100 ml LB medium were inoculated with 1 ml of a culture grown overnight. After 90 minutes, chloramphenicol was introduced such that the final concentrations were 0, 100, 200, and 300 μg/ml. The resulting growth curves are shown in Figure 1. Based on previous modelling predictions of completely inducible host/vector systems (not reported here), we anticipated an immediate lag followed by a slow recovery to a non-maximal but steady exponential growth period. We further anticipated that the longest lag period and the subsequently lowest growth rate would correspond to the 300 μg/ml flask, containing the highest examined antibiotic level. The anticipated growth dynamics, lag period followed by exponential growth, are not discernable from the data in Figure 1. This is most likely due to the non-linear nature of an ln(OD) vs time plot for cultures grown on LB media (even in the absence of antibiotics) after the cell mass becomes appreciable. This nonlinearity occurs because the undefined LB medium has no single limiting nutrient. It is obvious, however, that the highest level of chloramphenicol had the most

deleterious effect on the culture.

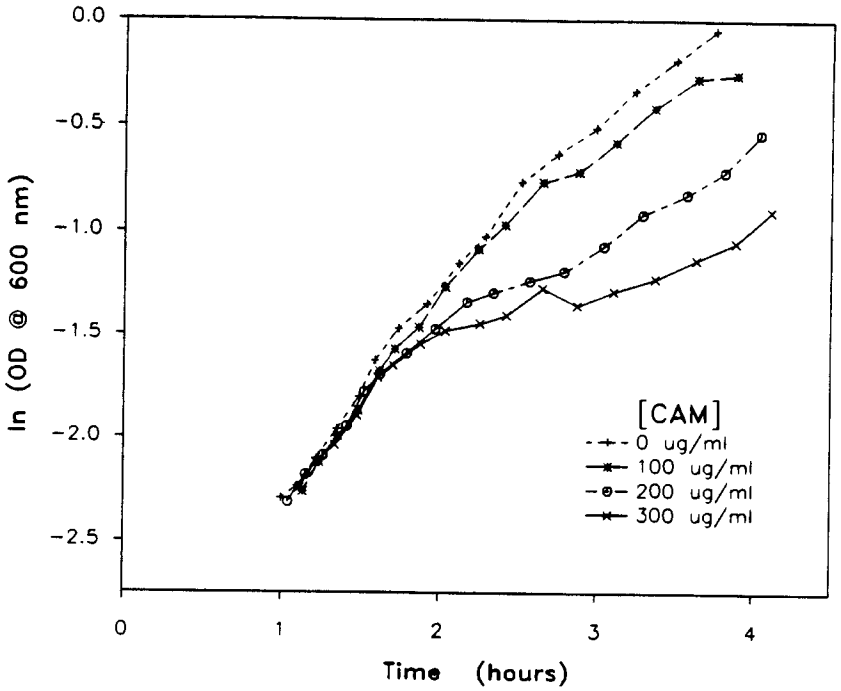

Figure 1. Dynamic Growth Response to CAM Spike.

B. Effect of Chloramphenicol on μ_{max}

The maximum specific growth rate was determined from initial growth measurements in both LB and M9 media with the previously mentioned levels of antibiotic. Surprisingly, the decrease in growth rate appears directly proportional to the increase in chloramphenicol (Figure 2). This linear decrease was observed in both media, and further, the slopes are nearly equal. This would suggest that external nutrient variations have no direct influence on the plasmid activity and its metabolic consequences.

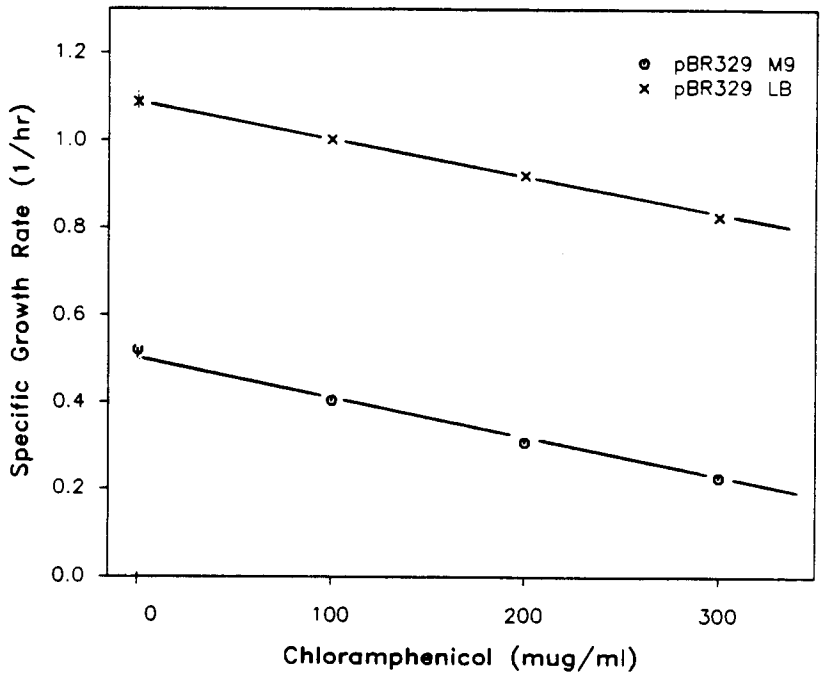

Figure 2. Effect of CAM on Growth Rate.

C. Expression of Foreign Protein, CAT

Increased resistance to chloramphenicol is due to an increase in chloramphenicol-acetyl-transferase activity. Indeed, measured quantities indicate a substantial increase in CAT activity in cultures having the highest chloramphenicol concentrations and, correspondingly, the lowest growth rates (Figure 3). It is interesting to note that the CAT activity increases nearly exponentially with the decrease in growth rate.

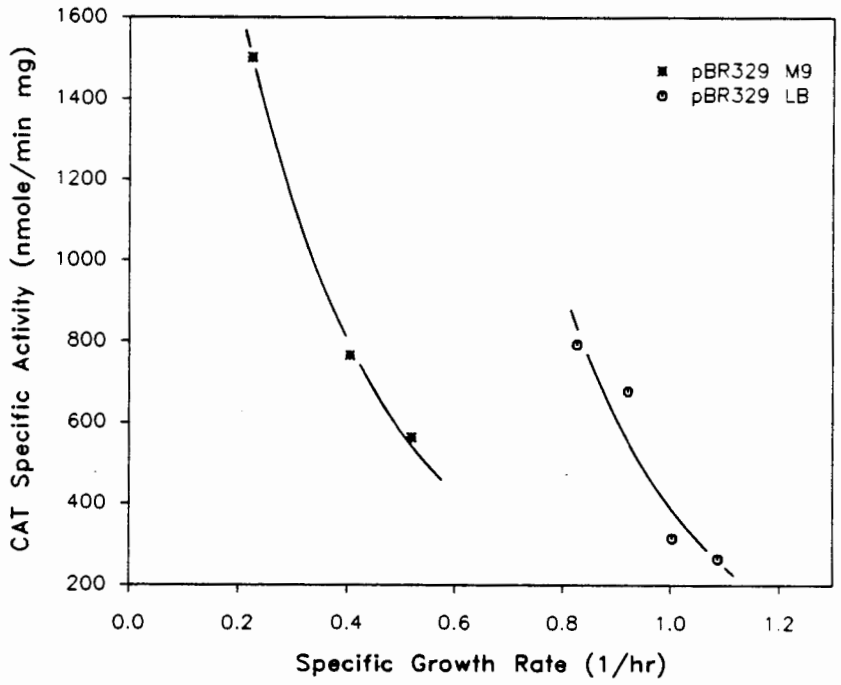

Figure 3. Highest CAT Activity corresponds to Highest CAM concentration and lowest growth rate.

D. Plasmid Content

The plasmid DNA per cell was highest at the lowest growth rate (Figure 4). Furthermore, a nearly linear increase in plasmid content with decreasing growth rate was observed. Previous researchers have found that the plasmid replication control mechanism for ColE1-like plasmids is regulated both positively (by RNA II) and negatively (by RNA I and rop polypeptide).[20,21] The net result is a monotonic increase in plasmid copy number per cell with decreasing cell growth rate (Lin-Chao and Bremer[22]), which is in complete agreement with our results. Other researchers have found, for a variety of host/colE1-vector systems where plasmid-encoded proteins are constitutively expressed, that the highest protein expression was in cultures having the lowest growth rate.[12–14,23,24] Since an increase in plasmid copy number is expected to yield a proportional increase in foreign protein content until high copy numbers[12,25], these results are consistent with and support our plasmid copy number observations. In fact, some of these researchers have reported the activity of constitutively expressed proteins (eg. β-lactamase activity from pBR322) as an indicator of plasmid copy number.[24,26] These studies have demonstrated that the number of plasmids within a specific host varies, and is regulated soley by the growth rate of the recombinant cells through the ratio RNAI/RNAII and the concentration of rop.

Thus, we expect that the growth rate is also the principal determinant in plasmid copy number regulation in our system. We assume, therefore, that there is no change in copy number due to the presence of chloramphenicol. The data from experiments on M9 media and LB media were consequently merged so that the dependence of plasmid content on growth rate was drawn as

indicated in Figure 4.

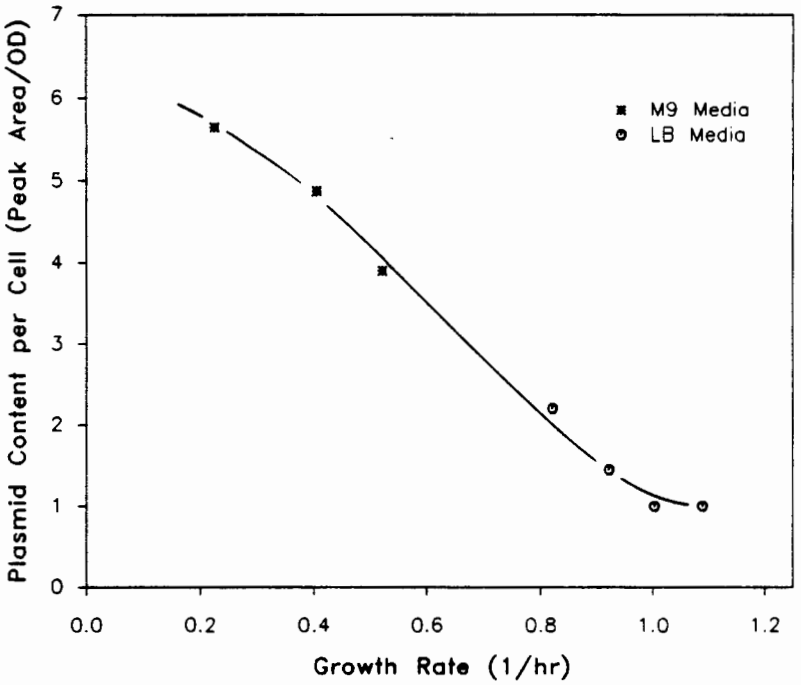

Figure 4. Plasmid Content Increases with Decreasing Growth Rate.

E. Induction of CAT and Effect on Growth

A major objective of this study was to elucidate the effect that foreign protein translation has on the growth rate of recombinant cells. This effect can be determined by measurements of protein activity at differing growth rates only after eliminating or correcting for all contributing factors such as variation in plasmid copy number (Np). Thus, in Figure 5, we have plotted the growth rate as a function of the ratio of specific CAT activity to plasmid content per cell. This ratio provides a measure of foreign mRNA translation activity since it expresses the amount of CAT produced from each plasmid. For both sets of data, an increase in CAT/Np was followed by a decrease in cell growth rate. Furthermore, the rate of decrease seems to be similar in both media.

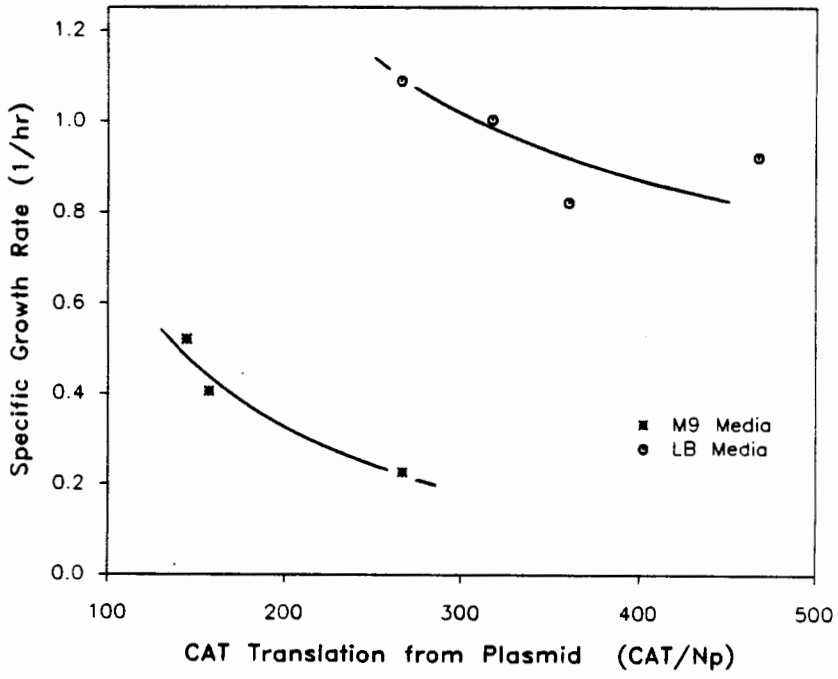

Figure 5. CAT Translation Decreases the Growth Rate.

IV. Concluding Remarks

For the first time, a reduction in cell growth has been linked to the translation of plasmid-encoded proteins. This has been predicted in our modelling work and has been quantitatively demonstrated here. We have not determined, however, the *independent* effect that plasmid replication has on cell growth. This is obscured experimentally by the expression of other proteins whose genes are transcribed from the plasmid. We have recently constructed a new plasmid, which utilizes a controllable tac promoter upstream of a transcriptionally and translationally regulated CAT gene and contains only one other significant protein gene (for β-lactamase). This should help differentiate replication from protein expression.

The authors wish to acknowledge the National Science Foundation (grant No. EET-8611305) and the Undergraduate Research Opportunities Program (UROP) of the University of Colorado (a grant to DCA) for support of this work.

References

[1] Imanaka, T. and S. Aiba. (1981) A Perspective on the Application of Genetic Engineering: Stability of Recombinant Plasmids. *Ann. N.Y. Acad. Sci.* 369:1-14.

[2] Fuller, F. (1982) A family of cloning vectors containing the *lac*UV5 promoter, *Gene* 19:43-54.

[3] Remaut, E., Stanssens, P. and W. Fiers (1981) Plasmid vectors for high-efficiency expression controlled by the p_L promoter of coliphage lambda, *Gene* 15:81-93.

[4] Amann E., Brosius, J. and M. Ptashne (1983) Vectors bearing a hybrid *trp* – *tac* promoter useful for regulated expression of cloned genes in *Escherichia coli*, *Gene* 25:167-178.

[5] Remaut, E., Tsao, H. and W. Fiers (1983) Improved plasmid vectors with a thermoinducible expression and temperature-regulated runaway replication, *Gene* 22:103-113.

[6] Larsen, J.E.L, Gerdes, K., Light, J. and S. Molin (1984) Low-copy-number plasmid-cloning vectors amplifiable by derepression of an inserted foreign promoter, *Gene* 28:45-54.

[7] Seressiotis, A. and J.E. Bailey (1987) Optimal gene expression and amplification strategies for batch and continuous recombinant cultures, *Biotechnol. Bioeng.* 29:392-398.

[8] Lauffenburger, D. (1986) Model for the dynamics of colicin plasmids in continuous culture, in *Biochemical Engineering IV*, Lim, H.C. and K. Venkatasubramanian, Eds., *Annals N.Y.A.S.* 469:97-103.

[9] Stephanopoulos, G. and G.R. Lapidus (1988) Chemostat dynamics of plasmid-bearing, plasmid-free mixed recombinant cultures, *Chem. Eng. Sci.* 43(1):49-57.

[10] DiBiasio, D. and C. Sardonini (1986) Stability of continuous culture with recombinant organisms, in *Biochemical Engineering IV*, Lim, H.C. and K. Venkatasubramanian, Eds., *Annals N.Y.A.S.* 469:111-117.

[11] Bailey, J.E., DaSilva, N.A., Peretti, W., Seo, J.-H. and F. Srienc (1986) Studies of host-plasmid interactions in recombinant microorganisms, in *Biochemical Engineering IV*, Lim, H.C. and K. Venkatasubramanian, Eds., *Annals N.Y.A.S.* 469:97-103.

[12] Seo, J. and J.E. Bailey (1985) Effects of recombinant plasmid content on growth properties and cloned gene product formation in *Escherichia coli*, *Biotechnol. Bioeng.* 27:1668.

[13] Siegel, R. and D.Y. Ryu (1985) Kinetic study of instability of recombinant plasmid pPlc23*trpAl* in *E. coli* using two-stage continuous culture system, *Biotechnol. Bioeng.* 27:28.

[14] Ataai, M.M. and M.L. Shuler (1987) A mathematical model for the prediction of plasmid copy number and genetic stability in *Escherichia coli*, *Biotechnol. Bioeng.* 30:389.

[15] Bentley, W.E. and D.S. Kompala (1987) A novel structured kinetic modeling approach for the analysis of plasmid instability in recombinant bacterial cultures, *Biotechnol. Bioeng.* (accepted for publication).

[16] Bentley, W.E. and D.S. Kompala (1988) Using structured kinetic model for analyzing instability in recombinant bacterial cultures, (accepted for publication in *Frontiers in Bioprocessing* CRC Press, Inc.), S. Sikdar and P. Todd, Editors.

[17] Maniatis, T., Fritsch, E.F. and J. Sambrook, (1982) *Molecular Cloning: A Laboratory Manual*, Cold Spring Harbor Laboratory, Cold Spring Harbor, New York.

[18] Rodriguez, R.L and R.C. Tait (1983) *Recombinant DNA Techniques: An Introduction*, The Benjamin/Cummings Publishing Company, Inc., Menlo Park, CA.

[19] Holmes, D.S. and M. Quigley (1981) A rapid boiling method for the preparation of bacterial plasmids, *Anal. Biochem.* 114:193.

[20] Davison, J. (1984) Mechanism of control of DNA replication and incompatibility in ColE1-type plasmids - a review, *Gene* 28:1-15.

[21] Lewin, B., (1987) *Genes III*, John Wiley & Sons, Inc., New York, 309.

[22] Lin-Chao, S. and H. Bremer (1986) Effect of the bacterial growth rate on replication control of plasmid pBR322 in *Escherichia coli*, *Mol. Gen. Gen.* 203:143-149.

[23] Stueber, D. and H. Bujard. (1982) Transcription from efficient promoters can interfere with plasmid replication and diminish expression of plasmid specified genes. *EMBO J.* 1(11):1399-1404.

[24] Klotsky, R.-A. and I. Schwartz (1987) Measurement of *cat* expression from growth-rate-regulated promoters employing β-lactamase activity as an indicator of plasmid copy number, *Gene* 55:141-146.

[25] Koizumi, J., Monden, Y. and S. Aiba (1985) Effects of temperature and dilution rate on the copy number of recombinant plasmid in continuous culture of *Bacillus stearothermophilus* (pLP11), *Biotechnol. Bioeng.* 27:721.

[26] Lupski, J.R., Ruiz, A.A. and G.N. Godson (1984) Promotion, termination, and anti-termination in the *rpsU-dnaG-rpoD* macromolecular synthesis operon of *E. coli*K-12, *Mol. Gen. Genet.* 195:391-401.

GENETIC ENGINEERING OF BETA-GALACTOSIDASE TO AID IN FERMENTATION PRODUCT RECOVERY BY POLYELECTROLYTE PRECIPITATION

D.E. Parker and C.E. Glatz
Department of Chemical Engineering

J. Zhao, C.F. Ford, and S.M. Gendel
Department of Genetics

M.A. Rougvie
Department of Biochemistry and Biophysics

Iowa State University, Ames, IA

ABSTRACT

Charged amino acid tails have been fused to the carboxyl end of the enzyme beta-galactosidase in order to increase the selectivity of polyelectrolyte precipitation of the enzyme. The beta-galactosidase was recovered from a disrupted culture of Escherichia coli (E. coli).

Synthetic oligonucleotides encoding the charged tail were inserted at the end of the beta-galactosidase gene on the plasmid vector pUR290 which was then transformed into E. coli. The bacteria were grown, expression of the enzyme was induced and the cells were disrupted by sonication. Two beta-galactosidases with negatively charged tails consisting of 5 and 11 aspartate residues were made. Enzyme from both crude cell extracts and purified preparations was precipitated with positively charged polyethyleneimine. The removals of total protein and beta-galactosidase were compared to determine the influence of the charged tails on the selective removal of the enzyme.

INTRODUCTION

The concentration and purification of a single protein fraction from a fermentation broth is the goal of many downstream processing operations. Often the desired product is in a dilute aqueous mixture consisting of other bioproducts with similar chemical and physical properties. Selective precipitation methods have the potential to be efficient, large-scale separation processes with important industrial applications (1). Polyelectrolyte precipitation of proteins is a separation and concentration method that involves the use of a polymer with repeating charged groups. The polyelectrolyte is used to precipitate proteins of opposite charge.

In this work we are genetically engineering a protein in an attempt to improve its separation behavior from a fermentation broth using polyelectrolyte precipitation. Negatively charged amino acid tails have been added to the carboxyl-terminus of the tetrameric enzyme beta-galactosidase by placing restriction fragments of DNA encoding the tails at the 3' end of the beta-galactosidase gene. The polycation polyethyleneimine (PEI) has been used to precipitate the tailed and untailed enzymes from both purified samples and crude cell extracts.

MATERIALS AND METHODS

Materials

Wild-type beta-galactosidase was obtained from Sigma Chemical Co. (St. Louis, MO) and PEI with an average molecular weight of 50,000-60,000 Daltons was from Aldrich Chemical Co. (Milwaukee, WI).

Protein and Enzyme Assays

The enzymatic activity of beta-galactosidase was determined by following the hydrolysis of o-nitrophenyl galactoside (ONPG) at 37°C (2). Total protein was determined using the Bio-Rad Protein Assay Reagent (Bio-Rad Co., Richmond, CA).

Cell Line and Vector

The E. coli strain F'11 rec A was used throughout the study and plasmid pUR290 was used as the vector (3). The plasmid pUR290 contains the lac Z gene (which encodes beta-galactosidase) with a multiple cloning site at the 3' end of the gene. This site contains several unique restriction endonuclease cleavage sites including Bam HI and Hind III. The plasmid also contains a gene coding for resistance to ampicillin so that E. coli transformed with the plasmid can be selected on media containing this antibiotic.

Media and Culture Conditions

The cells were grown at 37°C in LB medium containing 50 ug/ml of ampicillin (4). Overnight cultures were used to inoculate 1 liter of medium which was grown in shake flasks to late log phase.

Cloning of Tails

The tail segment was made by artificially synthesizing a segment of DNA that encodes the charged amino acid tail and that contains a Bam HI restriction site at one end and a Hind III site at the other end. Two partially complementary oligonucleotides were synthesized at the Iowa State University Nucleic Acid Facility. These were annealed, filled in, digested with the two restriction enzymes and inserted into pUR290 which had also been cut with Bam HI and Hind III.

The recombinant plasmid was then transformed (4) into E. coli F'11 rec A which does not contain a gene for beta-galactosidase. The beta-galactosidase gene was induced for expression by isopropylthiogalactoside (IPTG) and colonies expressing the enzyme were detected by the blue color they formed when grown on media plates containing the histochemical stain X-gal (5).

Sequence of Tails

The purification fusions consist of several amino acids added to the carboxyl end of the protein. The sequence of the tails past the last wild-type residue is: Asp-Pro-Met-Ala-$(Asp)_n$-Tyr.

One tail (T1) contains 5 aspartate residues (n=4) and the second (T2) contains 11 residues (n=10). The first aspartate and proline were part of the original Bam HI site and so were regenerated upon insertion of the tail segment. The methionine was included to allow cleavage of the tail by cyanogen bromide. The tyrosine and alanine were included to allow determination of the tail length.

Solubility

The solubility of the wild-type enzyme as a function of pH was determined by titrating samples of the protein to various values of pH, centrifuging for 30 minutes at 27,000 g and measuring the removal of beta-galactosidase.

Precipitation of Pure Enzyme

Cells were disrupted by two 2 and 1/2 minute bursts using the microtip of an Ultrsonics sonifier set at 40 watts. Beta-galactosidase was purified from sonicated cells by ammonium sulfate precipitation and affinity chromatography (6). PEI was added to 2 ml samples of beta-galactosidase at various dosage levels (mass PEI/mass protein) for the tailed and wild-type enzymes. The samples were mixed by inversion, centrifuged and supernatant beta-galactosidase activities measured to determine removals.

Precipitation of Cell Extracts

The crude cell extracts were adjusted to the same total protein concentration of approximately 1 mg/ml. PEI was added to 2 ml samples of extract at dosage levels ranging from 0 to 0.10 g PEI/g protein. Mixing was by inversion and the slurries were centrifuged at 27,000 g for 30 minutes. The total protein and beta-galactosidase removals were determined by measuring the concentrations of the supernatant.

RESULTS AND DISCUSSION

The solubility of wild-type beta-galactosidase as a function of pH is shown in Figure 1. Below the pH of approximately 5.5 the enzyme becomes insoluble. This is very near the isoelectric point of the protein. Precipitations with the positive PEI were done at pH 5.7 which is above the isoelectric point. Thus the protien has a net negative charge at this pH and the tailed enzymes should have an even greater net negative charge.

The results of the PEI precipitations done on separate purified samples of beta-galactosidase are shown in Figure 2. For a given dosage of PEI a larger percentage of the tailed enzymes was removed than was removed of the non-tailed enzyme. At the lower dosage of 0.01, more of T2 is precipitated than is T1. At the dosage level of 0.02, nearly all of T1 and T2 are precipitated while just under 60% of the wild-type enzyme is removed. More than enough PEI is present at this dosage to precipitate all of T1 or T2. While more of the wild-type enzyme is precipitated, its removals still do not match those of the negatively tailed enzymes. Thus the tails are effective in

increasing the affinity of purified beta-galactosidase for the polyelectrolye.

The results of the PEI precipitations done on two types of crude cell extracts of E. coli are shown in Figure 3. E. coli producing the T1 enzyme and the non-recombinant enzyme present on pUR290 (abbreviated as 290) have been studied so far. Dosages ranging from 0.02-0.10 g PEI/g total protein were examined and for both types of enzyme more total protein was removed than beta-galactosidase. The total protein removals are very similar for both extracts and range from 32% at the lowest dosage to nearly 90% at the highest dosage reported. The beta-galactosidase removals vary considerably between the two types of extracts. For all but the highest dosage a larger percentage of the 290 enzyme was removed than the T1 enzyme.

Nucleic acids present in the cell extract are probably interfering with the PEI precipitation of protein. Sassenfeld and Brewer (7) reported variable cation exchange chromatography when separating a protein with a positively charged polyarginine fusion from a bacterial extract. The nucleic acids present in the lysate competed with the negatively charged column for binding of the positive protein fusion. Nucleic acids are very negatively charged and so in our case would be strongly attracted to the positively charged PEI. Since nucleic acids are large polyelectrolytes they could be thought of as the precipitating agent, bringing down positively charged molecules including PEI. If this were the case then perhaps positively charged proteins would be brought down by the complex of nucleic acids and PEI. Thus the negative tail of the recombinant beta-galactosidase could actually play a detrimental role in its precipitation in the presence of nucleic acids.

Our hypothesis is that nucleic acids must first be removed from the cell extracts before beta-galactosidase can be selectively precipitated with PEI. We are presently working on a heat treatment to activate nucleases present within the E. coli cells (8). Further precipitation studies will then be conducted. Work is also under way on a third negative tail and a positive tail consisting of argininge residues.

REFERENCES

1. Michaels, A. S. 1984. Adapting modern biology to industrial practice. Chem. Eng. Prog. 80(6):19-25.

2. Sigma Chemical Co. product note. 1986. Enzyme Assay Procedure using ONPG as Substrate. Sigma Chemical Co., St. Louis, MO.

3. Ruther, U. and B. Muller-Hill. 1983. Easy identification of cDNA clones. EMBO J. 2:1791-1794.

4. Maniatis, T., E. F. Fritsch, and J. Sambrook. 1983. Molecular Cloning: A Laboratory Manual. Cold Spring Harbor Laboratory Press, Cold Spring Harbor, NY.

5. Miller, J. 1972. Experiments in Molecular Genetics. Cold Spring Harbor Laboratory Press, Cold Spring Harbor, NY.

6. Steers, E., P. Cuatrecasas, and H.B. Pollard. 1971. The purification of beta-galactosidase from Escherichia coli by affinity chromatography. J. Biol. Chem. 246:196-200.

7. Sassenfeld, H. M. and S. J. Brewer. 1984. A polypeptide fusion designed for the purification of recombinant proteins. Bio/Technology. 2:76-81.

8. Higgins, J. J., D. J. Lewis, W. H. Daly, F. G. Mosqueira, P. Dunnill, and M. D. Lilly. 1978. Investigation of the unit operations involved in continuous flow isolation of beta-galactosidase from Escherichia coli. Biotech. Bioeng. 20:159-182.

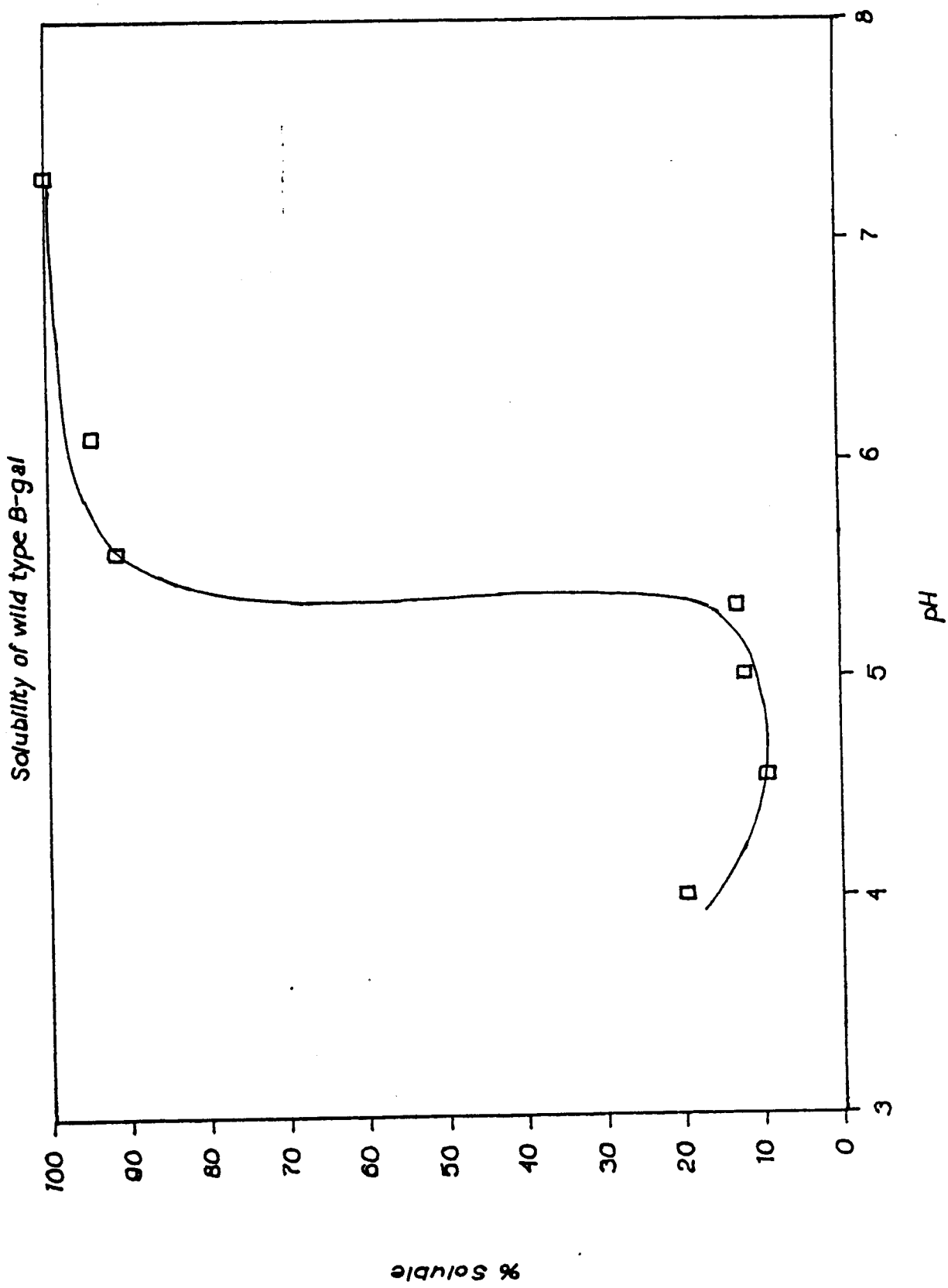
Solubility of wild type B-gal
% Soluble
pH
100
90
80
70
60
50
40
30
20
10
0
3
4
5
6
7
8

Figure 1.

PRECIPITATION OF β - GALACTOSIDASES WITH POLYETHYLENEIMINE

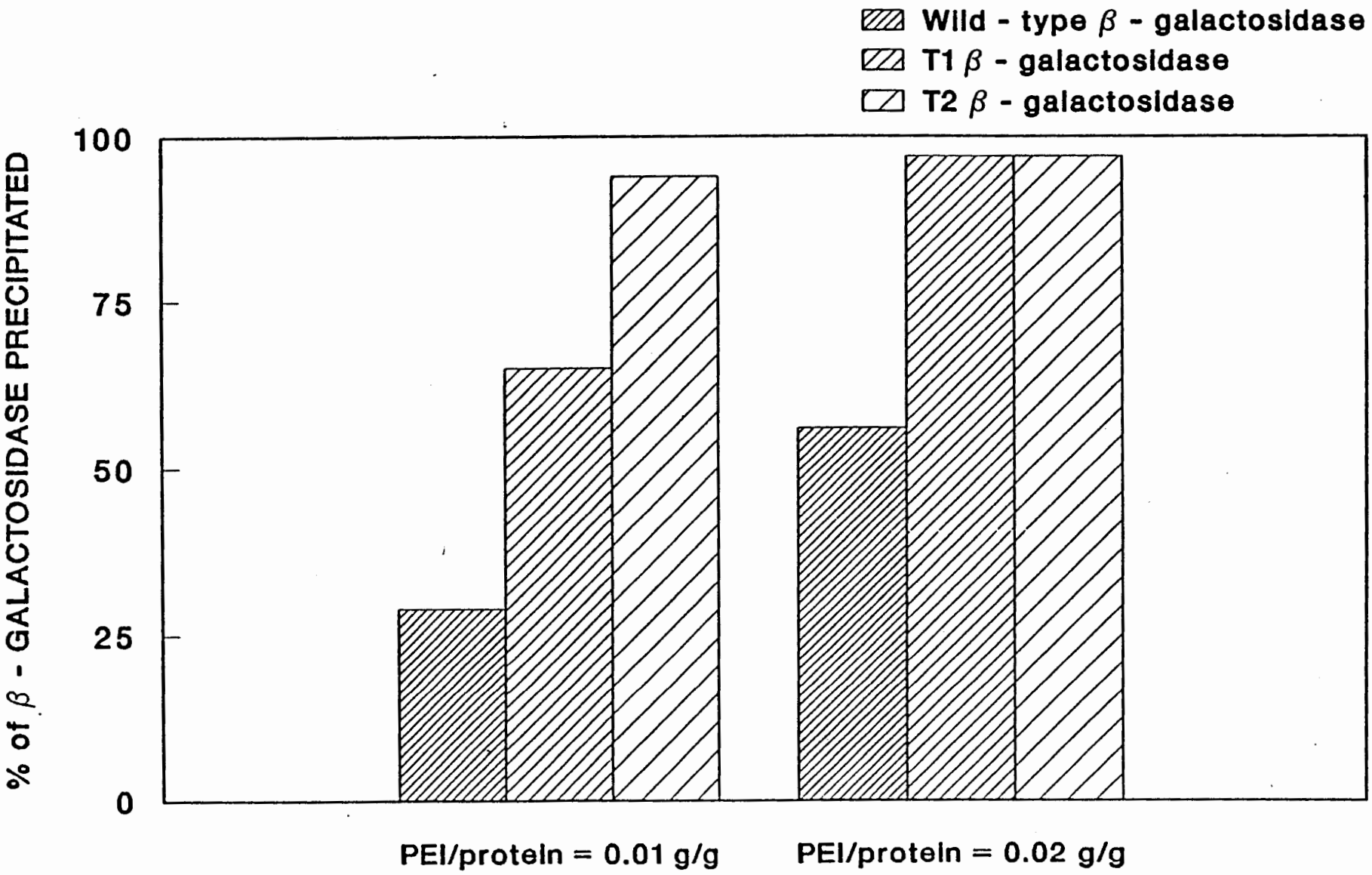

Figure 2.

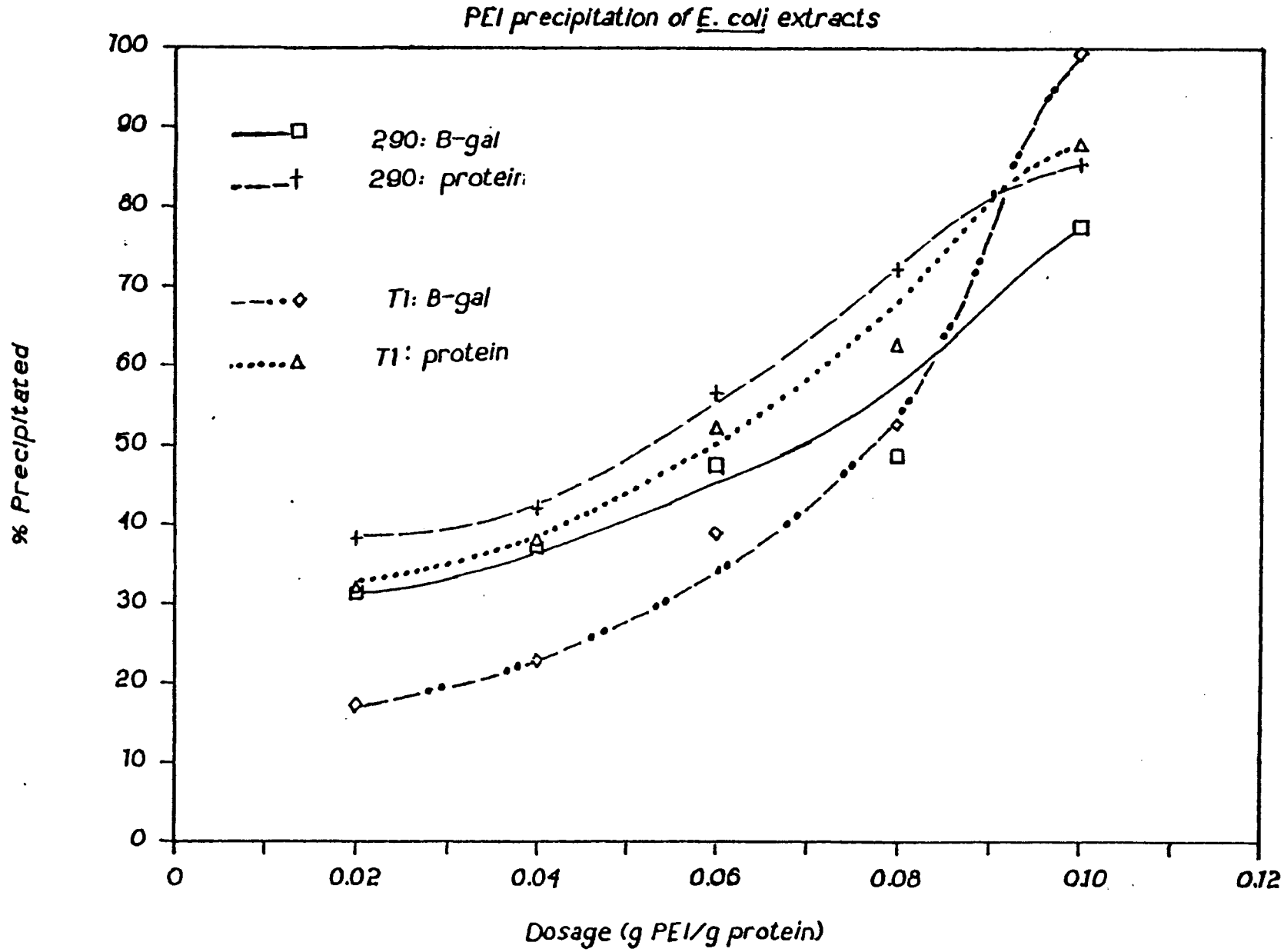
PEI precipitation of E. coli extracts
290: B-gal
290: protein
T1: B-gal
T1: protein
% Precipitated
Dosage (g PEI/g protein)
0
10
20
30
40
50
60
70
80
90
100
0
0.02
0.04
0.06
0.08
0.10
0.12

Figure 3.

BIODEGRADATION OF ORGANIC COMPOUNDS IN SOIL

Lourdes Taladriz, L.E. Erickson, and L.T. Fan

Department of Chemical Engineering
Kansas State University
Manhattan, Kansas 66502
April 23, 1988.

INTRODUCTION

It have been suggested that microorganisms exist which are capable of oxidizing all naturally produced organic compounds under suitable conditions. The problem is that a variety of environments, such as anaerobic or acidic ones, are not in such conditions, and numerous organic compounds may remain essentially unchanged over relatively long periods of time. This is what has occurred at the site under investigation.

An oil refinery operated in the vicinity of the site during the early part of the 20th century. After a fire in the mid 1920's, various waste materials from unknown sources were disposed of at the site. The Kansas Department of Health and Environment detected the presence of carcinogenic polynuclear aromatic compounds (PNA's) in soil and ground water samples (Spruill, 1987). Our interests are in the biodegradation of the aliphatic hydrocarbons and the polynuclear aromatic compounds.

The site, along with six others in the state of Kansas, is included in the Superfund list and is being studied at the present time for clean-up. The objective of this study was to assess biodegradation as a possible remedial means for the site.

MATERIAL AND METHODS

The soil samples tested in the experiments were obtained from the site under investigation. They were classified into three types according to location and are; acid sludge, soil found 10 feet below the surface, and soil found 20 feet below the surface. A mixed culture was cultivated from the surrounding soil of the acid sludge pond and used as inocula.

The acid sludge was treated under three conditions, namely, the unsaturated condition (experiment AU), saturated condition (experiment AS), and saturated condition with the addition of surfactant (experiment AT). The soil from ten feet below the surface was treated under the unsaturated condition (experiment 10U). The soil from twenty feet below the surface was treated under the saturated condition

(experiment 20S) and saturated condition with the addition of surfactant (experiment 20T).

The experiment lasted for 175 days with measurements taken every 14 days. The acid sludge with a pH of 1.0 was neutralized to a pH of 6.5 with calcium carbonate and water at the outset of each experiment. It was maintained at this pH with the nutrient media since it formed a phosphate buffer. Close to 500 grams of calcium carbonate were needed to bring 650 grams of soil to the pH of 6.5. All experiments were conducted at room temperature.

Since the samples contained PNA's, they were placed under a hood throughout each experiment. Each sample contained 650 grams of soil.

Samples were analyzed for the organic substrate concentration in terms of chemical oxygen demand (COD) and also with high pressure liquid chromatography (HPLC). They were also analyzed for cell concentration according to the standard plate count method.

RESULTS

The experimental data have been reported by Taladriz (1988). Estimates of the maximum specific growth rate based on cell number measurements are presented in Table I. Note that the samples in all the experiments exhibit some degree of degradation. The largest estimated values of the specific growth rate have been obtained in experiments AS and 20S. Surfactant, Tween 20, was not added in these experiments. The results of experiments AT and 20T indicate that the addition of Tween 20 affects the viability of the microbial population. The aqueous phase concentration of inhibitory and toxic substances would be expected to increase in the samples with the addition of Tween 20. For the acid sludge with the addition of Tween 20 (experiment AT), the maximum specific growth rate is less than that without its addition (experiment AS). The smallest value of the maximum specific growth rate reported in Table I is for experiment 10U. For the acid sludge samples, the estimate of the specific growth rate for experiment AU is considerably smaller than that for experiment AS.

The cell yields reported in Table II are considerably less for experiment AT than for experiment AS. This would be expected if the viability of the cells was affected by the addition of surfactant in the former.

The values of cell yield reported in Tables II and III are very low for experiment 10U, The viability of cells growing in soil under unsaturated conditions may be affected by soil moisture and water activity. In Figures 1 and 2 the biomass and substrate concentrations are plotted vs time for experiment 10U. The biomass concentration drops abruptly

between 56 and 70 days. This could be attributed to the loss of viability due to the low soil moisture and low water activity.

The model fitted to the biomass data assumes exponential growth. Figures 1 and 2 illustrate the fit of this model to the data from experiment 10U.

Various investigators have applied the first order kinetic model to biodegradation of PNA's; see Taladriz (1988) for a review of their works. The model is expressed as:

$$dC/dt = -kC$$

Figure 1 demonstrates the fit of the model to the substrate concentrations measured by the HPLC in experiment 10U. Figure 2 presents the corresponding fit for the substrate concentration in terms of COD.

The parameter estimates based on the model are presented in Tables II and III for the HPLC and COD data, respectively. The rate of transformation in these tables is the product of the first order rate constant, k, and the initial substrate concentration.

For the acid sludge, the value of the first order rate constant is considerably larger for experiment AT where surfactant is present than for experiment AS. This suggests that the surfactant enhances biodegradation; however, the lower values of cell yields and specific growth rate for experiment AT may be due to the inability of some of the cells to maintain their viability when the surfactant is present.

CONCLUSIONS

The materials in the contaminated site under investigation can be biodegraded by a mixed soil culture if it is neutralized and fed with a nutrient solution. The results of the present experiments indicate that 70 to 90% of the substrate is degraded in a period of 3 months. The rate constant of degradation for the acid sludge, based on a first order kinetic model, ranges from 0.0012 to 0.0080 $days^{-1}$. For the material ten and twenty feet below the surface, this rate constant ranges from 0.0027 to 0.021 $days^{-1}$. For the acid sludge, the addition of surfactant enhances degradation; however, it lowers the cell yield and maximum specific growth rate. For any sample, treatment under the saturated condition is more effective than that under the unsaturated condition.

The results of the present laboratory-scale study demonstrate that biodegradation is a potential technology for in situ treatment of contaminated soil. Nevertheless, it is highly desirable that a pilot-scale study be

undertaken to identify the limitations or difficulties not encountered in the laboratory experiments. For example, we may find oxygen transfer to be a difficult task to perform in such a study.

ACKNOWLEDGEMENTS

This work was partially supported by the Kansas State University Office of Hazardous Waste Research, the Kansas Department of Health and Environment, and the U.S. Geological Survey.

REFERENCES

1. Spruill, T., Written communications. *U.S. Geological Survey*, 1987.

2. Taladriz, L., *Biodegradation of Organic Compounds from an Abandoned Refinery*. M.S. Thesis, Kansas State University, 1988.

Table I. Specific growth rate estimates based on viable cell count measurements.

Experiment*	Maximum Specific Growth Rate ($days^{-1}$)	Correlation Coefficient for μ_m coeff.	Time Span for Estimating μ_m (days)
AU	0.047	0.87	0 to 70
AS	0.086	0.73	0 to 56
AT	0.04	0.89	0 to 56
10U	0.032	0.97	0 to 56
20S	0.0637	0.78	0 to 56
20T	0.061	0.79	0 to 70

*AU = acid sludge unsaturated
AS = acid sludge saturated
AT = acid sludge plus the addition of surfactant
10U = material 10 feet below the surface, unsaturated
20S = material 20 feet below the surface saturated
20T = material 20 feet below the surface plus the addition of surfactant.

Table II. Kinetic parameter values derived from the first order kinetic model: Data based on HPLC.

Experiment*	Biomass yield (No. cell/ g substrate)	Rate Constant ($days^{-1}$)	Rate of Transformation (mg Substrate/ g soil-day)
AU	5.0 E+10	0.0012	0.158
AS	1.2 E+11	0.0013	0.171
AT	2.4 E+10	0.0048	0.712
10U	1.2 E+09	0.0076	0.872
20S	1.2 E+10	0.014	1.43
20T	4.1 E+10	0.011	1.33

*AU = acid sludge unsaturated
AS = acid sludge saturated
AT = acid sludge plus the addition of surfactant
10U = material 10 feet below the surface, unsaturated
20S = material 20 feet below the surface saturated
20T = material 20 feet below the surface plus the addition of surfactant.

Table III. Kinetic parameter values derived from the first order kinetic model: Data based on COD.

Experiment*	Biomass yield (No.cell/ g COD)	Rate Constant ($days^{-1}$)	Rate of Transformation (mg COD/ g soil-day)
AU	6.7 E+10	0.0021	0.989
AS	5.5 E+10	0.0044	2.07
AT	2.1 E+10	0.0080	8.41
10U	1.5 E+09	0.021	9.61
20S	2.6 E+11	0.0027	0.497
20T	1.2 E+11	0.0067	3.86

*AU = acid sludge unsaturated
AS = acid sludge saturated
AT = acid sludge plus the addition of surfactant
10U = material 10 feet below the surface, unsaturated
20S = material 20 feet below the surface saturated
20T = material 20 feet below the surface plus the addition of surfactant.

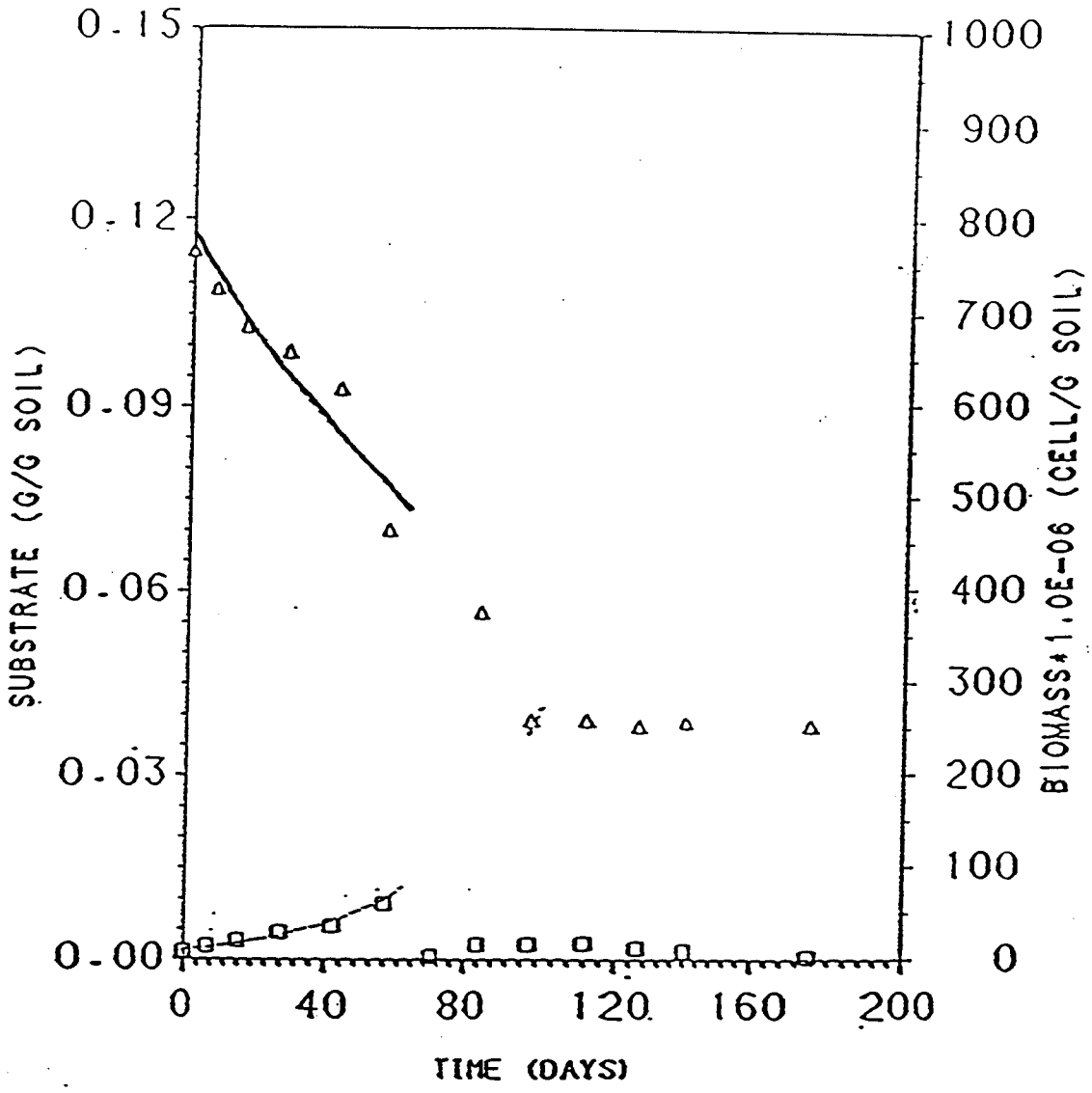

Figure 1. Substrate concentration, measured by HPLC, and the biomass concentration for ten feet unsaturated:

- **Δ substrate concentration;**
- **□ biomass concentration;**
- **——— substrate concentration predicted by first order kinetic model with k = 0.0076 days^{-1};**
- **---- biomass concentration predicted by an exponential model with μ = 0.032 days^{-1}.**

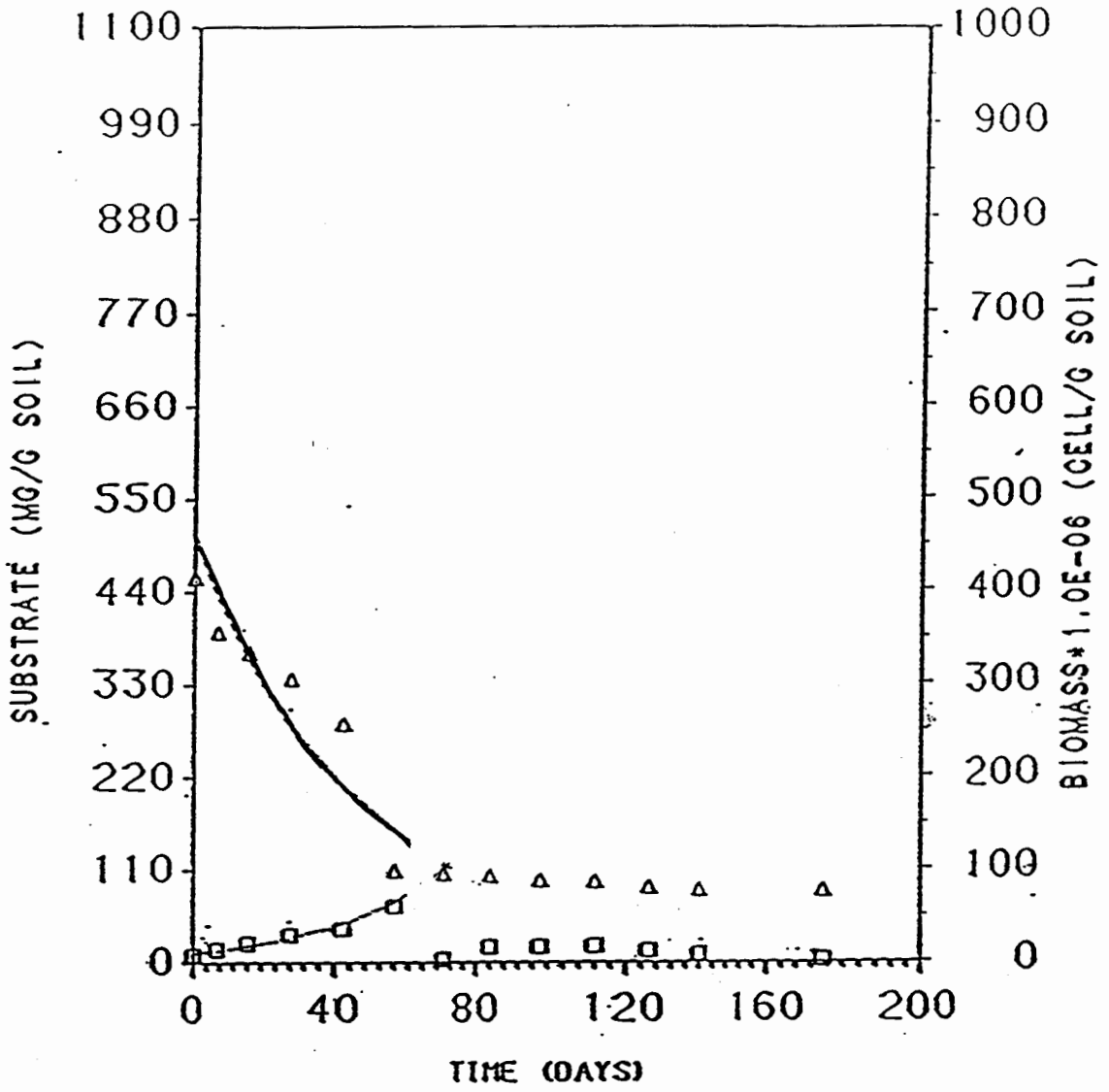

Figure 2. Substrate concentration, measured in terms of COD, and the biomass concentration for ten feet unsaturated:

- △ substrate concentration;
- □ biomass concentration;
- —— substrate concentration predicted by first order kinetic model with $k = 0.021$ days^{-1};
- ---- biomass concentration predicted by an exponential model with $\mu = 0.032$ days^{-1}.

EFFECT OF DILUTION, pH AND NUTRIENT COMPOSITION ON THE BIODEGRADATION OF METALWORKING FLUIDS

Ayush Gupta, L. E. Erickson, and L. T. Fan

Department of Chemical Engineering
Kansas State University
Manhattan, Kansas 66506

April 23, 1988

INTRODUCTION

With the emergence of synthetic and semisynthetic fluids in the metalworking industries, there is a great concern whether the waste is compatible with the existing wastewater treatment technology(Hunz, 1983; Lee, 1986; Lee et al., 1987; Lewis, 1987). Chemical emulsions by design are required to serve for extended periods in the metalworking industry, and thus, various preservatives are added to them to retard microbial contamination(Boswell, 1976). This gives rise to a two-fold problem. Firstly, most of the preservatives are xenobiotic and are hard to degrade. Secondly, they prevent microbial action necessary in the biological treatment of the waste fluids(Rossmore, 1985).

OBJECTIVE

An experimental study was undertaken to evaluate the effects of pH, initial oil concentration (dilution), and the inorganic nutrient media composition on the biodegradability of two metalworking fluid samples viz. IRMCO 141 and IRMCO 156 which contain Hexahydro-1,3,5 tris(2 hydroxy ethyl)-s-triazine as the preservative. The primary aim of the this work was to determine the biodegradability of the afore-mentioned fluids and to ascertain the most favorable conditions for the enhancement of degradation rates.

BATCH EXPERIMENTS

Experiments were carried out in 500 ml Erlenmeyer flasks with microbial populations of sewage origin along with metalworking fluids, each containing a synthetic medium as the inorganic nutrient source. The system parameters measured include biomass concentration in terms of the dry weight, chemical oxygen demand (COD), pH, and temperature. The experiments were continued for a period of over 30 days with the shake flasks maintained at 30 °C and at 175 rpm.

To study the effect of pH on biodegradation, six shake flasks were maintained at six different pH values. The initial oil concentration was maintained at 1% in all the flasks. The inorganic nutrient medium labelled as C of composition shown below was used to provide the essential nutrients to the microbial growth. The pH was controlled at 4.0, 5.0, 6.0, 7.0, 8.0 and 9.0 in the six shake flasks with the help of sulphuric acid (0.1 Molarity) and sodium hydroxide (0.1 Molarity). This procedure was repeated for both samples of oil. The biomass and COD concentration variation with time is shown in Figs. 1 and 2 for the samples of IRMCO 141 and IRMCO 156,

respectively. The COD removal percentages at various values of operating pH are shown in Fig. 3 for these two oil samples.

The dilution effect was studied by diluting the oil in four shake flasks to 0.5%, 1.0%, 2.0% and 5.0% by volume. The inorganic nutrient composition was that of the medium labelled as B for each of the dilutions. This set-up was used for both oil samples. The results of the COD removal percentages at each of the four dilutions for both oil samples is shown in Fig. 4.

Three inorganic nutrient compositions labelled as A, B and C were supplied separately to three different shake flasks containing oil at a concentration of 0.5%, to evaluate the effect of inorganic nutrient composition on the COD removal efficiency. The same scheme of experimentation was repeated for both the oil samples. The COD removal efficiencies for each of the three nutrient media compositions are presented in Fig. 5 for both oil samples. The compositions of these nutrient media are listed below.

Nutrient media A contained (in g/L): 7.5 $(NH_4)_2SO_4$; 1.5 Na_2HPO_4; 3.5 KH_2PO_4; 0.5 $MgSO_4.7H_2O$; 2.0 nutrient broth; $30 * 10^{-3}$ $FeSO_4.7H_2O$; $60 * 10^{-3}$ $CaCl_2.2H_2O$; $15 * 10^{-6}$ $CuSO_4.5H_2O$; $30 * 10^{-6}$ $Na_2B_2O_7.10H_2O$; $60 * 10^{-6}$ $MnCl_2.4H_2O$; $150 * 10^{-6}$ $ZnSO_4.7H_2O$; $30 * 10^{-3}$ $Na_2MoO_4.7H_2O$.

Nutrient media B contained (in g/L): 1.00 $(NH_4)_2SO_4$; 1.50 $CO(NH_2)_2$; 0.80 KH_2PO_4; 0.07 $MgSO_4.7H_2O$; 0.05 $CaCl_2.2H_2O$; 0.02 $ZnSO_4.7H_2O$; 0.02 $MnSO_4.4H_2O$; 0.005 $CuSO_4.5H_2O$; 0.10 $FeSO_4.7H_2O$; 1.00 Na_2SO_4.

Nutrient media C contained (in mg/L): 22.50 $MgSO_4.7H_2O$; 27.50 $CaCl_2$; 0.25 $FeCl_3.6H_2O$; 1.57 Na_2SO_3; 8.50 KH_2PO_4; 21.75 K_2HPO_4; 33.40 $Na_2HPO_4.7H_2O$; 1.70 NH_4Cl.

CONCLUSIONS

The significant conclusions of this work are as follows:

1. Occurance of multiple lag, exponential and death phases is common with a microbial population of the mixed origin. An antagonistic relationship exists among bacteria, fungi and protozoans.

2. Metalworking fluids are designed to minimize bacterial contamination while they are in use. In contrast, their biodegradation requires a condition without inhibitory factors detrimental to microbial growth. The pH appears to be an important factor; the biocidal effect of the preservatives added to the oil samples is a strong function of the operating pH.

3. The optimum pH for maximum biodegradation of oil sample IRMCO 141 was 6.0. For oil sample IRMCO 156, there was a range of pH between 5.0 and 7.0 in which maximum biodegradation was observed.

4. Dilution of the oil sample is necessary to economically optimize the biodegradation. The optimum concentration for IRMCO 141 is 2% and that for IRMCO 156 is 1%.

5. Urea as an additive to the nutrient media appears to have beneficial results.

ACKNOWLEDGEMENTS

This work was made possible through the financial support of Advanced Engineering Staff, General Motors Corporation, Warren, Michigan. Thanks are also due to P. N. Mishra of the General Motors Corporation for his assistance.

REFERENCES

Boswell, D. E., The biocidal requirements of cutting fluids, **Proceedings of the Third International Biodegradation Symposium**, J. M. Sharpley and A. M. Kaplan (Eds.), pp. 215-220, Allied Science Publishers, London (1976).

Hunz, R. P., Water-based metalworking lubricants, **Lubrication Engineering**, 40, 549-553 (1983).

Lee, S. M., Biodegradation of metalworking fluids, Masters Thesis, Kansas State University, Manhattan, Kansas (1986).

Lee, S. M., Ayush Gupta, L. E. Erickson, and L. T. Fan, Biodegradation of metalworking fluids, **Proceedings of the 17th Annual Biochemical Engineering Symposium**, ISU-ERI-Ames-88069, P. J. Reilly (Ed.), pp. 125-134, Iowa State University, Ames, Iowa (1987).

Lewis, R. B., Oil-degrading microorganisms, **Chemical Engineering Progress**, 83(10), 35-41 (1987).

Rossmoore, H. W., Microbial degradation of water-based metalworking fluids, **Comprehensive Biotechnology**, 4, 249-269, Pergamon Press, London (1985).

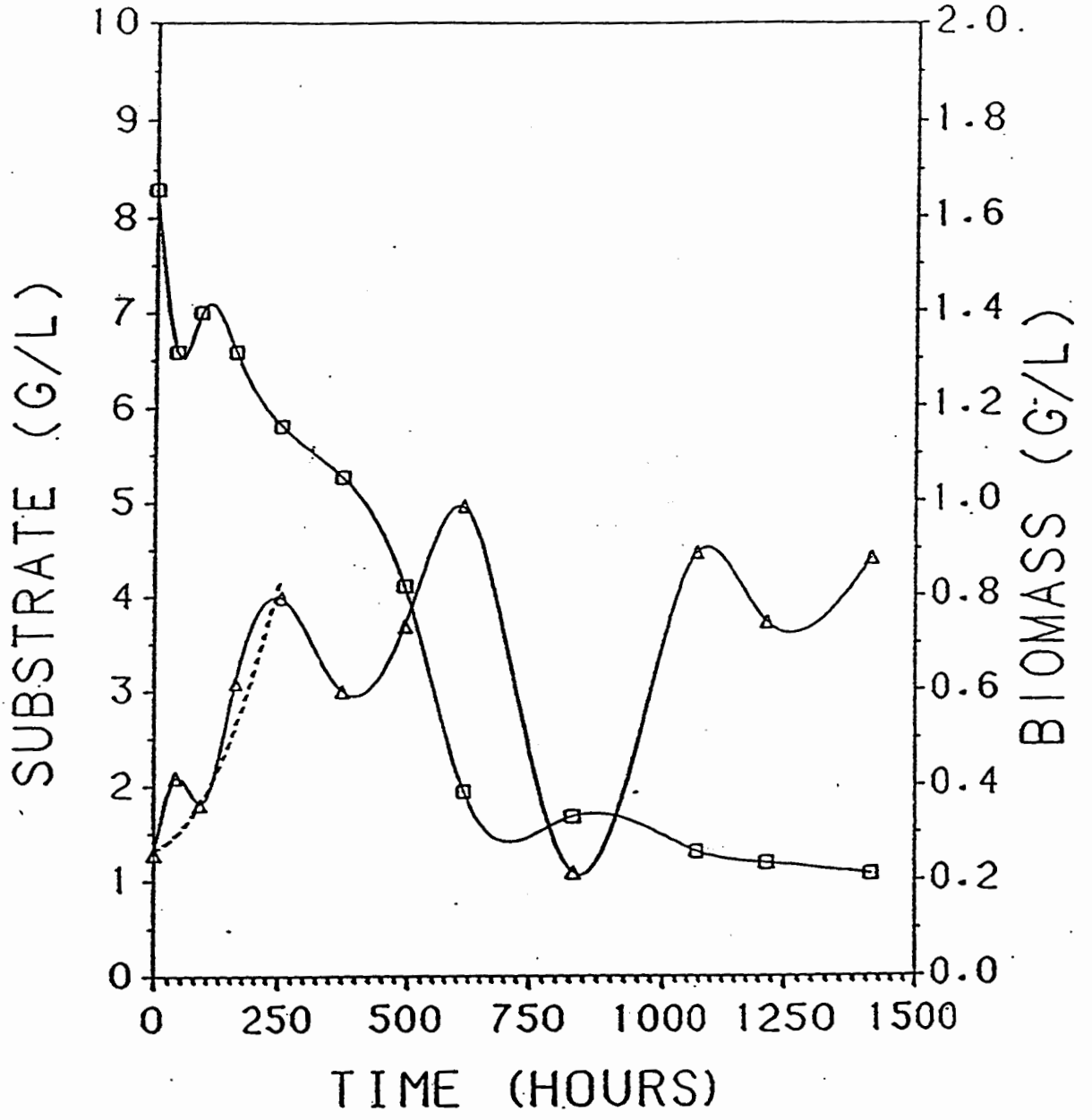

Figure 1. Biomass(Δ) and COD(□) variations with time for the mixed population of microorganisms growing on oil sample IRMCO 141 at a controlled pH of 6.0: dashed line represents the exponential growth model.

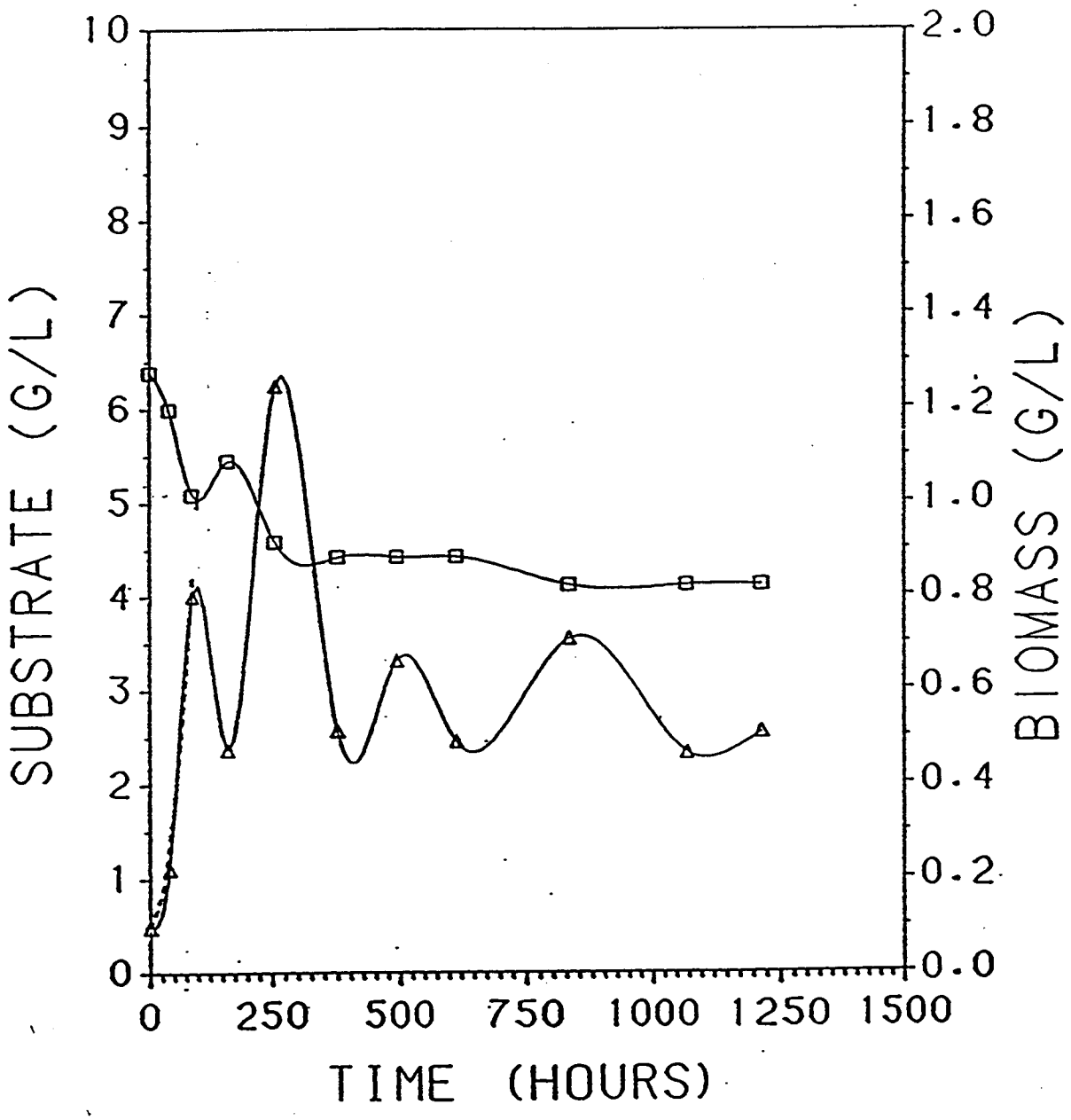

Figure 2. Biomass(Δ) and COD(□) variations with time for the mixed population of microorganisms growing on oil sample IRMCO 156 at a controlled pH of 7.0: dashed line represents the exponential growth model.

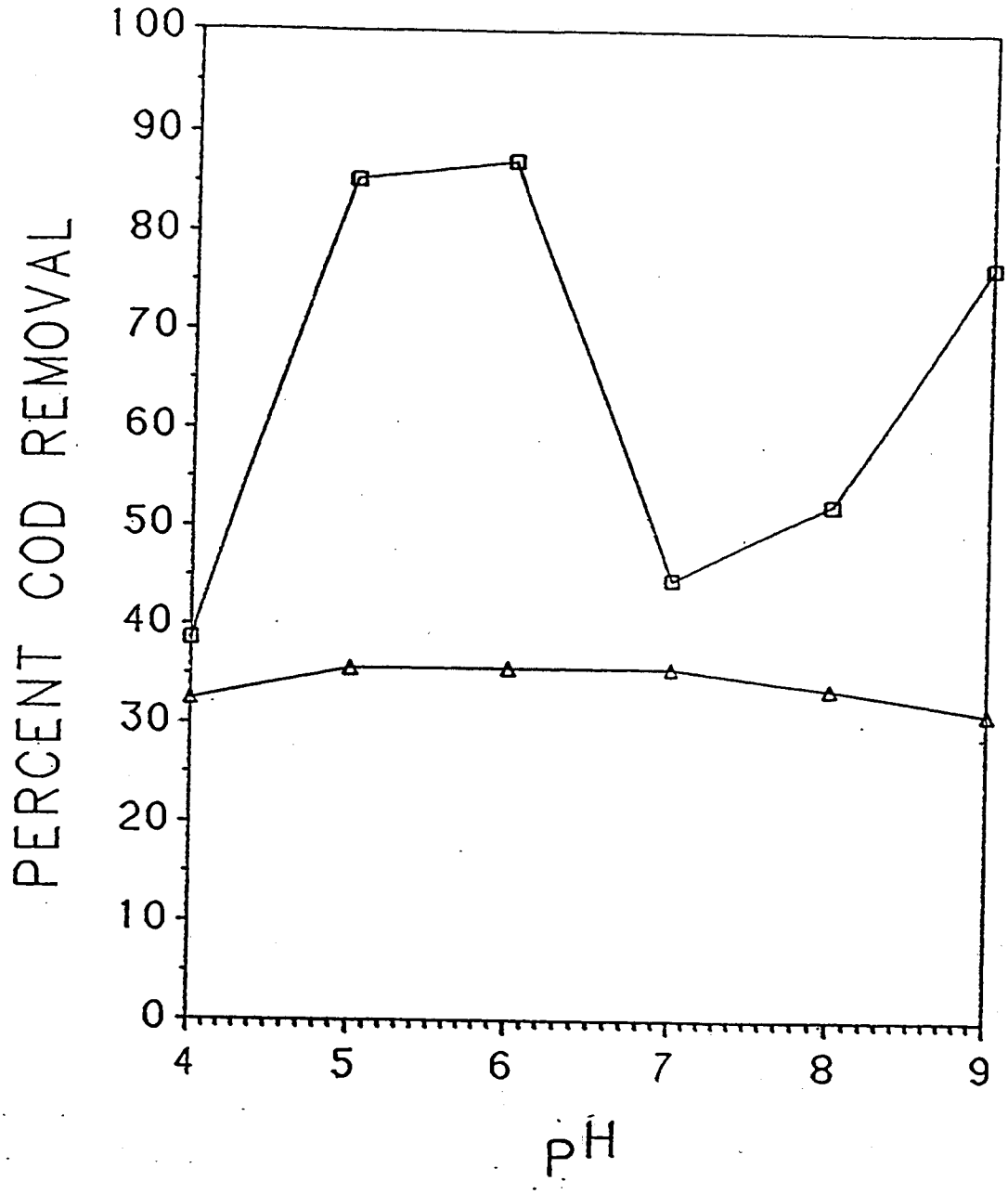

Figure 3. Percent COD removal at various pH values for the mixed population of microorganisms growing on oil samples IRMCO 141(□) and IRMCO 156(Δ).

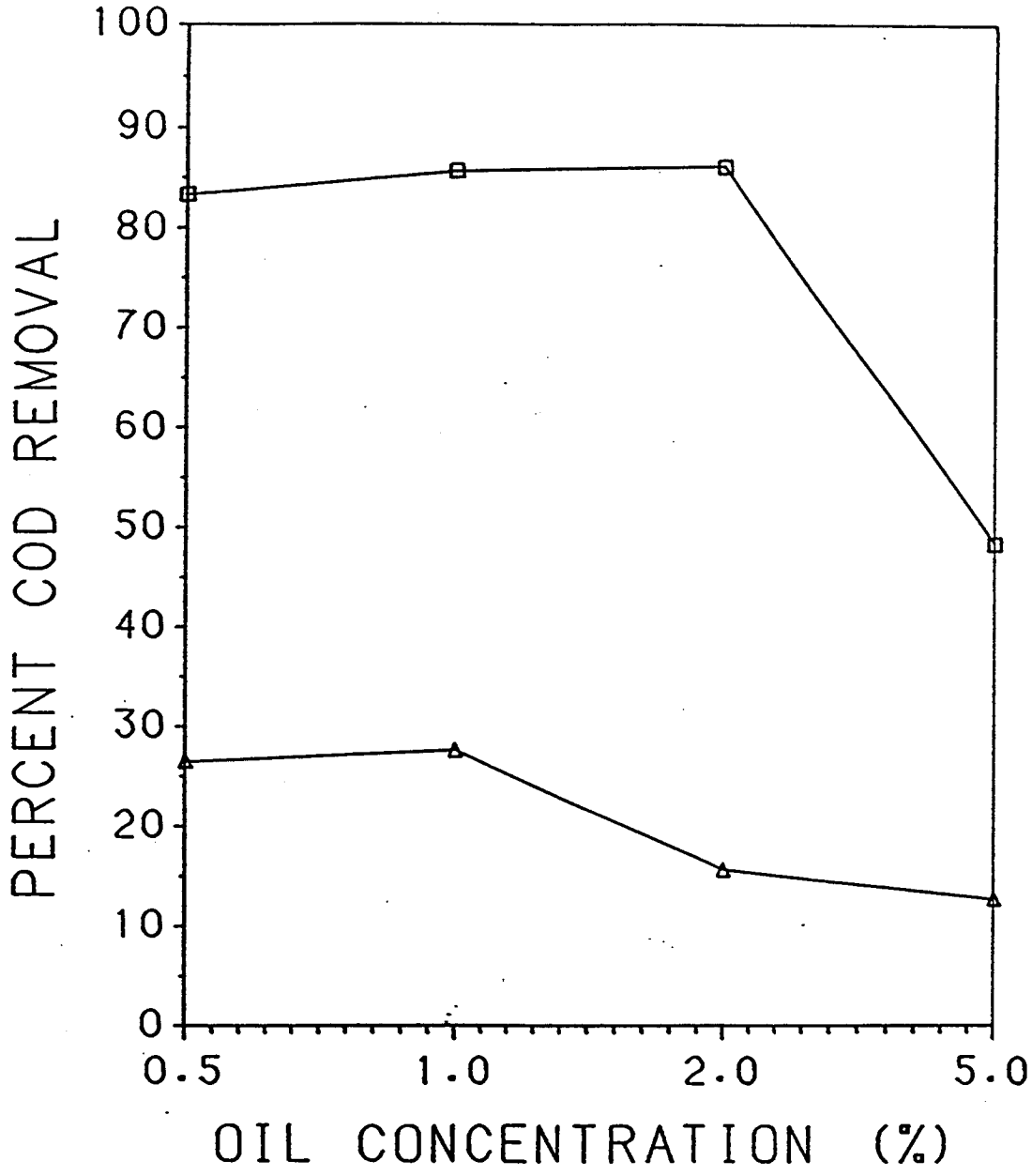

Figure 4. Percent COD removal at various initial oil concentrations for the mixed population of microorganisms growing on oil samples IRMCO 141(□) and IRMCO 156(Δ).

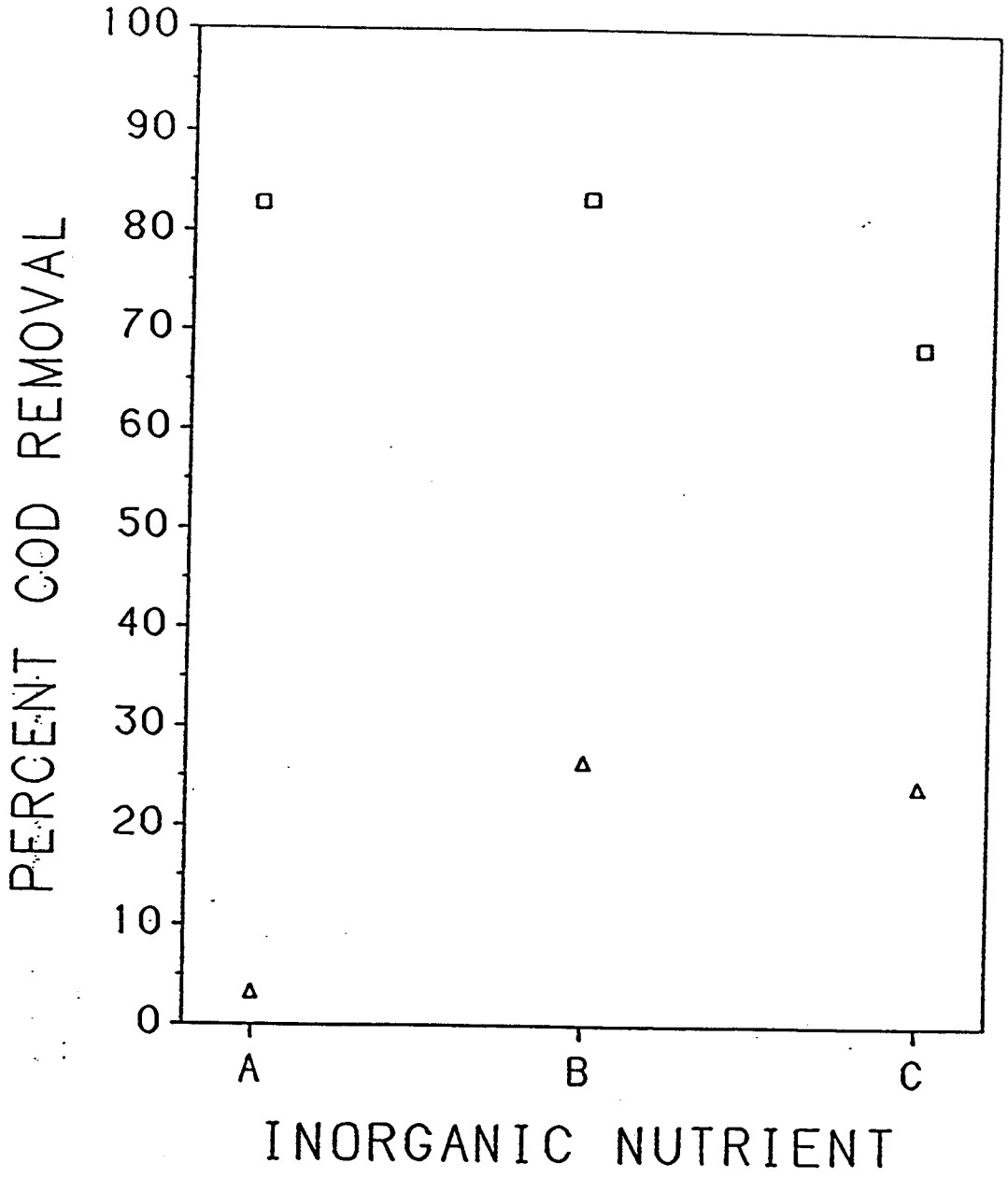

Figure 5. Percent COD removal at various inorganic nutrient compositions for the mixed population of microorganisms growing on oil samples IRMCO 141(□) and IRMCO 156(Δ).

DISSOLVED HYDROGEN CORRELATION WITH REDOX POTENTIAL IN ACETONE-BUTANOL FERMENTATION

Xiangdong ZHOU

Department of Microbiology
Colorado State University, Fort Collins, CO 80523

INTRODUCTION

Dissolved hydrogen has tremendous influence on fermentation pattern, metabolic regulation and end product formation in several anaerobic fermentations. Regulation of the fermentation pattern and end product formation by hydrogen pressure have been shown in ethanologenic anaerobes, e.g., Clostridium thermocellum (7), Clostridium saccharolyticum (6) and Thermoanaerobium brockii (5). These studies indicated that increased hydrogen concentration in the system inhibited the production of hydrogen and altered the flow of electrons in the biochemical pathway of the microorganisms. As a result, the composition of end products was changed and more ethanol, which is the major reduced end product, was produced in the system.

It is also well known that hydrogen plays an important role in the acetone-butanol fermentation. The effect of hydrogen on the regulation of the biochemical pathway of Clostridium acetobutylicum was studied by Yerushalmi and co-workers (8) and Doremus et al. (2) in terms of butanol accumulation. They found that the production of butanol was increased by the high level of dissolved hydrogen which was created at low agitation rates and/or high head-space partial pressure of hydrogen. However, in all the studies mentioned above the methods for determining the dissolved hydrogen concentration in the fermentation broth were complicated and time consuming. In order to control hydrogen concentration at optimal level, it is necessary to develop an on-line method for the measurement of dissolved hydrogen.

It was known that the direction and intensity of microbiological reactions depend considerablly on oxidation-reduction (redox) conditions in the system. Jacob (3) pointed out that the redox potential change to more negative values was correlated with the decrease of dissolved oxygen caused by the respiration of the bacteria in aerobic cultures. The rate and extend of decrease in redox potential were dependent on the growth rate and the physiological type of bacteria. Thus, it is obvious that the redox potential can be used as a good indicator for cell growth and oxygen level in aerobic cultures. It was also shown (4) in cultures of facultatively anaerobic bacteria that the metabolically produced hydrogen has a strong influence on the redox potential of the culture. The culture of Proteus vulgaris indicated an intense and fast redox potential negativation caused by hydrogen during the logarithmic growth phase. This finding indicated that the increase of dissolved hydrogen was associated with the decrease of redox potential. Here, the redox potential serves as a predictor for dissolved hydrogen level in the

anaerobic fermentation. Based on the above discussion, it is appearent that there would be a correlation between dissolved hydrogen and redox potential. Therefore, the major objective of this study is to determine the correlation between dissolved hydrogen and redox potential, and finally establish an on-line method to measure dissolved hydrogen in the anaerobic fermentation using a commercially available redox probe.

MATERIALS AND METHODS

In this study, the correlation between dissolved hydrogen and redox potential has been studied by using following three systems: (1) Distilled water.

(2) Media for Methanobacterium thermoautotrophicum and Clostridium acetobutylicum.

(3) Fermentation with Clostridium acetobutylicum.

The fermentor used was a Chemap Model CF fermentor manufactured in Switzerland with 7 liter total volume and 5 liter working volume. In distilled water and the medium systems, the experiments were designed to systematically change one of the four variables: temperature, agitation rate, head space pressure and hydrogen gas flow rate. Every time, when one variable was changed, both redox potential and dissolved hydrogen correspondingly changed. In this way, the correlation between dissolved hydrogen and redox potential was determined.

A strain of Clostridium acetobutylicum (ATCC 824) was used for the fermentations. The cultures were started from spores in corn-mash tubes stored at 5°C in the refrigerator. The inoculated tube was sealed, heat shocked by placing the tube in a beaker of boiling water for one minute, and then placed inside a temperature-controlled incubator at 37°C in the anaerobic chamber (Coy, Ann Arbor, MI). The fermentations were performed in the Chemap fermentor described above with 3 liters of liquid medium. The medium contained the following components in g/L: KH_2PO_4, 0.75; K_2HPO_4, 0.75; $MgSO_4$, 0.20; $MnSO_4$ H_2O, 0.01; $FeSO_4$ $7H_2O$, 0.001; NaCl, 1.00; Yeast extract, 5.00; Asparagine H_2O, 2.00; and $(NH_4)_2SO_4$, 2.00. Glucose, 50. L(+)-cysteine was left out since it has strong influence on redox potential. Both batch and continuous fermentations were conducted. All fermentations were run at 37°C. The agitation rate was set at 150 rpm throughout the fermentation. The pH was controlled at approximate 5.0 by automatic addition of 2.0 N KOH. Three parallel samples were taken simultaneously every two hours; 25 mL broth was withdrawn from the fermentor for each sample. These liquid samples were then placed in the refrigerator overnight for the equilibration of dissolved and headspace hydrogen in the airtight sampling bottles. 1 mL headspace gas samples were withdrawn from the sampling bottles for hydrogen concentration analysis using gas chromatograph. A Gow-Mac Series 550 Gas Chromatograph equipped with a thermal conductivity detector was used, and argon was used as the carrier gas. Solvents were analyzed by High Pressure Liquid Chromatography (HPLC) according to Buday (1).

After medium sterilization, the fermentor was sparged with nitrogen both previous to and during inoculation to keep

the sterile medium anaerobic. In the continuous fermentation, the dilution rates were set at 0.2 /h by setting a constant volume through a weight controller equipped with the fermentor. The components of fresh medium for feed substrate was the same as that in the fermentor. The feeding substrate was also kept free of oxygen by sparging with nitrogen.

RESULTS AND DISCUSSION

A. PARAMETER EFFECTS ON MASS TRANSFER OF HYDROGEN IN WATER SYSTEMS

A.1. Head Space Pressure

Figure 1 shows the effect of head space pressure on dissolved hydrogen and redox potential in water system. The dissolved hydrogen was found to increase linearly with the head space pressure in the range of 0 to 1.2 bars (gauge pressure), while all other conditions (temperature 20^{o}C, agitation rate 300 rpm, hydrogen gas flow rate 0.5 L/min) were kept constant. According to Henry's Law C=P/H (where C is gas concentration in the solution, P is partial pressure and H is Henry's constant), gas solubility was proportional to its partial pressure. Enhanced head space pressure resulted in an increase of hydrogen partial pressure, which in turn increased dissolved hygrogen concentration in the solution. As expected, a good correlation between dissolved hydrogen and redox potential was observed based on changing head space pressure. A straight line with r^2 (r is correlation coefficient about the straight line) value equal to 0.99 is shown in Figure 2 to illustrate the correlation between dissolved hydrogen and redox potential.

A.2. Agitation Rate

Dissolved hydrogen concentration increased almost linearly with agitation rate as the agitation rate was changed from 200 rpm to 400, 600, and 800 rpm, while all other conditions (including temperature 20^{o}C, hydrogen gas flow rate 0.5 L/min, pressure 0 bar) were maintained constant. Dissolved hydrogen concentration depended on the gas-liquid mass transfer rate which was directly related to agitation rate. Enhanced agitation rate resulted in the increase of mass transfer coefficient and/or interfacial area, which in turn improves gas-liquid mass transfer efficiency leading to a higher dissolved hydrogen concentration in the liquid. It was also found that a good correlation exists between redox potential and dissolved hydrogen by changing agitation rate with r^2=0.94.

A.3. Hydrogen Gas Flow Rate

In this set of experiments, hydrogen gas flow rate was changed, while temperature (20^{o}C), head space pressure (0 bar), agitation rate (300 rpm) were kept constant. It was found that dissolved hydrogen concentration increased linearly with the increase of hydrogen gas flow rate. Increased hydrogen gas flow rate probably made the solution more turbulent. Thus, the resistance to gas-liquid exchange was reduced, and the mass

transfer rate of hydrogen in the liquid was increased. Dissolved hydrogen was also a strong linear function of redox potential with r^2 equal to 0.91 under these experimental conditions.

A.4. Temperature

Dissolved hydrogen was observed to decrease with the increase of temperature in the range of 20°C to 60°C, while all other experimental conditions (including agitation rate 250 rpm, pressure 0 bar, and hydrogen gas flow rate 0.5 L/min) were maintained constant. When all other conditions are kept constant, gas solubility would normally decrease with the increased temperature. The higher the temperature, the lower the hydrogen gas solubility, and the lower the dissolved hydrogen concentration. The correlation between dissolved hydrogen and redox potential in water system by changing temperature also showed a straight line with r^2 equal to 0.99.

B. CORRELATION BETWEEN DISSOLVED HYDROGEN AND REDOX POTENTIAL IN MEDIA SYSTEMS

The same sets of experiments were conducted in C. acetobutylicum medium and M. thermoautotrophicum medium by changing temperature, head space pressure, hydrogen gas flow rate and agitation rate. The major results derived from media systems were similar to those obtained in water systems. The effects of parameters on dissolved hydrogen in media systems were observed to have the same general pattern as that derived from water systems. The corresponding correlation curves between dissolved hydrogen and redox potential in media systems also showed the same trends as that illustrated in water systems (Table 1).

In spite of the similarities between water systems and media systems, some different results were obtained. First, it was found that the redox potential values in media systems were generally higher than that measured in water systems. This was probably due to buffer capacity of the media systems. In a buffered solution like a microbiological medium, a low redox-transformation rate was caused by the strong buffer capacity. This low rate of redox transformation resulted in a slow formation of the potential at the electrode. Finally, it turns out to be true that the redox potential in a microbiological medium usually had slower changes than that in pure water. Based on above discussion, the amount of decrease of redox potential caused by dissolved hydrogen in the medium would be much smaller than that observed in pure water, since the medium had buffer capacity which led to a slower change of redox potential.

Second, the slopes of the linear regression for the media systems were generally greater than those derived for the water systems; an exception was the temperature run in M. thermoautotrophicum medium. This finding demonstrated that the dissolved hydrogen in media systems had less influence on redox potential. The possible reason for this observation was that the organic substance and inorganic salts in the medium may weaken the influence on redox potential exerted by dissolved hydrogen.

Third, the r^2 values, which represent the strength of

linear relationship between dissolved hydrogen and redox potential, were observed to be generally smaller in media systems; an exception was the pressure run in C. acetobutylicum medium.

C. REGULATORY FUNCTION OF HYDROGEN METABOLISM IN FERMENTATION BY CLOSTRIDIUM ACETOBUTYLICUM

C.1. Batch fermentation

Figure 3 shows the change of dissolved hydrogen and redox potential during the course of one batch fermentation. The dissolved hydrogen increased rapidly at the early stage, maximized at about 10 hours, then dropped quickly. Towards the end of the fermentation after about 25 hours, the dissolved hydrogen diminished to zero.

In the acetone-butanol fermentation, the rate of hydrogen production is controlled by hydrogenase activity. During the acid phase (usually within 10 hours) accompanying by a rapid increase of hydrogen production, intracellular electron flow is mainly directed to hydrogen formation whereas carbon flow principally to acid products. The hydrogenase activity is high, and the organism has a very efficient route for the disposal of internal electrons by producing gaseous hydrogen. Therefore, for maximum hydrogen production to occur during the acid phase of the fermentation is expected as shown in Figure 3. On the other hand, in the solvent phase (after about 10 hours) the electron flow and carbon flow are diverted to the solvent end products. The solventogenesis is associated with decrease of hydrogenase activity, and the organism diverts intracellular protons and electrons to neutral solvents in order to maintain electron balance and physiological function. This is why the dissolved hydrogen is observed to decrease quickly after the peak at about 10 hours (Figure 3).

The correlation between dissolved hydrogen and redox potential in the batch fermentation is given in Figure 4. The linear relationship between these two variables is unsatisfactory with r^2 value only 0.305. This is because the redox potential in the second phase no longer follows the trend of dissolved hydrogen, as shown in Figure 3. Since the redox potential is not a strong function of dissolved hydrogen in batch fermentation, the approach for on-line measurement of dissolved hydrogen using a redox potential probe may not be practical in batch fermentations of C. acetobutylicum.

C.2. Continuous Fermentation

The changes of dissolved hydrogen and redox potential in one continuous fermentation are shown in Figure 5 with dilution rate of 0.2/h. The dissolved hydrogen increased quickly at the early stage just like in batch fermentation. But after the fermentation was operated in continuous mode, unlike in batch fermentation the dissolved hydrogen did not drop down, but was constant. This is probably due to the continuous addition of fresh medium to the fermentor. The organism can continuously consume nutrients and produce hydrogen. When the fermentation was performed in continuous mode, the system was kept in a relative

steady-state. The physiological status and enzyme activities inside the cell were also kept fairly stable. Thus, the dissolved hydrogen level in continuous culture can be maintained relatively constant due to the rather stable hydrogenase activity. However, the actual reasons for this constant level of dissolved hydrogen concentration in the continuous culture are remained unknown. The redox potential in the continuous culture first showed a great change to more negative values, accompanied by a rapid increase of dissolved hydrogen. This redox potential change was undoubtedly caused by the increase of dissolved hydrogen which was created by the rapid growth of microorganisms. Then, the redox potential was maintained almost constant, after the fermentation was conducted in continuous mode. This constant redox potential may be controlled by the strong redox buffer capacity of the microbial culture. It is apparent from Figure 5 that the redox potential curve followed exactly the same pattern as dissolved hydrogen. This finding would suggest that there is a good correlation between redox potential and dissolved hydrogen in continuous culture. The correlation curve between these two variables in continuous culture is given in Figure 6. As expected, the curve was straight line with r^2 value equal to 0.989. Thus, we can conclude that a strong linear relationship exists between dissolved hydrogen and redox potential in continuous culture system.

CONCLUSION

The interrelationship between dissolved hydrogen and redox potential was investigated in this study in three systems: distilled water, media for C. acetobutylicum and M. thermoautotrophicum, and fermentation with C. acetobutylicum. The main results are summarized in Table 1. The r^2 values were generally very high with only one exception of 0.305 in batch fermentation. Therefore, we can conclude that a strong linear relationship between redox potential and dissolved hydrogen was observed in most systems tested. There is potential for on-line measurement of dissolved hydrogen in the anaerobic fermentation of C. acetobutylicum using a commercially available redox probe. The redox potential is a useful indicator of disslved hydrogen in anaerobic fermentation, since our results shown that the redox potential was a strong function of dissolved hydrogen in continuous culture of C. acetobutylicum. Therefore, it is highly recommended to consider the redox poptential as a parameter that can be used to control the dissolved hydrogen concentration in anaerobic fermentations.

REFERENCES

1. Buday, Z. 1988. Improved Acetone-Butanol Fermentation Analysis. Proceedings of the 18th Biochem. Eng. Symp.
2. Doremus, M.G., J.C. Linden, and A.R. Moreira. 1985. Agitation and pressure effects on acetone-butanol fermentation. Biotechnol. Bioeng. 27:852-860.
3. Jacob, H.E. 1970. Redox potential. Methods in Microbiol.

2:91-123.
4. Jacob, H.E. 1974. Reasons for the redox potential in microbial cultures. Adv. Microbial Eng. part 2, pp. 781-788.
5. Lamed, R., and J.G. Zeikus. 1980. Ethanol production by thermophilic bacteria. J. Bacteriol. 144: 569-578.
6. Murray, W.D., and A.W Khan. 1983. Ethanol production by a newly isolated anaerobe Clostridium saccharolyticum. Can. J. Microbiology. 29:342-347.
7. Su, T.M., R. Lamed, and J.H. Lobos. 1981. Effect of stirring and hydrogen on ethanol production by thermophilic fermentation. Proceedings of the 2nd World Cong. of Chem. Eng. and World Chem. Exposition. 1:352-356.
8. Yerushalmi, L., B. Volesky, and T. Szczesny. 1985. Effect of increased hydrogen partial pressure on the acetone-butanol fermentation by Clostridium acetobutylicum. Appl. Microbiol. Biotechnol. 22:103-107.

Table 1. Summary of the Results from All Three Systems

Working System	Variable	Slope	r^2	Redox Range
Methanobacterial Medium	Agitation Rate	1.2×10^{-4}	0.85	-356 to -364
Methanobacterial Medium	Temperature	2.8×10^{-5}	0.80	-356 to -405
Clostridial Medium	Pressure	2.8×10^{-4}	0.92	-378 to -386
Clostridial Medium	Gas Flow Rate	1.3×10^{-4}	0.81	-359 to -373
Distilled Water	Agitation Rate	5.5×10^{-5}	0.94	-702 to -735
Distilled Watwer	Temperature	6.9×10^{-5}	0.99	-702 to -727
Distilled Water	Pressure	7.5×10^{-5}	0.99	-716 to -740
Distilled Water	Gas Rate	1.4×10^{-5}	0.91	-728 to -753
Batch Fermentation		1.1×10^{-5}	0.305	-280 to -508
Continuous Ferm.		1.7×10^{-5}	0.989	-298 to -520

** The values of slope and r^2 are from correlation curves.

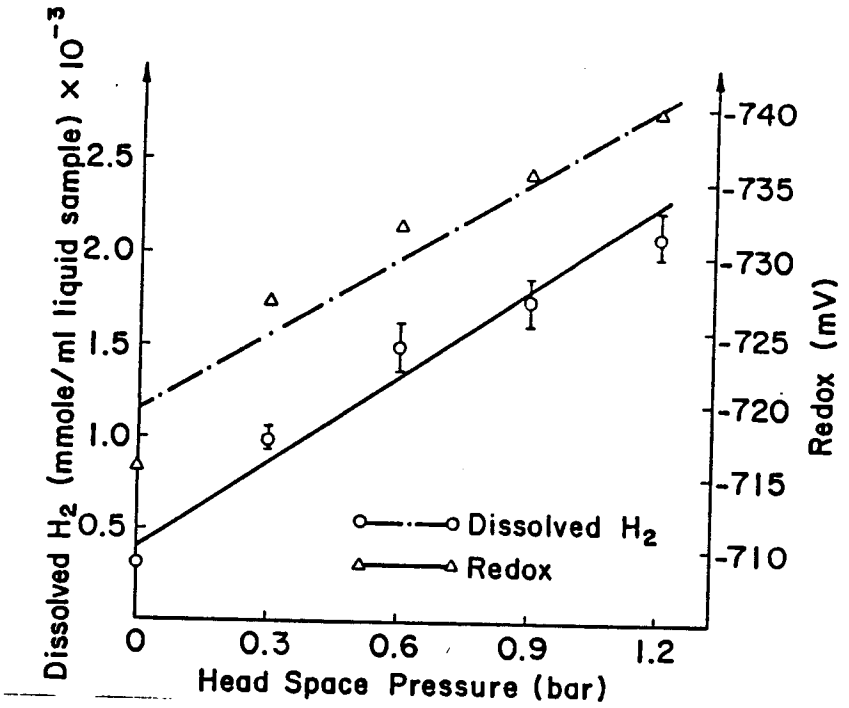

Figure 1. The Effect Of Head Space Pressure On Dissolved Hydrogen And Redox Potential In Distilled Water.

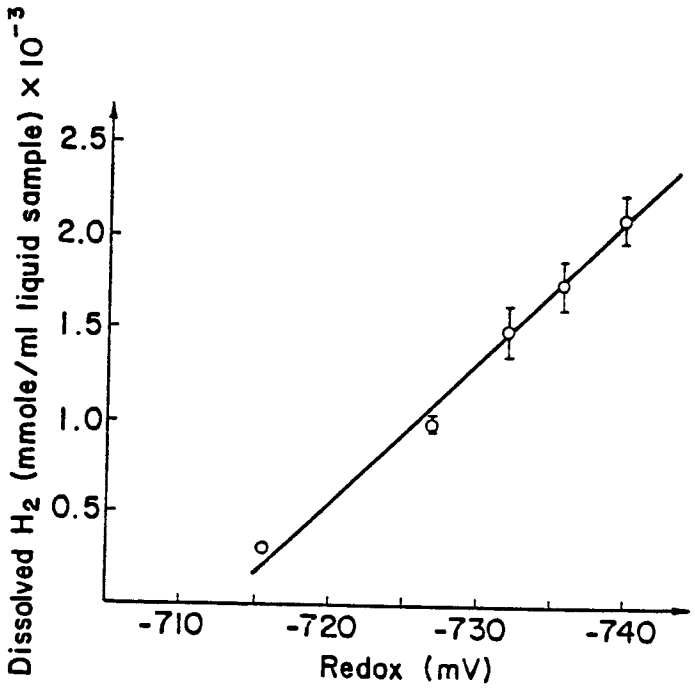

Figure 2. Dissolved Hydrogen ---- Redox Potential Correlation In Distilled Water By Changing Head Space Pressure.

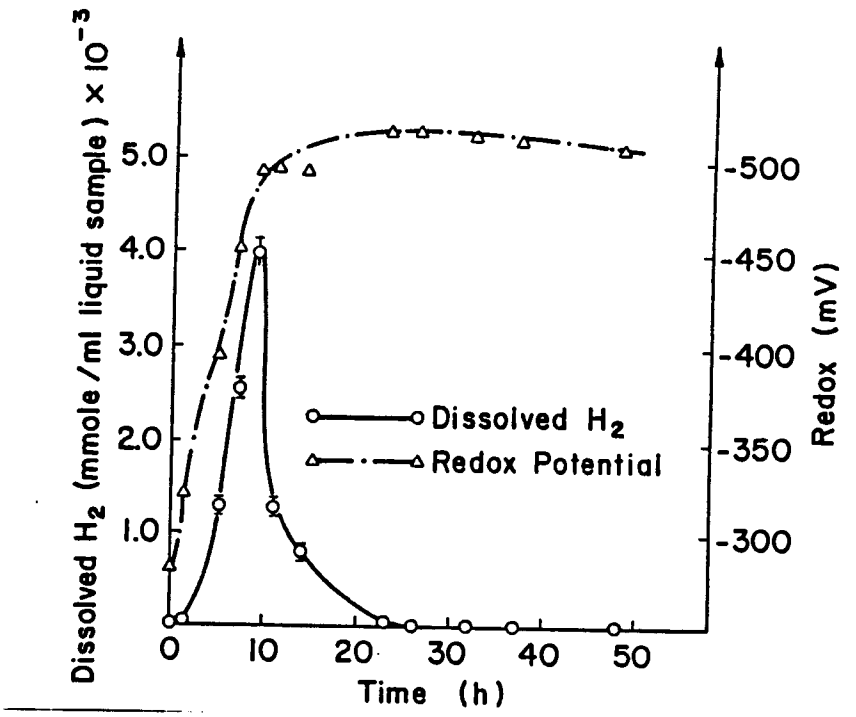

Figure 3. Redox Potential and Dissolved Hydrogen Time Course in Batch Fermentation with C. acetobutylicum.

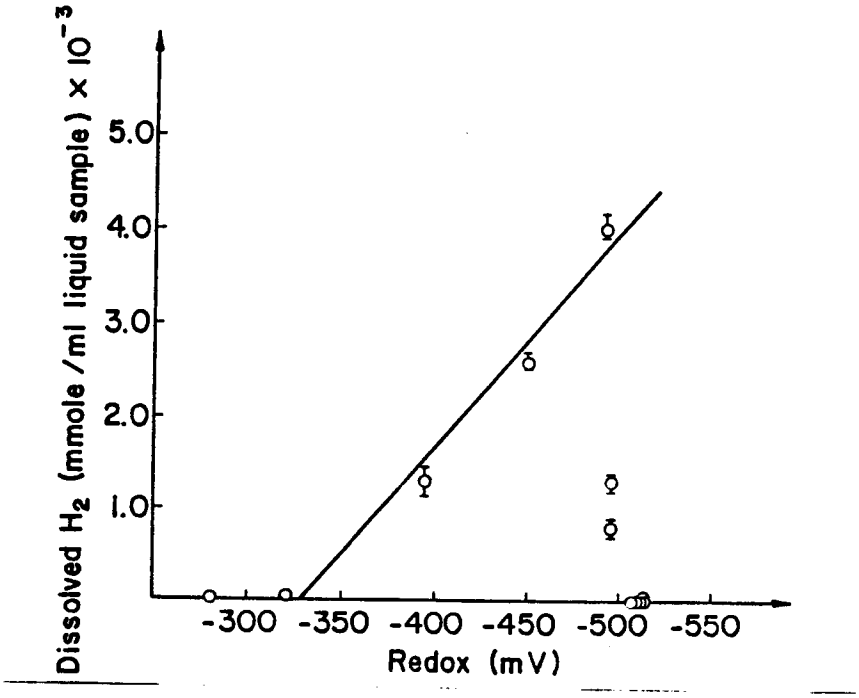

Figure 4. Dissolved Hydrogen-----Redox Potential Correlation in Batch Fermentation with C. acetobutylicum.

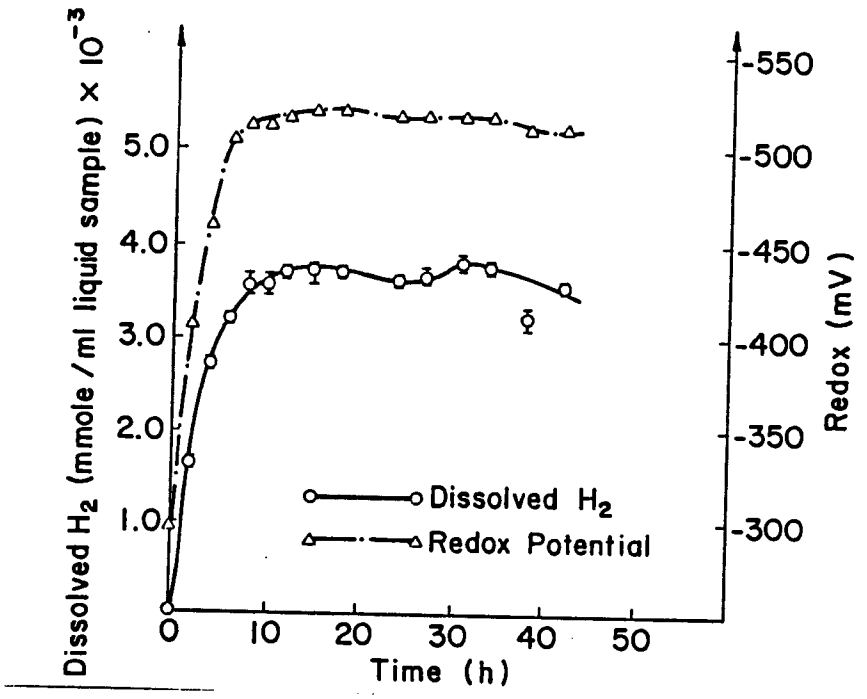

Figure 5. Redox Potential and Dissolved Hydrogen Time Course in Continuous Fermentation with C. acetobutylicum.

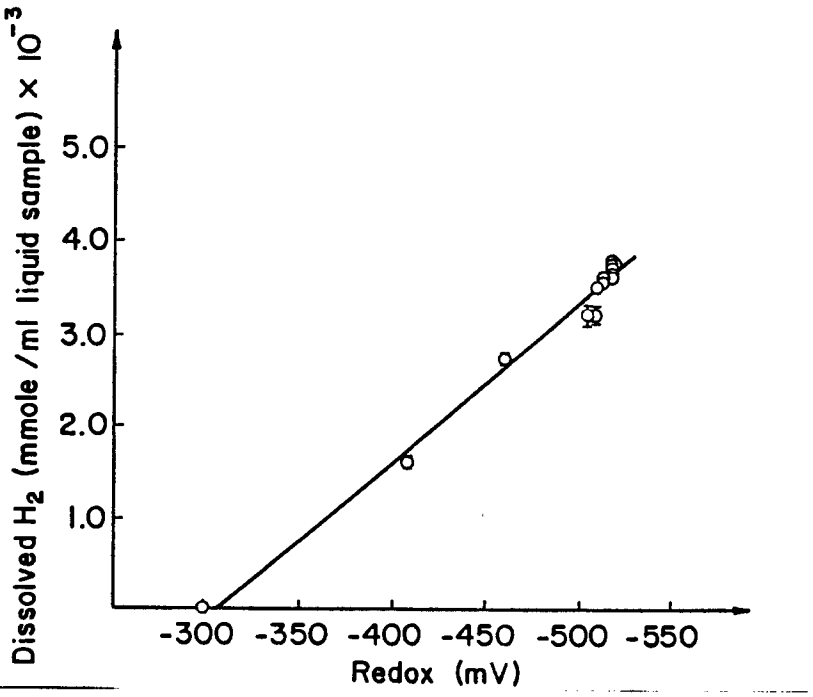

Figure 6. Dissolved Hydrogen-----Redox Potential Correlation in Continuous Fermentation with C. acetobutylicum.

"Modeling of Ensiling Fermentation of Sweet Sorghum"

A. K. Hilaly
Department of Agricultural and Chemical Engineering
Colorado State University, Fort Collins, CO 80523

INTRODUCTION :

Ensiling is a complicated microbial anaerobic process which results in significant biochemical changes in the forage material placed in the silo and thus leads to its preservation for subsequent uses. There is sufficient historical evidence which suggests that the ensiling process had been practiced for centuries in many parts of the world as a means of preserving crops. However, due to the complicated nature of the process and lack of knowledge of the biochemical changes in the silage, the process was not being carried out efficiently. Recently the process has drawn attention of many investigators and it is gaining ever increasing significance as a useful storage method for forage materials.

Sweet sorghum may be used as a convenient raw material for the production of fuel alcohol and chemical feedstocks through fermentation process. Ensilage of sweet sorghum enables one to preserve it with expenditure of little energy and thus makes it available as the source of fermentable carbohydrates over a considerable portion of the year. The objective of this work is to develop a mathematical model of the ensilage process of sweet sorghum in order to simulate the major biochemical changes during the process. In this modeling approach several simplifying assumptions were made which will be pointed out in the subsequent sections while developing the model.

MODEL DEVELOPMENT :

The rate of change of water soluble carbohydrate (WSC) concentration may be expressed as

$$\frac{dS}{dt} = -\frac{X.Gr}{Y_g} + X.Dr.Y_d \qquad (1)$$

where X = concentration of bacterial mass, Gr = specific growth rate, Dr = specific death rate, S = concentration of WSC. The value of the growth yield coefficient Y_g is assumed to be 0.05 based on our experimental data. The coefficient of bacterial mass released as WSC, Y_d, is assumed to be equal to 0.166 based on the data collected by Stouthamer. The first term in the right hand side of equation (1) is the amount of WSC consumed by the growing bacteria while the second term is the WSC released by bacterial death.

The rate of change of bacterial mass is given by

$$\frac{dX}{dt} = (Gr - Dr).X \qquad (2)$$

The specific growth rate Gr is dependent on various environmental factors, such as, temperature (T), pH, water activity (a_w) and water soluble carbohydrate concentration (S). Therefore, Gr may be expressed as

$$Gr = Gr^m . f_{gpH} . f_{aw} . f_s \qquad (3)$$

where Gr^m = maximum specific growth rate dependent upon temperature, f_{gpH} = fraction of Gr^m as dependent on pH, f_{aw} = fraction of Gr^m as dependent on a_w, f_s = fraction of Gr^m as dependent on S.

The maximum specific growth rate may be calculated from the relation

$$Gr^m = \exp[\ E1 - E2/RT\ ] \qquad (4)$$

where R is the universal gas constant and E1 & E2 are Arrhenius constants depending on the species of the bacteria. In our experiments Lactobacillus. plantarum and Streptococcus. faecium were used. Data for the former is available only and hence we assumed the same values of E1 and E2 for the second microorganism. Between 30 C and 35 C, the values of E1 and E2 are thus 17.22 J/mole & 42307 J/mole respectively.

Pitt et al. did regressional analysis of experimental data on Pediococcus. pentosaceus and Streptococcus. faecalis and found the following relations respectively to describe the effect of pH on growth.

$$\begin{aligned} f_{gpH} &= -3.45 + 1.27pH - 0.0899pH^2, \quad 3.7<pH<6.3 \\ &= -23.2 + 7.62pH - 0.6pH^2 \quad , \quad 6.3<pH<7.3 \\ \text{and } f_{gpH} &= -3.48 + 1.27pH - 0.09pH^2 \quad , \quad 3.72<pH<10 \end{aligned} \qquad (5)$$

We used the average of the above two relations in our model.

The effect of WSC on growth follows Michaelis-Menten kinetics and hence given by

$$f_s = \frac{S}{K_s + S} \qquad (6)$$

There are some controversy about the exact value of K_s. Pitt et al. calculated K_s from various sources of experimental data and suggested a value of 3.2×10^{-5} g WSC/g silage.

Growth rate depends on osmotic potential through water activity. Pitt et al. regressed the experimental data (collected by Lanigan) on L. plantarum and obtained the following relation.

$$f_{aw} = -5.55 + 6.64a_w - 268.7(a_w - 0.98)^2, \quad 0.93<a_w<0.99$$
$$= 1.0, \quad a_w>0.99 \qquad (7)$$

When the concentration of acetic acid reaches a threshold concentration for inhibition, the maximum specific growth rate is reduced according to the following relation

$$Gr^{mi} = Gr^m.[\ 1 - (\ A - A_o)/K_p\ ] \text{ for } A > A_o \qquad (7b)$$

where A_o is the threshold concentration of acetic acid for inhibition and K_p is the inhibition constant.

There is not sufficient information on death rates in the literature. Pitt et al. proposed

$$Dr = Dr^m.f_{dpH} \qquad (8)$$

where Dr^m = maximum specific death rate and f_{dpH} = fraction of maximum death rate as dependent on pH. The maximum death rate may be calculated from

$$Dr^m = \frac{Gr}{f_{dpH}} \text{ at } pH = pH^* \qquad (9)$$

where pH* is the modified pH dependent on dry matter content (DM) of the silage and is given by the relation

$$pH^* = -2.16 + 47.5DM - 81.7DM^2, \quad 0.206<DM<0.33$$
$$= 4.15, \quad DM<0.206 \qquad (10)$$

Pitt et al. obtained the above relation from regressional analysis of data on ensilage of ryegrass and alfalfa.

The value of f_{dpH} may be calculated from

$$f_{dpH} = 15.09 - 4.96pH + 0.409pH^2, \quad 5.98<pH<7.6$$
$$= 12.98 - 6.44pH + 1.289pH^2 - 0.0959pH^3, \quad 5.04<pH<5.98$$
$$= 1.0, \quad pH<5.04 \qquad (11)$$

The fermentation products in the silage are primarily lactic acid (L), acetic acid (A), and ethanol (E). The rate of change of total products (P) may be written as

$$\frac{dP}{dt} = (1 - Y_g).\frac{Gr.X}{Y_g} \qquad (12)$$

If f_L, f_A and f_E represent the fraction of lactic acid, acetic

acid and ethanol, respectively of total product, the rate of change of concentration of L, A and E may be expressed as

$$\frac{dL}{dt} = f_L \cdot \frac{dP}{dt} \qquad (13)$$

$$\frac{dA}{dt} = f_A \cdot \frac{dP}{dt} \qquad (14)$$

$$\frac{dE}{dt} = f_E \cdot \frac{dP}{dt} \qquad (15)$$

where $f_L + f_A + f_E = 1$ and f_L is given by

$$\begin{aligned} f_L &= 2.454 - 0.391pH + 51.0, \quad S/DM < 0.01 \\ &= 1.58 - 0.153pH \qquad\quad , \quad S/DM > 0.01 \end{aligned} \qquad (16)$$

The fraction $(1 - f_L)$ is divided into two equal parts to obtain f_A and f_E.

The pH of the silage depends on production of lactic acid and acetic acid as well as buffer index of the silage. The rate of change of pH is given by the following equation

$$\frac{dpH}{dt} = \frac{1}{B} \cdot \left[\frac{1}{MWL} \cdot \frac{dL_D}{dt} + \frac{1}{MWA} \cdot \frac{dA_D}{dt} \right] \qquad (17)$$

where L_D and A_D denotes the concentration of dissociated lactic acid and acetic acid, respectively. B is the buffer index of the silage; MWL and MWA are the molecular weight of lactic acid and acetic acid. The concentration of dissociated lactic acid and acetic acid is given by the following equations

$$L_D = \frac{10^{(pH - pKL)}}{1 + 10^{(pH - pKL)}} \cdot L \qquad (18)$$

and

$$A_D = \frac{10^{(pH - pKA)}}{1 + 10^{(pH - pKA)}} \cdot A \qquad (19)$$

where pKL and pKA are the pK values of lactic acid and acetic acid, respectively. The equation to calculate buffer index is given by

$$B = L.B_L + A.B_A + (1 - L - A).B_h \qquad (20)$$

where B_L = buffer index of lactic acid

$$= \frac{2.303.10^{(pH - pKL)}}{MWL[1 + 10^{(pH - pKL)}]^2} \qquad (21)$$

B_A = buffer index of acetic acid

$$= \frac{2.303.10^{(pH - pKA)}}{MWA[1 + 10^{(pH - pKA)}]^2} \qquad (22)$$

B_h = buffer index of herbage
= $(2.982 - 0.861pH + 0.661pH^2)/1000$ (23)

The equation describing the rate of change of water activity is given by

$$\frac{da_w}{dt} = (-a_w).\frac{1 - 2Y_g}{10(1-DM)}.\frac{Gr.X}{Y_g} \quad (24)$$

Greenhill proposed the following relation between dry matter content and water activity

$$a_w = 1 - \frac{b.DM}{1 - DM} \quad (25)$$

where b is a constant depending upon the forage material. We assumed a value of 0.04 in our model, which is the average value for alfalfa, white clover and ryegrass.

SOLUTION METHOD :

The simultaneous differential equations describing the change of concentration of WSC, lactic acid, acetic acid, ethanol, bacterial cell, pH and water activity were solved numerically by Runge-Kutta method with a step size of 0.25 day. There was no problem of instability of solution and computational time for the program was only 30 sec in cyber machine CDC 7600.

DISCUSSION :

Figure 1, 2, 3, 4 & 5 show the experimental and predicted time course of concentration of WSC, lactic acid, acetic acid, ethanol and pH. Experimental data were from Lindel et al. Good agreement can be seen between experiment and prediction in case of WSC and pH profile. However, it should be mentioned here again that WSC consists of glucose, fructose, xylose and mannitol. One limitation of our model is that it cannot estimate the amounts of these substances individually. It can also be seen that small discrepancies exist between experiment and prediction for lactic acid, acetic acid and ethanol concentration profiles.

Possible sources of error that led to some discrepancy are : (1) uncertainty of accuracy of the death parameter which affects the growth of bacteria as well as production of various metabolites. The technique for estimating the parameter Dr needs to be investigated more; (2) the assumed constant values of Y_g (growth yield) and Y_d (fraction of bacterial mass released as WSC). In actuality Y_g will vary during the course of fermentation and Y_d value needs to be estimated experimentally for the particular system of interest; (3) the assumption of maintaining a constant proportion between ethanol and acetic acid production

during the whole fermentation process. This may not be true since the microorganism may switch from one pathway to another according to its need depending upon the environment; (4) absence of appropriate product (lactic acid, acetic acid and ethanol) inhibition parameter. Although in our model, inhibition caused by acetic acid was considered, we assumed the parameter values to be the same as in acetone-butanol fermentation(Costa and Moreira). Therefore, the values of the inhibition parameters need to be estimated accurately for the particular system concerned.

Figure 6 shows the time course of bacterial population. As can be seen, only at the earlier portion of fermentation there is increase of cell mass concentration and thereafter it falls off gradually. Probably the high value of the death parameter Dr results in this type of profile. However, we do not have experimental data on cell mass concentration to verify the predicted curve.

REFERENCES :

1. Costa, J. M. & A. R. Moreira."Growth inhibition kinetics for acetone-butanol fermentation".In Foundation of Biochemical Engineering, Kinetics and Thermodynamics in Biological Systems, H. W. Blanch, E. T. Papoutsakis and G. Stephanopoulas,(eds). ACS Symposium Series No. 207, p.501-504. American Chemical Society, Washington D.C.,1983.

2. Pitt. R. E. & R. Y. Leibensperger. "A quantitative model of the silage process in lactate silages". Grass and Forage Science, vol 40, p.279-303, 1985.

3. Neal, H. D. & J. H. Thornby. " A model of the anaerobic phase of the ensiling". Grass and Forage Science, vol 38, p.121-134, 1983.

4. Stouthamer, A. H. "A theoretical study on the amount of ATP required for the systhesis of mirobial cell material" Antonic van Leewenhoek, vol 39, p.545-565, 1973

5. Greenhill, W. L. "Plant juices in relation to silage fermentation.III Effect of water activity of juice" Journal of British Grassland Society,vol 19, p.336-339, 1964.

6. Lanigan, G. W. "Silage bacteriology.I.Water activity and temperature relationships of silage strains of Lactobacillus plantarum, Lactobacillus brevis and Pediococcus cerevisae." Aus. J. of Biological Science,vol 16, p.606-615, 1963.

7. Linden, J. C., Henk, L. L.,Murphy, V. G., Smith, D. H., Gabrielsen, B. C., Tengerdy, R. P. and L. Czako. "Preservation of potential fermentables in sweet sorghum by ensiling." Biotechnology and Bioengineering, vol 30, p.860-867, 1987.

NOMENCLATURE :

Gr = specific growth rate (day^{-1})
Gr^m = maximum specific growth rate
f_{gpH} = fraction of maximum growth rate dependent on pH.
f_s = fraction of maximum growth rate dependent on WSC.
f_{aw} = fraction of maximum growth rate dependent on water activity
Dr = specific death rate (day^{-1})
Dr^m = maximum specific death rate
f_{dpH} = fraction of maximum specific death rate dependent on pH
Y_g = growth yield
Y_d = fraction of bacterial mass released as WSC
f_L = lactic acid fraction of product
f_A = acetic acid fraction of product
f_E = ethanol fraction of product
B = buffer index of silage {eq acid(pH g silage)$^{-1}$}
B_L =buffer index of lactic acid{eq acid(pH g lactic acid)$^{-1}$}
B_A =buffer index of acetic acid{eq acid(pH g acetic acid)$^{-1}$}
B_h = buffer index of herbage {eq acid(pH g herbage)$^{-1}$}
L_D = dissociated lactic acid { g acid/(g silage)$^{-1}$}
A_D = dissociated acetic acid { g acid/(g silage)$^{-1}$}
pH^* = modified pH
MWL = molecular weight of lactic acid
MWA = molecular weight of acetic acid
DM = dry matter fraction
b = constant dependent on forage material.

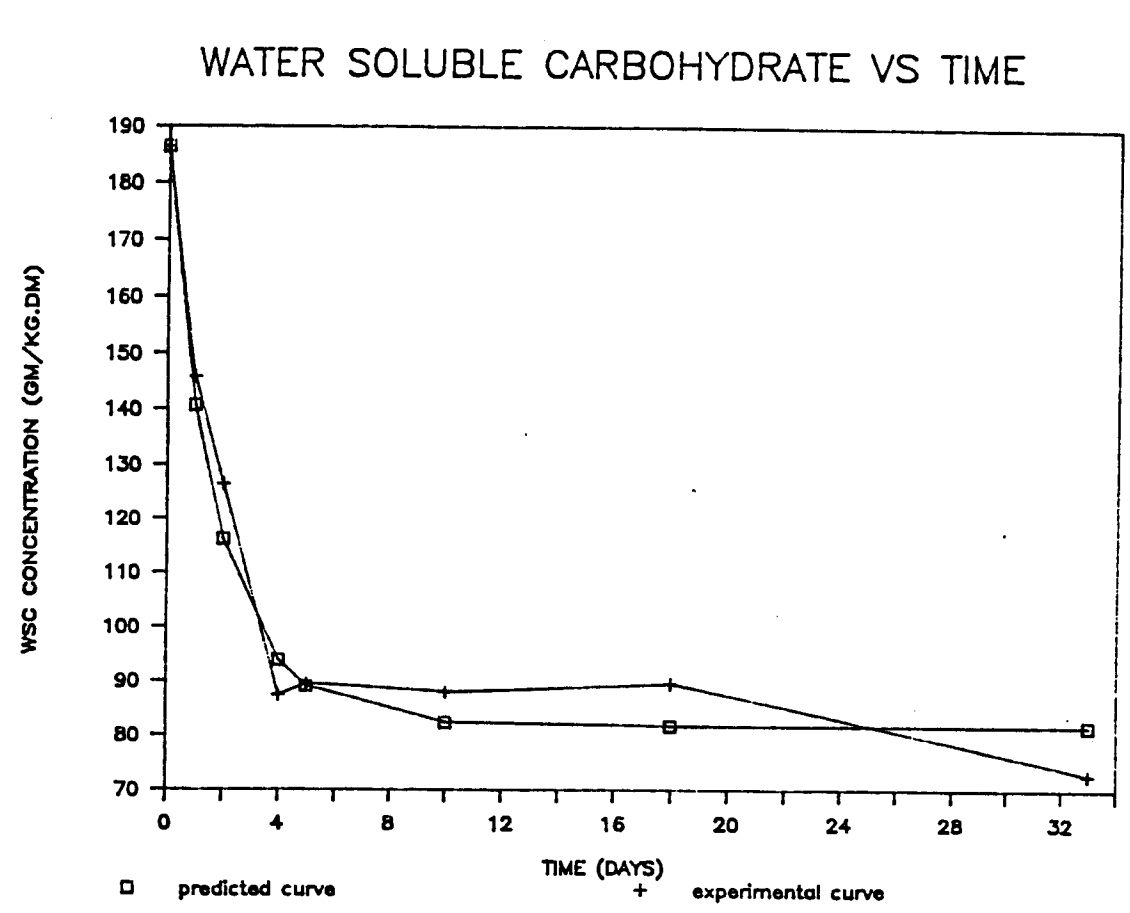
WATER SOLUBLE CARBOHYDRATE VS TIME
WSC CONCENTRATION (GM/KG.DM)
190
180
170
160
150
140
130
120
110
100
90
80
70
0
4
8
12
16
20
24
28
32
TIME (DAYS)
predicted curve
experimental curve

Fig 1

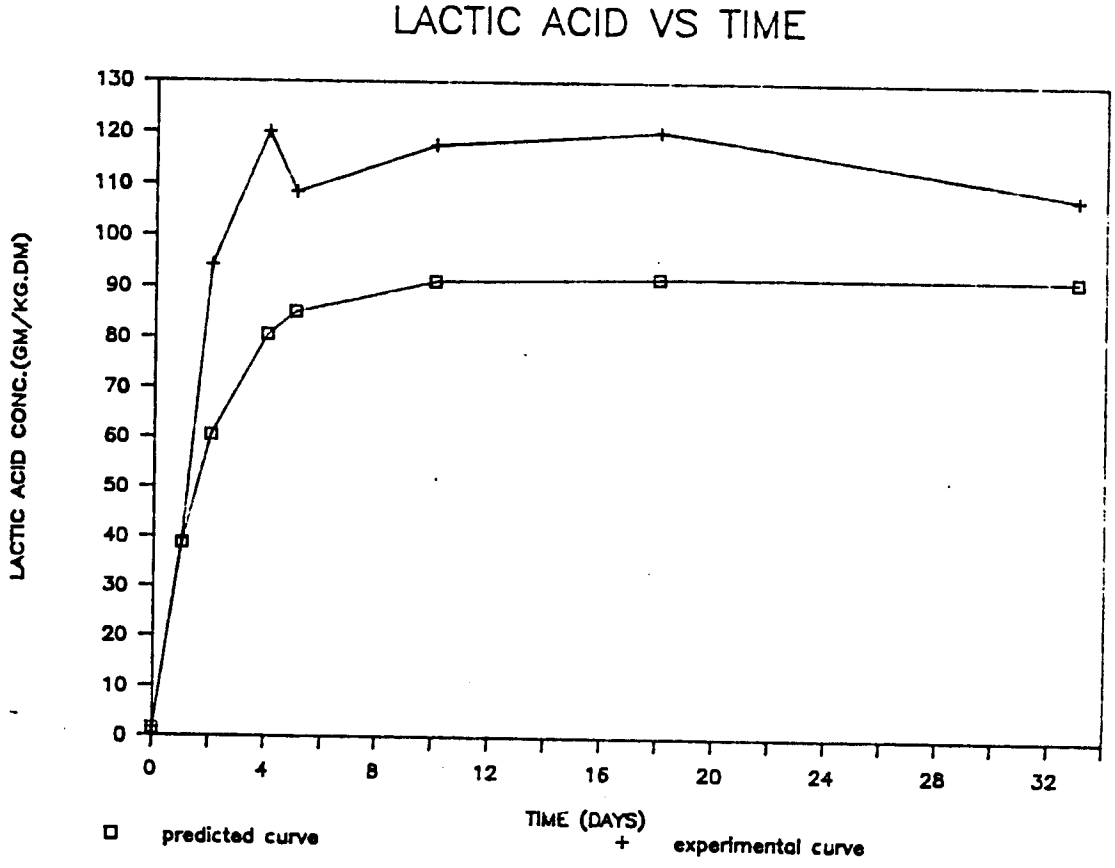
LACTIC ACID VS TIME
LACTIC ACID CONC.(GM/KG.DM)
130
120
110
100
90
80
70
60
50
40
30
20
10
0
0
4
8
12
16
20
24
28
32
TIME (DAYS)
predicted curve
experimental curve

Fig 2

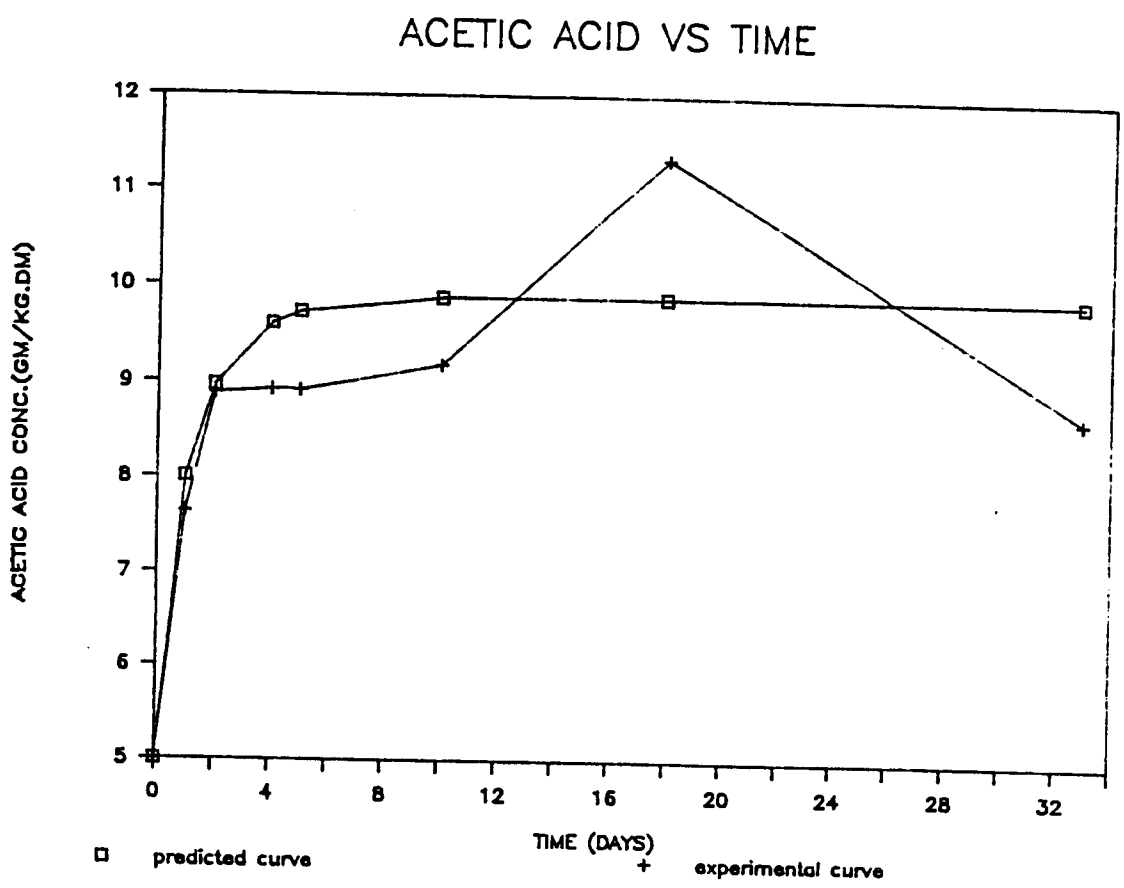
ACETIC ACID VS TIME
ACETIC ACID CONC.(GM/KG.DM)
12
11
10
9
8
7
6
5
0
4
8
12
16
20
24
28
32
TIME (DAYS)
predicted curve
experimental curve

Fig 3

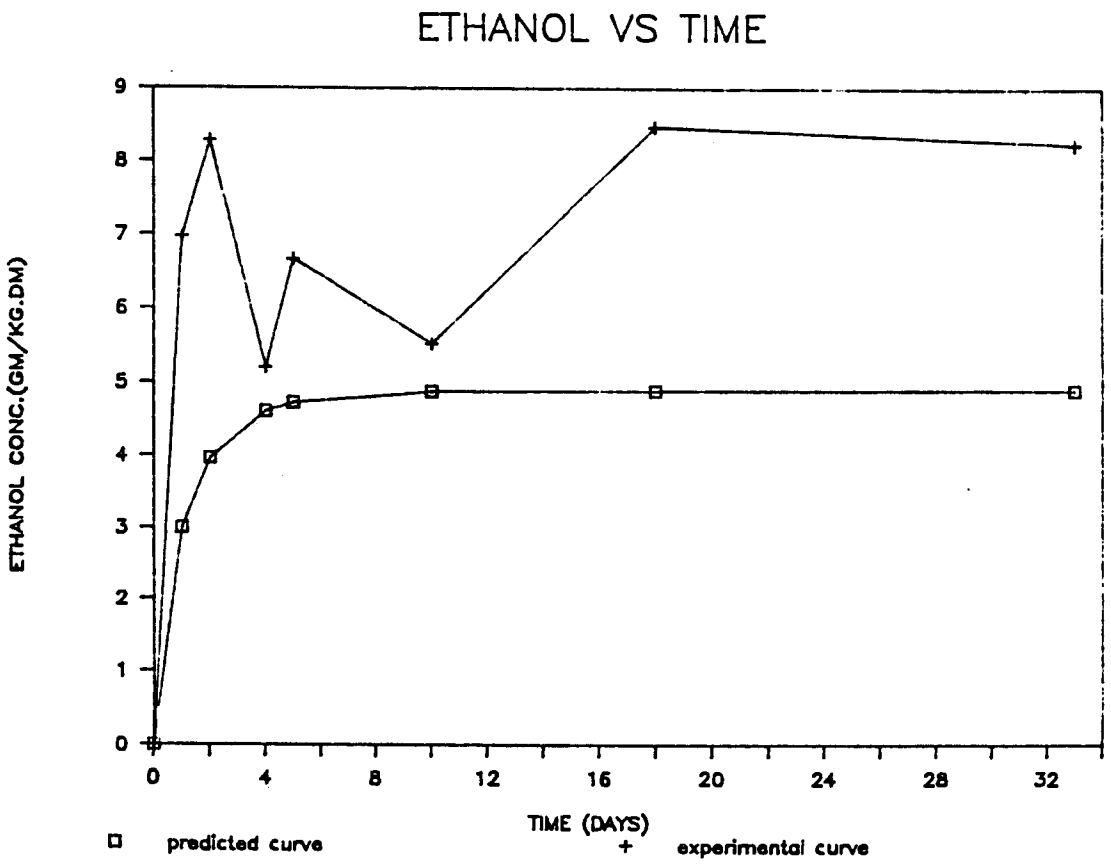
ETHANOL VS TIME
ETHANOL CONC.(GM/KG.DM)
9
8
7
6
5
4
3
2
1
0
0
4
8
12
16
20
24
28
32
TIME (DAYS)
predicted curve
experimental curve

Fig 4

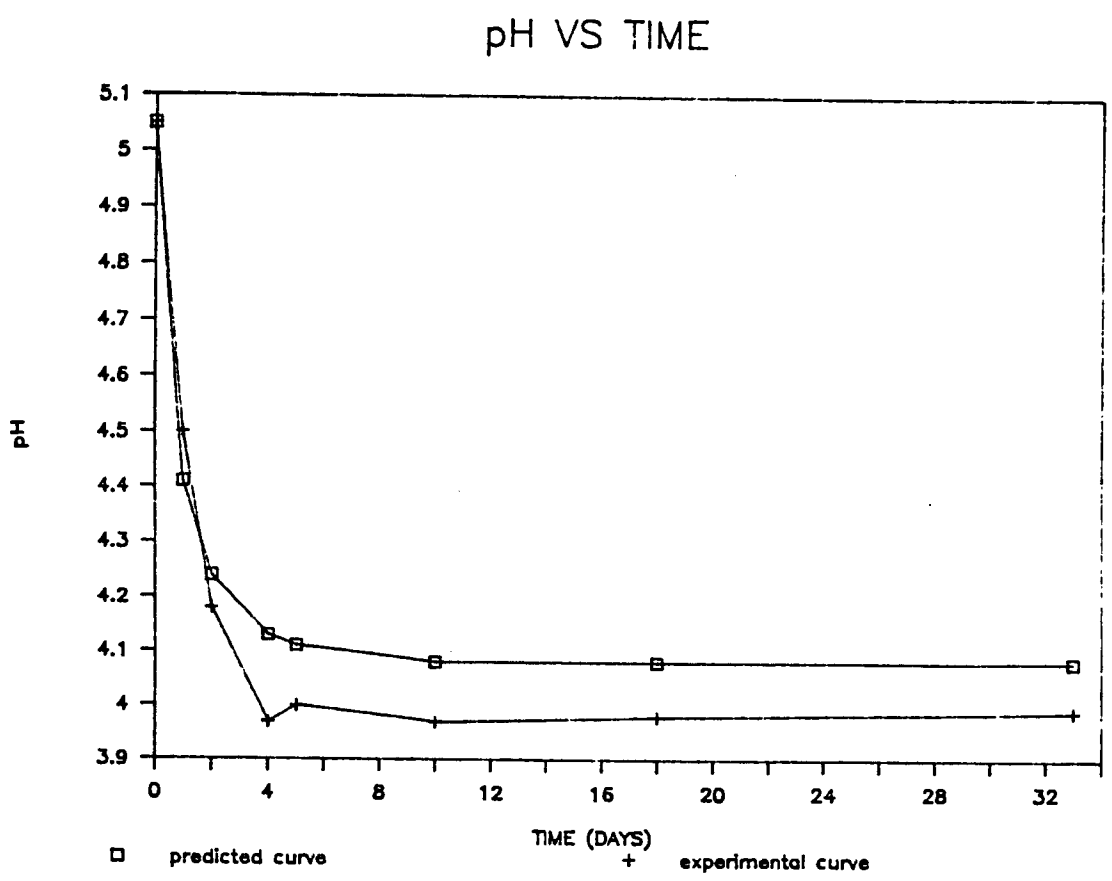
pH VS TIME
pH
5.1
5
4.9
4.8
4.7
4.6
4.5
4.4
4.3
4.2
4.1
4
3.9
0
4
8
12
16
20
24
28
32
TIME (DAYS)
predicted curve
experimental curve

Fig 5

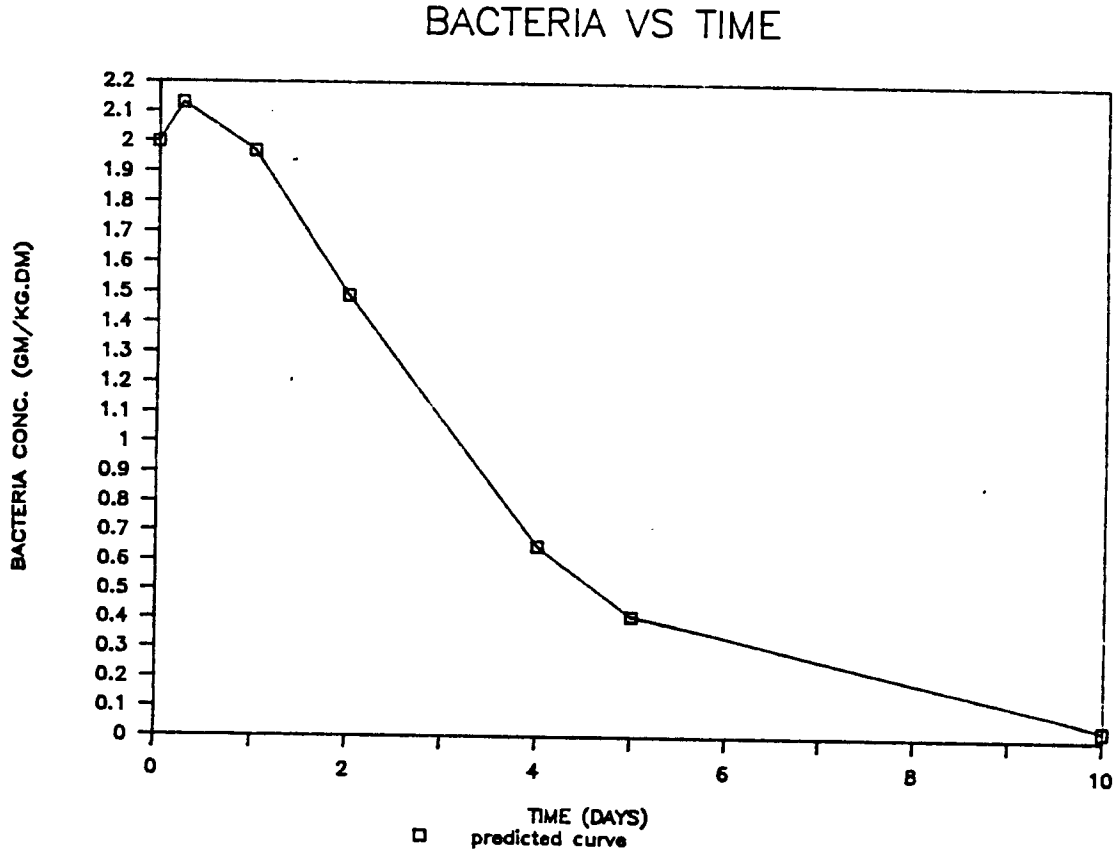
BACTERIA VS TIME
BACTERIA CONC. (GM/KG.DM)
2.2
2.1
2
1.9
1.8
1.7
1.6
1.5
1.4
1.3
1.2
1.1
1
0.9
0.8
0.7
0.6
0.5
0.4
0.3
0.2
0.1
0
0
2
4
6
8
10
TIME (DAYS)
predicted curve

Fig 6